PICOSECOND LASER PULSES

REPORT J920479-21
ANNUAL REPORT

PERIOD COVERED: 1 MARCH 1969 TO 28 FEBRUARY 1970

PREPARED UNDER CONTRACT N00014-66-C0344
SPONSORED BY
ADVANCED RESEARCH PROJECTS AGENCY ARPA ORDER NO. 306 A#15

United Aircraft Research Laboratories
UNITED AIRCRAFT CORPORATION
EAST HARTFORD, CONNECTICUT

160

DISCLAIMER NOTICE

THIS DOCUMENT IS THE BEST QUALITY AVAILABLE.

COPY FURNISHED CONTAINED A SIGNIFICANT NUMBER OF PAGES WHICH DO NOT REPRODUCE LEGIBLY.

Copy #23

J920479-21

UNITED AIRCRAFT CORPORATION
RESEARCH LABORATORIES
East Hartford, Connecticut

J920479-21
Annual Report Under Contract N00014-66-C0344
1 March 1969 to 28 February 1970

ARPA Order No.: 306A#15
Program Cost Code: 9E30K21
Contractor: United Aircraft Research Laboratories
Effective Date of Contract (Modification G06: 1 August 1969
Contract Expiration Date: 31 July 1970
Amount of Contract: $333,916.00
Contract No.: N00014-66-C0344
Principal Investigator: Dr. Anthony J. DeMaria, Area Code 203, 565-3545
Project Scientist: Dr. William H. Glenn, Area Code 203, 565-5411
Short Title: Picosecond Laser Pulses
Date: 26 March 1970

This research is part of Project DEFENDER under the joint sponsorship of the Advanced Research Projects Agency, the Office of Naval Research and the Department of Defense.

Reported by: A. J. DeMaria
A. J. DeMaria
Senior Principal Scientist
Quantum Physics Laboratory

W. H. Glenn
Principal Scientist
Quantum Physics

E. B. Treacy
Senior Research Scientist

M. E. Mack
Senior Research Scientist

G. L. Lamb, Jr.
Senior Theoretical Physicist

C. M. Ferrar
Senior Research Scientist

Approved by: A. J. DeMaria
A. J. DeMaria
Senior Principal Scientist
Quantum Physics Laboratory

Report J920479-21

Annaul Report Under Contract N00014-66-C0344
for the Period 1 March 1969 through 28 February 1970

RESEARCH INVESTIGATION OF PICOSECOND LASER PULSES

ARPA Order No. 306 A # 15, Project Code No. 9E30K21

TABLE OF CONTENTS

TABLE OF CONTENTS
(Continued)

Section 1

INTRODUCTION AND SUMMARY

Q-switched laser pulses have found wide applications in diverse areas of pure and applied research. Some fields which have been opened to investigation by the availability of such pulses include gas breakdown at optical frequencies, plasma production for thermonuclear research, optical harmonic generation and parametric amplification, stimulated scattering effects and coherent propagation effects. Q-switeched pulses have also been used for ranging and guidance systems, high speed photography, medical research, precision machining and other applications. The minimum pulse durections obtainable with the various existing Q-switching techniques are limited to approximately 10^{-8} seconds because of the time required for the buildup of the pulse in the laser cavity.

The advent of the mode-locked laser has brought about a four to five order of magnitude decrease in pulse duration, from 10^{-8} sec to less than 10^{-12} sec and a three order of magnitude increase in peak power, from 10^{9} watts to 10^{12} watts or greater. Detection systems capable of resolving events on a time scale as short as 10^{-13} sec have been developed. It is expected that these developments should open more areas of investigation and should lead to additional scientific, military and commercial applications. The short time duration of the pulses allows the investigation of atomic and molecular processes and coherent interaction effects on a time scale that was previously inaccessible to direct observation and high power available with these pulses allows the investigation of nonlinear effects that were previously unobservable.

The United Aircraft Research Laboratories have been conducting under the present contract a continuing investigation of short time duration laser pulses and their interactions with matter. This investigation, while primarily concerned with the picosecond duration pulses produced by mode-locking, has also been extended to transient phenomena involving longer pulses. During the period covered by this report, work has been conducted in the following areas: (a) the analysis of the propagation of ultrashort pulses in a resonant medium, (b) the analysis of the generation of Cerenkov-like radiation by nonlinear optical effects, (c) the development and demonstration of a novel technique for the measurement of a phase structure of picosecond pulses, (d) the study of stimulated transient Raman Scattering in liquids and gases,(e) the development of extremely fast pumping sources for organic dye lasers, (f) the mode locking of a flashlamp pumped organic dye laser, (g) the demonstration of traveling wave laser action in an organic dye, (h) the investigation of the possibility of obtaining stimulated emission from laser produced plasmas, (i) the investigation of nonlinear polarization effects in anisotropic molecular liquids.

In the area of the analysis of pulse propagation, the major portion of time has been directed toward the formation of a unified synthesis of advances thus far achieved by various workers in obtaining analytical results in the field of ultrashort optical pulse propagation. In the course of reformulating the results of these workers, a number of minor extensions and simplifications of their work have been

obtained. Although the results of some investigators have not been incorporated at this time, it is expected that the material reported herein will constitute a major step toward the compilation of a complete summary of the current status of this field.

During this period, consideration was given to the "dc" component of the nonlinear polarization induced in a dielectric by the passage of a high power optical pulse. This component constitutes a polarization source that moves through the dielectric with the group velocity of the optical pulse. This polarization can lead to Cerenkov radiation at frequencies whose velocity of propagation is less than that of the pulse. This effect is of fundamental interest in itself as it represents a completely new technique for the generation of Cerenkov radiation. It could have application to millimeter and submillimeter wave generation and noise sources. Of even more general importance is the realization that many experiments in beam-wave interactions that can be performed with difficulty using megavolt electron beams can be performed easily using the nonlinear polarization associated with a propagating picosecond pulse.

Since the first measurement of the time duration of the pulses produced by mode-locking of neodymium-glass lasers, it has been apparent that the duration of the pulses are considerably in excess of the minimum possible duration as determined from the reciprocal of the bandwidth. A time-bandwidth product in excess of unity implies a phase or amplitude structure in the pulses. The first measurement of this structure was obtained at this laboratory in 1968. It was found that the pulses could be compressed in time by passing them through a dispersive optical system. The dispersion of the system that was capable of compressing the pulses was such that the transit time increased with increasing wavelength. The compression of the pulses indicated the presence of a linear component of the frequency vs time of the pulses, with longer wavelengths or lower frequencies coming earlier. The compression also indicated that a significant fraction of the observed bandwidth was due to the frequency sweep. While the compression experiments serve to demonstrate the presence of a frequency sweep, it is difficult to extract more detailed information about the phase structure from them. During this reporting period a technique has been devised to extract the maximum available information on the phase structure of the pulses subject to the constraint of present detectors. The information that can be obtained from this technique consists of essentially $\sqrt{N}$ resolvable points on a frequency vs time curve. Here N represents the time-bandwidth product of the pulse. Initial experimental results have been obtained and indicate that the technique works as designed. These results also are consistent with the compression experiments and reconfirm the presence of a linear component of the frequency sweep.

Experiments in stimulated scattering with picosecond pulses have continued. During this period emphasis has been placed on the investigation of stimulated Raman scattering in liquids and gases, and a number of new results have been obtained. The essential difference between stimulated Raman scattering with nanosecond duration pulses from a Q-switched laser and that produced with picosecond duration pulse from a mode-locked laser lies in the finite build-up time of the associated phonons. In the case of picosecond pulse excitation, the phonon population does not reach its steady state value and the transient nature of the scattering must be considered. An important consequence of the transient nature is the fact that in the extreme transient limit, the Raman gain is determined not by the peak value of the spontaneous

Raman cross section but by the total area under the curve of cross section vs frequency. It is possible therefore to excite Raman lines in the transient limit that cannot be excited in the steady state due to competition with other narrower lines that have a higher peak cross section but lower integrated cross section.

Using a mode-locked ruby laser that produced pulses of 5 - 10 picoseconds duration and approximately 56 watts of power, transient stimulated Raman scattering was observed in all liquids that were tested including liquids such as water, carbon tetrachloride and methanol in which stimulated scattering is normally difficult to obtain. Energy conversions as high as 20% were observed together with multiple order Stokes generation and beam trapping. Stimulated scattering was also observed in a variety of gases including N_2, O_2, CO_2, N_2O, SF_6, CH_4, C_2H_4, C_3H_6, HCl and HBr. Prior to these experiments, stimulated Raman scattering had been observed only in H_2, D_2 and CH_4. Self trapping in a collimated beam was observed for the first time in gases, and evidence of a strong optical Stark shift was observed. It is felt that stimulated Raman scattering could have important application in the determination of relaxation rates of materials of interest for chemical lasers. The scattering provides a means of selectively exciting a non-equilibrium population on a very short time scale. The subsequent decay can then be monitored to determine the relaxation rates.

The work on stimulated Raman scattering was carried out in collaboration with N. Bloembergen, R. L. Carman, F. Shimizu and J. Reintjes of Harvard University. All of the experimental results on stimulated scattering reported herein were obtained at United Aircraft Research Laboratories.

The continuing effort in organic dye laser technology has led to improved pumping and modulation capabilities. Dye lasers are capable of producing energetic short pulses at a wide variety of wavelengths and should have significant military and industrial as well as basic research applications.

Initial investigations of the feasibility of obtaining stimulated emission from laser produced plasmas have been carried out. Picosecond pulse excitation provides an extremely fast pumping rate and might be used to populate levels having a very rapid decay time. With such a pumping technique it might be possible to obtain stimulated emission at ultraviolet or shorter wavelengths. Further experiments in this area will be carried out upon completion of a corporation owned 10 joule, .1 nanosecond neodynium laser facility.

The extension of the ideas of magnetic adiabatic passage into the optical region and the first experimental demonstration of the optical adiabatic rapid passage were carried out under the present contract and are reported in detail in the Third Annual Report, H920479-13, March 31, 1969. A separate research program on optical adiabatic passage in gases has been established and is being funded under contract with the Army Research Office, Durham, North Carolina (Contract DAHC04-70=C-0014). Work in this area under the present contract has, therefore, been discontinued.

Section 2

ANALYTICAL DESCRIPTION OF ULTRASHORT OPTICAL PULSE PROPAGATION IN A RESONANT MEDIUM

2.1 Introduction

Recent advances in laser technology have led to the production of coherent optical pulses having durations in the picosecond (10^{-12} sec) regime[1,2]. Such time intervals are comparable to or shorter than the relaxation times associated with the energy levels of many atomic systems. The interaction of radiation with matter on such short time scales gives rise to phenomena which, as a result of quantum mechanical coherence effects, cannot be described by the rate equation analysis developed previously [3-5] for the treatment of much longer pulses.

The novelty of the effects which may appear in the short time resonant response of atomic systems has been brought out quite strikingly by the recent discovery of self-induced transparency [6,7,8]. In this effect, the leading edge of an optical pulse is used to invert an atomic population while the trailing edge returns the population to its initial state by means of stimulated emission. The process is realizable if it takes place in a time that is short compared to the incoherent damping time of the resonant atomic systems, i.e., to the homogeneous broadening time of the medium. When all conditions for this process are met, it is found that a steady state pulse profile is established and that this pulse envelope then propagates through the medium at a velocity which may be considerably less than the light velocity in the medium. What is perhaps most remarkable is that even those atoms that are off resonance due to inhomogeneous broadening can partake of this process in such a way that they are returned to their initial state. Within the theoretical framework that has been used to describe this effect it has been shown [7,8] that such steady state propagation can take place only if the profile of the electric field is of a special form, namely that of a hyperbolic secant. Many salient features of this effect have been considered[7] since its discovery. The possibility of analogous effects in semiconductors has also been proposed[73] and somewhat similar effects have been observed in the study of neuristor waveforms.

In addition to the anomalous transmission property of ultrashort optical pulses, the amplification of such pulses has also drawn considerable attention. A number of analytical results have been obtained here as well[9,10,11]. One expects that amplification processes will ultimately be limited by non-resonant loss mechanisms. If these are introduced in a phenomenological way through a conductivity, then the ad hoc assumption that there is a steady state pulse propagating at the light velocity may be verified by direct computation.

Whenever it becomes necessary to extend the range of validity of a theory to encompass new phenomena, it is useful to seek limiting cases of the new formalism[8,12,13,14] which admit of exact solutions of the type referred to above. While the experimentalist is rarely moved by theoretical descriptions that fail to provide for all facets of a phenomenon as it is known to exist in the experimental situation, such as relaxation times, inhomogeneous broadening, etc., it should be emphasized that many of the most interesting effects in ultra-short pulse propagation appear

already in much simpler theoretical contexts and an understanding of even these simpler equations, as opposed to the new generation of numerical results, is far from complete. The most promising method of attack is clearly through a simultaneous application of both analytical and computational techniques and the field of optical pulse propagation provides an ideal opportunity for the application of this "synergetic" approach. In fact, self induced transparency was discovered from an analysis of numerical solutions of the appropriate equations.

The present paper summarizes the success that has thus far been achieved in describing the novel aspects of ultrashort optical pulse propagation by analytical treatment. In addition to the above-mentioned results, two relatively simple models have been devised which describe a number of other effects that have been observed both experimentally[8,15] and as output from machine computations based upon more complete theoretical descriptions[12-14]. The first model[9,17] is one in which inhomogeneous broadening is neglected. The physical situation most closely related to such a model is that of propagation under conditions of extreme saturation broadening[18,19]. Although the problem under consideration involves a coupling between radiation and matter that is too strong to be treated by perturbation theory, a fairly extensive analytical treatment of this model is still possible since it expresses this interaction in terms of a single nonlinear partial differential equation which arose long ago in differential geometry. The techniques developed about the turn of the century for obtaining solutions to this equation may be employed to great advantage.

Certain other phenomena, notably that of photon echo[20-23], require for their explanation the relative dephasing of atoms that results when inhomogeneous broadening is present. This effect is also an example of the collective superradiant state[7,4] in which energy is radiated coherently into the electromagnetic field. Here again, it is possible to construct a soluble model[24] in which the reaction of stimulated emission back on the incident wave is taken into account. If one is willing to forgo consideration of the detailed structure of pulse shapes, the time dependence of the pulse may be assumed to be that of a delta function and interest confined to the spatially dependent amplitude of such delta function pulses. Only the time integral of such a pulse shape is meaningful, of course, but such a time integral has been shown to be precisely the quantity of interest in the treatment of ultrashort pulses. The area theorem[7,8], which is so useful in understanding short pulse phenomena, is also found to govern the spatial evolution of the amplitude functions introduced in this model.

Although much of the physical insight required for an understanding of these propagation effects may be obtained from a consideration of the interaction of light with a system of two-level atoms, it should be emphasized that the results thus obtained may require modification when level degeneracy is included[8,18].

2.2 Basic Equations

We begin by summarizing the standard semiclassical description of the interaction of an electromagnetic wave with an assembly of two-level systems. The optical field in the form of a plane polarized electromagnetic pulse may be characterized by its electric field vector $\underset{\sim}{E}(\underset{\sim}{r},t)$ which satisfies the usual wave equation

$$\nabla^2 \underset{\sim}{E} - \frac{4\pi\sigma}{c^2}\frac{\partial \underset{\sim}{E}}{\partial t} - \frac{1}{c^2}\frac{\partial^2 \underset{\sim}{E}}{\partial t^2} = \frac{4\pi}{c^2}\frac{\partial^2 \underset{\sim}{P}}{\partial t^2} \tag{2.1}$$

where σ is a conductivity that is introduced to simulate nonresonant losses in the medium, c is the velocity of light in the medium and $\underset{\sim}{P}$ is the polarization of the medium that is induced by the electromagnetic wave. For a medium consisting of an assemblage of noninteracting two-level systems distributed with a uniform density n_o, this polarization is $n_o p$ where p is the polarization of an individual two-level system.

The polarization of an individual system may in turn be obtained from its microscopic description by the usual prescription

$$p = \mathrm{Tr}(\rho \underset{\sim}{P}) \tag{2.2}$$

where ρ is the density matrix of the two-level system[25], and $\underset{\sim}{P}$ is the polarization operator. The time dependence of ρ is given by the quantum mechanical Liouville theorem

$$i\hbar\frac{\partial \rho}{\partial t} + [\rho, \mathcal{H}] = 0 \tag{2.3}$$

where $\mathcal{H}$ is the total Hamiltonian of an individual two-level system. The time dependence of an arbitrary operator, $\mathcal{O}$ is governed by the relation

$$i\hbar\frac{d\mathcal{O}}{dt} = i\hbar\frac{\partial \mathcal{O}}{\partial t} + [\mathcal{O}, \mathcal{H}] \tag{2.4}$$

For later use, it proves convenient to recognize that operators not containing explicit time dependence also satisfy

$$\hbar^2\frac{d^2\mathcal{O}}{dt^2} + [[\mathcal{O}, \mathcal{H}], \mathcal{O}] = i\hbar\left[\frac{\partial \mathcal{H}}{\partial t}, \mathcal{O}\right] \tag{2.5}$$

The Hamiltonian of a two level system interacting with a classical electromagnetic field may be adequately represented by

$$\mathcal{H} = \mathcal{H}_0 + V \tag{2.6}$$

where $\mathcal{H}_0$ is the Hamiltonian of the isolated two-level system and

$$V = -\underset{\sim}{E} \cdot \underset{\sim}{P} \tag{2.7}$$

is the interaction energy in dipole approximation.

The wave function for the isolated two-level system may be written

$$\psi(\underset{\sim}{r}, t) = a_a(t)u_a(\underset{\sim}{r}) + a_b(t)u_b(\underset{\sim}{r}) \tag{2.8}$$

where u_a and u_b are eigenfunctions of the system and satisfy

$$\mathcal{H}_0 u_a = E_a u_a \, , a = a,b \tag{2.9}$$

Such energy eigenfunctions provide the specific representations

$$\mathcal{H}_0 = \begin{pmatrix} E_a & 0 \\ 0 & E_b \end{pmatrix} , \underset{\sim}{P} = \begin{pmatrix} 0 & \underset{\sim}{P}_{ab} \\ \underset{\sim}{P}_{ba} & 0 \end{pmatrix} , \rho = \begin{pmatrix} \rho_{aa} & \rho_{ab} \\ \rho_{ba} & \rho_{bb} \end{pmatrix} \tag{2.10}$$

where

$$\underset{\sim}{P}_{\alpha\beta} = -e \int d^3 \underset{\sim}{r} \, u_\alpha^* \underset{\sim}{r} \, u_\beta \tag{2.11}$$

$$\rho_{\alpha\beta} = a_\alpha^* a_\beta$$

and the levels are labeled such that $E_a > E_b$. The vanishing of the diagonal elements in $\underset{\sim}{P}$ signifies the assumed absence of any permanent dipole moment in the system under consideration.

In addition to the polarization $\underset{\sim}{P}$, the difference in population between upper and lower states n, is also of interest and may be expressed in the form

$$n = n_0 (\rho_{aa} - \rho_{bb}) = n_0 \, \mathrm{Tr}(\rho \sigma_z) \tag{2.12}$$

where σ_z is the Pauli spin matrix

$$\sigma_z = \begin{pmatrix} 1 & 0 \\ 0 & -1 \end{pmatrix} \tag{2.13}$$

The time dependence of p can be conveniently obtained by taking the trace of the operator equation

$$\hbar^2 \ddot{\underset{\sim}{P}} + \left| \left[\underset{\sim}{P}, \mathcal{H} \right], \mathcal{H} \right| = i\hbar \left| \frac{\partial \mathcal{H}}{\partial t} \, , \underset{\sim}{P} \right| \tag{2.14}$$

which follows from Eq. (2.4). With the representations given above, the right-hand side of this equation vanishes while

$$\left[\underset{\sim}{P}, \mathcal{H} \right] = \left[P, \mathcal{H}_0 \right] = -\hbar \omega_{ab} \begin{pmatrix} 0 & \underset{\sim}{P}_{ab} \\ \underset{\sim}{P}_{ba} & 0 \end{pmatrix} \tag{2.15a}$$

$$\left| \left[\underset{\sim}{P}, \mathcal{H} \right], \mathcal{H}_0 \right| = \hbar \omega_{ab}^2 \underset{\sim}{P} \tag{2.15b}$$

and

$$\left| \left[\underset{\sim}{P}, \mathcal{H} \right], V \right| = 2\hbar \omega_{ab} \underset{\sim}{E} \cdot \begin{pmatrix} \underset{\sim}{P}_{ab} \underset{\sim}{P}_{ba} & 0 \\ 0 & - \underset{\sim}{P}_{ba} \underset{\sim}{P}_{ab} \end{pmatrix} \tag{2.15c}$$

where

$$\hbar\omega_{ab} = E_a - E_b \tag{2.16}$$

Equation (2.12) therefore reduces to

$$\ddot{\underset{\sim}{P}} + \omega_{ab}^2 \underset{\sim}{P} = -\frac{2\omega_{ab}}{\hbar} \underset{\sim}{E} \cdot \underset{\sim}{p}_{ab} \underset{\sim}{p}_{ba} \sigma_z \tag{2.17}$$

Application of the trace operation converts this operator equation into

$$\ddot{\underset{\sim}{p}} + \omega_a^2{}_b \underset{\sim}{p} = -\left(\frac{1}{3}\right)\frac{2\omega_{ab}\wp^2}{\hbar n_o} \underset{\sim}{E} n \tag{2.18}$$

where it has been assumed that $p_{ab} = p_{ba} = \wp$. The factor of 1/3 in parenthesis is to be included if all possible spatial orientations of the two level systems are permitted[26,75].

From a direct multiplication of the quantities involved there follows

$$i\hbar \dot{\underset{\sim}{P}} = \left[\underset{\sim}{P}, \mathcal{H}\right] = -\frac{\hbar\omega_{ab}}{2}\left[\sigma_z, \underset{\sim}{P}\right] \tag{2.19}$$

On the other hand, multiplication of Eq. (2.3) by $n_o\sigma_z$ and application of the trace operation yields

$$i\hbar\dot{n} = n_o \underset{\sim}{E} \cdot \mathrm{Tr}\left\{\rho\left[\underset{\sim}{P}, \sigma_z\right]\right\} \tag{2.20}$$

Calculation of the trace of Eq. (2.19) then finally leads to the equality

$$\dot{n} = \frac{2n_o}{\hbar\omega_{ab}} \underset{\sim}{E} \cdot \dot{\underset{\sim}{P}} \tag{2.21}$$

Equations (2.18) and (2.21) provide a convenient starting point for describing the response of a two-level system to an external electromagnetic field.

Having formulated the response of the two-level systems to the incident optical field, we now turn to a consideration of the reaction of the medium back upon the incident wave. It is the self-consistent evolution of these two processes that is the essence of the problem under consideration. On the right-hand side of Eq. (2.1), the term $\partial^2\underset{\sim}{p}/\partial t^2$ may be approximated by $-\omega_o^2\underset{\sim}{p}$ where ω_o is the carrier frequency of the incident pulse. This follows immediately if ω_{ab} is replaced by ω_o in Eq. (2.18) and the term of the right-hand side of that equation is neglected. Neglect of this term is equivalent to a neglect of the backscattered wave that is produced as the incident wave traverses the medium. From Eqs. (2.1) and (2.18), one sees that this neglect is permissible provided that $n_o\wp^2/\hbar\omega_o \ll 1$ which will be nearly always satisfied.

Since even the shortest pulses produced to date contain many optical cycles, it is appropriate to write the electric field in terms of a carrier wave as well as envelope and phase functions $\mathcal{E}(\underset{\sim}{r},t)$ and $\Phi(\underset{\sim}{r},t)$ respectively which vary slowly on the length and time scales of the carrier wave. Hence we write

$$E(\underset{\sim}{r},t) = E_0 \mathcal{E}(\underset{\sim}{r},t) \cos\left[\underset{\sim}{k}_0 \cdot \underset{\sim}{r} - \omega_0 t + \phi(\underset{\sim}{r},t)\right] \tag{2.22}$$

and assume $\omega_0 \mathcal{E} \gg \partial \mathcal{E}/\partial t$, $k_0 \mathcal{E} \gg \partial \mathcal{E}/\partial x$ plus similar inequalities for Φ. A characteristic field magnitude E_0 has also been extracted from the amplitude. Because of the assumption that $\mathcal{E}(\underset{\sim}{r},t)$ and $\Phi(\underset{\sim}{r},t)$ vary slowly compared to the carrier wave, Eq. (2.1) may be reduced to a much simpler form. In particular, only first derivatives of $\mathcal{E}(\underset{\sim}{r},t)$ and $\Phi(\underset{\sim}{r},t)$ need be retained on the left-hand side of this equation when it is expressed in terms of $\mathcal{E}$ and Φ. The solution thus obtained is customarily referred to as the solution in the slowly varying envelope approximation.

In general, it is appropriate to consider not a single transition frequency ω_{ab} but a spread in transition frequencies about ω_{ab}, so called inhomogeneous broadening. It is convenient to analyze the situation in which this distribution is symmetric about ω_{ab} and the carrier frequency of the incident optical pulse is at this frequency, i.e., $\omega_0 = \omega_{ab}$.

Equation(2.1), specialized to a plane wave traveling in a positive x direction now becomes

$$\left(\frac{d\mathcal{E}}{dt} + 2\pi\sigma\mathcal{E}\right)\sin\Phi(x,t) + \frac{d\phi}{dt}\cos\Phi(x,t) = \frac{2\pi\omega_0 \mathcal{N}_0}{E_0}\int_{-\infty}^{\infty} d\Delta\omega\, g(\Delta\omega)\, p(\Delta\omega, x, t) \tag{2.23}$$

where

$$\Phi(x,t) = k_0 x - \omega_0 t + \phi(x,t)\,, \quad \frac{d}{dt} = \frac{\partial}{\partial t} + c\frac{\partial}{\partial x} \tag{2.23a}$$

and $\Delta\omega = \omega - \omega_0$. Although the idealization of an infinite plane wave front is convenient for theoretical purposes, it should be emphasized that transverse mode structure may be important in experimental situations.

The spectrum $g(\Delta\omega)$ which characterizes the inhomogeneous broadening is assumed to be normalized so that

$$\int_{-\infty}^{\infty} d\Delta\omega\, g(\Delta\omega) = 1 \tag{2.24a}$$

The causal Green's function for Eq. (2.18), i.e., the solution of

$$\frac{d^2G}{dt^2} + \omega_{ab}^2 G = -\delta(t-t') \tag{2.24b}$$

which satisfies $G = 0$ for $t < t'$ is

$$G(t\,|\,t') = -\frac{1}{\omega_{ab}}\mathcal{U}(t-t')\sin\omega_{ab}(t-t') \tag{2.25}$$

in which u(t) is the unit step function. Multiplication of Eqs. (2.18) and (2.25) by $G(t|t')$ and p respectively, subtracting and integrating over all time yields

$$p(\Delta\omega,x,t) = -2\wp\Omega\int_{-\infty}^{t} dt' \sin\omega(t-t') N(\Delta\omega,x,t')\mathcal{E}(x,t')\cos\Phi(x,t') \tag{2.26}$$

where $N = n/n_0$, and Ω, the Rabi frequency, is given by $\Omega = E_0\wp/\hbar$. The factor of 1/3 due to orientational averaging is neglected. This expression for the polarization may now be decomposed into parts which are in phase and $\pi/2$ out of phase with the electric field. One finds that

$$p = \wp\left[\rho(\Delta\omega,x,t)\sin(\Phi(x,t)) + \mathcal{Q}(\Delta\omega,x,t)\cos(\Phi(x,t))\right] \tag{2.27}$$

where

$$\mathcal{P} = \Omega\int_{-\infty}^{t} dt' \mathcal{E}(x,t') N(\Delta\omega,x,t')\cos\left[\Delta\omega(t-t') + \phi(x,t) - \phi(x,t')\right] \tag{2.28a}$$

$$\mathcal{Q} = -\Omega\int_{-\infty}^{t} dt' \mathcal{E}(x,t') N(\Delta\omega,x,t')\sin\left[\Delta\omega(t-t') + \phi(x,t) - \phi(x,t')\right] \tag{2.28b}$$

In obtaining this result, terms near the second harmonic of ω_0 have been discarded. However, it should be emphasized that in obtaining these results there has been no assumption that ρ, $\mathcal{Q}$, and N vary slowly compared to the carrier wave.

Equation (2.23) may now be decomposed into the pair of relations

$$\frac{d\rho}{dt} + 2\pi\sigma\mathcal{E} = (c\alpha'/\Omega)\int_{-\infty}^{\infty} d\Delta\omega\, g(\Delta\omega)\rho(\Delta\omega,x,t) \tag{2.29a}$$

$$\mathcal{E}\frac{d\phi}{dt} = -(c\alpha'/\Omega)\int_{-\infty}^{\infty} d\Delta\omega\, g(\Delta\omega)\mathcal{Q}(\Delta\omega,x,t) \tag{2.29b}$$

where

$$\alpha' = 2\pi n_0\omega_0\wp^2/\hbar c \tag{2.30}$$

The functions ρ and $\mathcal{Q}$ are readily shown to satisfy the differential equations

$$\frac{\partial\rho}{\partial t} = \Omega\mathcal{E}N + \left(\Delta\omega + \frac{\partial\phi}{\partial t}\right)\mathcal{Q} \tag{2.31a}$$

$$\frac{\partial\mathcal{Q}}{\partial t} = -\left(\Delta\omega + \frac{\partial\phi}{\partial t}\right)\rho \tag{2.31b}$$

When time dependence near the second harmonic of ω_o is also neglected in Eq. (2.21) it is equivalent to

$$\frac{\partial N}{\partial t} = -\Omega \mathcal{E}\left(\rho - \frac{1}{\omega_0}\frac{\partial \mathcal{Q}}{\partial t}\right) \tag{2.32}$$

When the slowly varying envelope approximation is used, the second term on the right-hand side may be discarded. It is convenient to introduce the transformation

$$t = \Omega(t - x/c), \xi = (\Omega\epsilon/c)x \tag{2.33}$$

The constant ϵ is essentially the ratio of energy stored in the medium to the energy of the wave, i.e.

$$\epsilon = n_0 \hbar_0 \omega_0 / (E_0^2/2\pi) \tag{2.34}$$

Neglecting the conductivity at this point, Eqs. (2.29) are transformed to

$$\frac{\partial \mathcal{E}}{\partial \xi} = \int_{-\infty}^{\infty} d\Delta\omega\, g(\Delta\omega)\rho(\Delta\omega,\xi,\tau) \tag{2.35}$$

$$\mathcal{E}\frac{\partial \phi}{\partial \xi} = \int_{-\infty}^{\infty} d\Delta\omega\, g(\Delta\omega)\mathcal{Q}(\Delta\omega,\xi,\tau) \tag{2.36}$$

while Eqs. (2.31) and (2.32), in the slowly varying envelope approximation, become

$$\frac{\partial N}{\partial \tau} = -\mathcal{E}\rho \tag{2.37a}$$

$$\frac{\partial \rho}{\partial \tau} = \mathcal{E}N + \left(f + \frac{\partial \phi}{\partial \tau}\right)\mathcal{Q} \tag{2.37b}$$

$$\frac{\partial \mathcal{Q}}{\partial \tau} = -\left(f + \frac{\partial \phi}{\partial \tau}\right)\rho \tag{2.37c}$$

where $f = \Delta\omega/\Omega$. Equations (2.37) describe how the field amplitude $\mathcal{E}$ and phase ϕ determine ρ, $\mathcal{Q}$ and N for a two-level system that is off resonance by an amount $\Delta\omega$. Equations (2.35) and (2.36) show how the polarization due to a distribution of such systems reacts back on the amplitude and phase.

Equations (2.37) also arise in nuclear magnetic resonance studies in which an oscillating magnetic field interacts with an assemblage of two level systems which possess a magnetic moment. Such studies have been confined to samples that are of a sufficiently small size that the reaction of the induced field back on the exciting

field could be ignored. Equations (2.37) may then be solved for a specified external field. This is not the case in the situation envisioned here. A satisfactory description of optical pulse propagation is only obtained when Eqs. (2.36) and (2.37) are solved self consistently.

At this point, it may be noted that Eqs. (2.35) and (2.37) contain two conservation laws. Conservation of energy follows upon multiplication of Eq. (2.35) by $\mathcal{E}$ and introduction of Eq. (2.37a) which yields

$$\frac{1}{2}\frac{\partial \mathcal{E}^2}{\partial \xi} + \frac{\partial}{\partial \tau}\int_{-\infty}^{\infty} d\Delta\omega g(\Delta\omega) N = 0 \qquad (2.38$$

Multiplication of Eqs. (2.37) by N, ρ and $\mathcal{Q}$ respectively along with summation of the resulting equations yields an exact differential which is equivalent to

$$N^2 + \rho^2 + \mathcal{Q}^2 = 1 \qquad (2.39)$$

In this result, a constant of integration has been set equal to unity since in the usual applications of the theory one has $\rho(\zeta, -\infty) = \mathcal{Q}(\zeta, -\infty) = 0$, $N(\zeta, -\infty) = \pm 1$. The form of Eq. (2.39) enables one to interpret the response of a two level system in terms of the motion of a vector on the surface of a sphere in a ρ, $\mathcal{Q}$, N space.

2.3 Self-Induced Transparency and the Area Theorem

Up to the present time, the full set of equations given by Eq. (2.35 - 2.37) has received little attention. However, if one adopts the consistent set of assumptions that the phase term φ is initially zero, that the carrier frequency is at the center of a symmetrically broadened line (i.e., $g(\Delta\omega) = g(-\Delta\omega)$, and that $\mathcal{Q}$ is an odd function of $\Delta\omega$. Then from Eq. (2.36) one sees that the source term governing variations in φ is zero so that φ will remain zero. This form of the theory, particularly with the aid of numerical computations,[14] has provided considerable insight into the subject of ultrashort pulse propagation.

Even this specialized form of the basic equations has yielded only steady state solutions. These include both the solitary wave solution of self-induced transparency[7,8] and infinite wave train solutions[27,28,29] which contain the solitary wave as a limiting case. Only the former will be discussed here; infinite wave train solutions will be discussed later in connection with a somewhat more specialized theoretical model.

For a steady state solution, one may assume that $\mathcal{E}$, ρ, $\mathcal{Q}$, and N are functions of a single dimensionless variable $w = (t - x/V)/\tau_p$ where V is the velocity of the pulse and τ_p is a parameter having the dimensions of time. It will be shown that τ_p may be directly related to the pulse width.

Equations (2.35) and (2.37c) may now be combined and integrated to yield

$$\left(1 - \frac{c}{V}\right)\mathcal{E}(w) + \epsilon\Omega\int_{-\infty}^{\infty} d\Delta\omega\, g(\Delta\omega)\mathcal{Q}(\Delta\omega, w)/\Delta\omega = 0 \tag{2.40}$$

An integration constant has been set equal to zero in this result since $\mathcal{E}$ and $\mathcal{Q}$ are zero before arrival of the pulse. If this equation is divided by $\mathcal{E}(w)$ and differentiated with respect to w, one obtains

$$\int_{-\infty}^{\infty} d\Delta\omega\, \frac{g(\Delta\omega)}{\Delta\omega}\, \frac{d}{dw}\left(\frac{\mathcal{Q}}{\mathcal{E}}\right) = 0 \tag{2.41}$$

Now the function $g(\Delta\omega)$ contains a parameter such as T_2^* that determines the width of the inhomogeneous broadening, e.g.

$$g(\Delta\omega) = \frac{T_2^*}{2\sqrt{\pi}} \exp\left[-(\Delta\omega T_2^*/2)^2\right] \tag{2.42}$$

Although τ_p and V, and hence ω depend in an implicit way upon T_2^*, there is no explicit dependence of $\mathcal{E}$ upon T_2^*. Also, since $\mathcal{Q}$ is the response of an individual two-level system, it is also independent of T_2^* except for the implicit dependence contained in w. Consequently, the function in parentheses, the integral of Eq. (2.41), does not contain explicit dependence upon T_2^*. Now if it is assumed that the theory must be valid for arbitrarily large values of T_2^*, then one may invoke Lerch's theorem[30] to justify the conclusion that the term multiplying $g(\Delta\omega)$ in the integrand must itself be equal to zero. It then follows that

$$\mathcal{Q}(\Delta\omega, w) = \chi(\Delta\omega)\mathcal{E}(w) \tag{2.43}$$

where $\chi(\Delta\omega)$ is an as yet unknown function of the detuning. When this result is introduced into Eq. (2.40), one finds that the velocity of the envelope function is given by

$$\frac{1}{V} = \frac{1}{c}\left(1 + \epsilon\Omega\int_{-\infty}^{\infty} d\Delta\omega\, g(\Delta\omega)\chi(\Delta\omega)/\Delta\omega\right) \tag{2.44}$$

To obtain the form of the envelope function $\mathcal{E}$, it is first noted that Eqs. (2.37b, c), with the phase term φ set equal to zero, are equivalent to the linear equation

$$\frac{\partial\lambda}{\partial\tau} + i\mathcal{E}\lambda = f\mathcal{Q} \tag{2.45}$$

where $\lambda = \rho + i\mathcal{Q}$. Setting

$$\phi(w) = \Omega\tau_p\int_{-\infty}^{w} dw'\mathcal{E}(w') \tag{2.46}$$

and introducing Eq. (2.43), one finds that the solution of Eq. (2.45) which reduces to $\rho(-\infty) = 0$, $N(-\infty) = -1$ is

$$\rho = -(1 - f\chi)\sin\phi \tag{2.47}$$

$$N = -f\chi - (1 - f\chi)\cos\phi \tag{2.48}$$

Substitution of Eq. (2.43), (2.47) and (2.48) into Eq. (2.39) yields

$$\chi(\Delta\omega) = \frac{\Omega\tau_p\Delta\omega}{1 + (\Delta\omega\tau_p)^2} \tag{2.49}$$

Also, from Eq. (2.38), the energy conservation law,

$$\left(\frac{d\phi}{dw}\right)^2 = 2\gamma^2(1 - \cos\phi) = 4\gamma^2\sin^2(\phi/2) \tag{2.50}$$

where

$$\gamma^2 = \epsilon\Gamma(\Omega\tau_p)^2/\left(\frac{c}{v} - 1\right) \tag{2.51}$$

and

$$\Gamma \equiv 1 - \frac{1}{\Omega}\int_{-\infty}^{\infty} d\Delta\omega\, g(\Delta\omega)\,\Delta\omega\,\chi(\Delta\omega) \tag{2.52}$$

The solution of Eq. (2.50) that vanishes as $w \to \pm\infty$ is

$$\phi = 4\tan^{-1}e^{\gamma w} \tag{2.53}$$

Hence the electric field envelope is

$$\frac{\wp}{\hbar}E_0\mathcal{E} = \frac{1}{\tau_p}\frac{d\phi}{dw} = \frac{2\gamma}{\tau_p}\operatorname{sech}\gamma w \tag{2.54}$$

and one sees from the definition of w that τ_p will play the role of pulse half width provided γ is set equal to unity.

If the maximum pulse height is equated to $2E_0$, then Eq. (2.54) yields

$$\Omega\tau_p = 1 \tag{2.55}$$

which determines the pulse width in terms of its amplitude and $\wp$ which characterizes the medium.

From Eqs. (2.43), (2.47), (2.48) and (2.49) one finds that the response of a given two-level system is[3]

$$\begin{aligned} N &= -1+2D\sin^2(\phi/2) \\ \rho &= -D\sin\phi \\ \mathcal{J} &= 2\,\Delta\omega\tau_p D\sin(\phi/2) \end{aligned} \tag{2.56}$$

where

$$D = \left[1+(\Delta\omega\tau_p)^2\right]^{-1} \tag{2.57a}$$

Also, it is now possible to return to Eq. (2.44) for the envelope velocity and consider its dependence upon T_2^*. Combining Eqs. (2.44) and (2.49), one finds that V is given by

$$\frac{1}{V} = \frac{1}{c} + \alpha' \tau_p^2 \int_{-\infty}^{\infty} d\Delta\omega g(\Delta\omega) D \tag{2.57b}$$

$$\frac{1}{V_0} - \frac{1}{V} = (1-\Gamma)\left(\frac{1}{V_0} - \frac{1}{c}\right) \tag{2.58}$$

Here V_o is the velocity in the limit of no inhomogeneous broadening. For $g(\Delta\omega)$ given by Eq. (2.42), one obtains

$$\Gamma = \int d\Delta\omega g(\Delta\omega) D = 2k\exp(k^2) E_N \, fc(k) \tag{2.59}$$

where

$$K = T_2^*/2\tau_p \tag{2.60}$$

and Erfc(k) is the compliment of the error function[31]. For $T_2^* \gg \tau_p$, $\Gamma \to 1$ and $V \to V_0$. As T_2^* becomes much less than τ_p, a much smaller percentage of the atoms are on resonance. One then finds $I \to 0$ and hence $V \to c$.

Finally, it has been noted[32] that if the carrier frequency is not confined to the center of a symmetric line but is in fact far-off resonance, the expression for the velocity given in Eq. (2.44) goes over to the usual result for the velocity of a wave in a dispersive medium.

The above results, along with the infinite wave train solutions which correspond to libration and oscillation solutions of Eq. (2.50) are the only analytical solutions of the inhomogeneously broadened version of Eqs. (2.35 - 2.37) that have been reported to date. However, further analytical progress is still possible if one confines attention to the area under the envelope curve[7,8]. Defining

$$\theta(x) = \Omega \int_{-\infty}^{\infty} dt' \mathcal{E}(x,t') \tag{2.61}$$

the equation governing the variation in θ is readily obtained by integrating Eq. (2.29a) over all time. Using Eqs. (2.28b) and (2.31b) with φ again set equal to zero one finds

$$\frac{d\theta}{dx} + \kappa\theta = \alpha'\Omega \int_{-\infty}^{\infty} d\Delta\omega \, \frac{g(\Delta\omega)}{\Delta\omega} \int_{-\infty}^{\infty} dt' \mathcal{E}(x,t') N(x,t') \lim_{t\to\infty} \sin \Delta\omega (t-t') \tag{2.62}$$

where $k = 2\pi \sigma/c$. Since the indicated limiting process is somewhat delicate, a method of carrying it out is now given in some detail. First, one may introduce the well known forms

$$\lim_{t\to\infty} \frac{\sin\Delta\omega t}{\Delta\omega} = \pi\delta(\Delta\omega)$$

$$\lim_{t\to\infty} \frac{\cos\Delta\omega t}{\Delta\omega} = \left(\frac{1}{\Delta\omega} - \frac{P}{\Delta\omega}\right) \tag{2.63}$$

where P denotes a principal value. Using another standard representation for the delta function and the principal value,

$$\lim_{t\to\infty} \frac{\cos\Delta\omega t}{\Delta\omega} = \lim_{\epsilon\to 0} \left[\frac{1}{\Delta\omega} - \frac{\Delta\omega}{\epsilon^2 + (\Delta\omega)^2} \right]$$

$$= \pi \frac{\delta(\Delta\omega)}{\omega} \lim_{\epsilon\to 0} \epsilon \to 0 \tag{2.64}$$

When these results are used in Eq. (2.62), one obtains

$$\frac{d\theta}{dx} + \kappa\theta = \frac{\alpha\Omega}{2} \int_{-\infty}^{\infty} dt' \mathcal{E}(x,t') N(0,x,t') \tag{2.65}$$

where

$$\alpha = 2\pi g(0)\alpha' \tag{2.66}$$

and α' is as defined in Eq. (2.30). As will be shown later, the population of on-resonance atoms, i.e., those represented by $N(0,x,t)$, may be expressed as

$$N(0,x,t) = \pm \cos\left[\Omega \int_{-\infty}^{t} dt' \mathcal{E}(x,t')\right] \tag{2.67}$$

where the upper sign is to be used if the population is initially inverted while the lower sign is used if the population is initially in the lower level. Hence Eq. (2.65) finally takes the form

$$\frac{d\theta}{dx} + \kappa\theta = \pm \frac{\alpha}{2} \sin\theta \tag{2.68}$$

Equation (2.68) is the area theorem[7,8]. It contains the key to an understanding of many of the effects which occur in the propagation of ultrashort optical pulses. Again, if orientational averaging is included, the factor α should be replaced by $\alpha/3$.

For $\sigma = 0$, the solution of Eq. (2.68) which satisfies $\theta = \theta_o$ at $x = x_o$ is

$$\tan\frac{\theta}{2} = \tan\frac{\theta_o}{2}\exp\left[\pm\frac{a}{2}(x-x_o)\right] \tag{2.69}$$

and is depicted schematically in Fig. 1. Modifications of this result due to nonvanishing conductivity have been inferred[16] from numerical solutions of Eq. (2.68).

Since Eq. (2.68) contains a choice of signs, it is actually two distinct differential equations. The two solutions are obtained from Fig. 1 by reading the diagram from right to left for the plus sign (amplifier) and from left to right for the minus sign (attenuator). Hence one sees that an infinitesimal area will grow to π in an amplifier while any area less than π will evolve to zero in an attenuator. This second result allows for not only the well-known decay of a pulse as it propagates in an attenuator, but also for evolution into a nonvanishing zero π pulse, i.e., one in which the total area under the pulse envelope is zero but the area under the pulse energy ($\sim\mathcal{E}^2$) is not zero. This is of course possible if the positive portions of a pulse envelope are equal in area to the negative portions. Physically, the regions of positive and negative envelope are merely regions in which there is a relative difference of 180 degrees in the phase of the carrier wave. In an attenuator, initial pulse areas between π and 3π will evolve into the steady state 2π pulse of self-induced transparency. One also sees that the 2π pulse is unstable in an amplifier and will evolve into either a π or 3π pulse.

Figure 1 refers only to the total area of a pulse and gives no information at all about the possible breakup of a pulse into two or more pulses with the same total area or of whether a continually amplifying pulse will retain an area of π by virtue of pulse narrowing or by developing negative regions in the pulse envelope.

2.4 Steady State Pulse in an Amplifier

In addition to the self-induced transparency solution in an attenuator, a somewhat similar steady state result may be obtained in an amplifer if the loss term σ is retained in Eq. (2.29a). This was first recognized by observation of machine computations[13] and subsequently obtained analytically[9]. Both results have been obtained in the limit of no inhomogeneous broadening although certain cases in which homogeneous broadening is retained have also been treated[9]. From Eqs. (2.29), (2.31) and (2.32) the relevant equations are

$$\frac{\partial\mathcal{E}}{\partial t} + c\frac{\partial\mathcal{E}}{\partial x} + 2\pi\sigma\mathcal{E} = \frac{ca'}{\Omega}\rho \tag{2.70}$$

$$\mathcal{E}\left(\frac{\partial\phi}{\partial t} + c\frac{\partial\phi}{\partial x}\right) = -\frac{ca'}{\Omega}2 \tag{2.71}$$

as well as Eqs. (2.37). The ad hoc assumption which renders the analysis tractable is that both $\mathcal{E}$ and φ travel at the velocity c. The differential operators in Eqs. (2.70) and (2.71) then vanish identically and the problem is greatly simplified.

It should be emphasized that there is no rigorous justification for this assumption. However, it has recently been noted[16] that if a steady state pulse at any velocity $v \neq c$ is assumed, then the resulting numerical solution is unstable and evolves asymptotically into a pulse propagating at $v = c$.

From Eq. (2.71) one then sees that $\mathcal{Q} = 0$ and hence from Eq. (2.37b) that

$$\Delta\omega + \frac{\partial\phi}{\partial t} = 0 \tag{2.72}$$

Consequently,

$$\phi = (\omega - \omega_0)t \tag{2.73}$$

and from Eq. (2.22) one sees that the frequency of the steady state pulse is always equal to ω the transition frequency of the two-level system[9]. Since $\mathcal{Q} = 0$, Eq. (2.37a) follows from Eq. (2.32) without the use of the slowly varying envelope approximation. The remaining equations are now

$$\zeta\mathcal{E} = \rho \tag{2.74}$$

$$\dot{\rho} = \Omega\mathcal{E}N \tag{2.75}$$

$$\dot{N} = -\Omega\mathcal{E}\rho \tag{2.76}$$

where the dot signifies differentiation with respect to $t - x/c$ and

$$\zeta = \sigma E_0 / N_0 \omega_0 \wp \tag{2.77}$$

Since Eq. (2.75) and (2.76) have the parametric representation

$$\rho = \sin\phi \tag{2.78a}$$

$$N = \cos\phi \tag{2.78b}$$

with

$$\Omega\mathcal{E} = \dot{\phi} \tag{2.79}$$

Eq. (2.74) is equivalent to the differential equation

$$\Omega \zeta \dot{\phi} = \sin \phi \tag{2.80}$$

The solution is immediate and leads to

$$\mathcal{E} = \frac{1}{\zeta} \operatorname{sech}\left[\Omega(t - x/c)/\zeta \right] \tag{2.81}$$

Also, the population is seen to be inverted by the pulse since Eq. (2.78b) is now equivalent to

$$N = -\tanh\left[\Omega(t - x/c)/\zeta \right] \tag{2.82}$$

Since

$$\Omega \int_{-\infty}^{\infty} dt \mathcal{E} = \pi \tag{2.83}$$

and also because the vector whose components are ρ and $\mathcal{D}$ is rotated through an angle π during the passage of the pulse, the result given in Eq. (2.81) is customarily referred to as a π pulse.

Steady state pulse propagation in an amplifier has also been analyzed without the assumption of a slowly varying envelope and phase[10]. The assumption of propagation at the light velocity of the medium is retained, however, and provides the simplification that is sufficient to permit an exact solution. For pulses that are many optical cycles in duration, there is very little difference between the pulse shape obtained with this more exact treatment and the method described above, as is to be expected. What is of great interest, however, is the prediction of phase variation in the carrier wave. The "chirp" predicted by the theory is proportional to the square of the ratio of optical period to pulse width. Such a result could not be obtained in the slowly varying phase and envelope approximation since it is equivalent to an expansion to only first order in this ratio.

The method has subsequently been extended[11] to include the effect of dispersion in the host medium. In the limit of large dispersion it was found that a monotonic frequency sweep is predicted. Such chirping of ultrashort pulses has been observed experimentally and offers new opportunities for pulse compression[33,34] and population inversion[35]. The chirp that developes in the presence of large dispersion is found to be proportional to the first power of the ratio of optical period to pulse width. This suggests that such a result can be obtained with the framework of the slowly varying phase and envelope approximation and in the following development, the problem will be approached from this point of view.

When no dispersion is present and the pulse is assumed to propagate at the velocity of light in the host medium, Eq. (2.21) reduces to

$$\sigma E = -\frac{\partial P}{\partial w} \tag{2.84}$$

where w = t - x/c. When E and P are written in the form of Eq. (2.22) and (2.27) respectively but without any assumption that $\mathcal{E}$ and φ are slowly varying, Eq. (2.80) yields the pair of relations

$$\zeta \mathcal{E} = \rho - \omega_0^{-1}\left(\rho \frac{\partial \phi}{\partial w} + \frac{\partial \mathcal{Q}}{\partial w}\right) \tag{2.85}$$

$$\frac{\partial \rho}{\partial w} + 2\left(\omega_0 - \frac{\partial \phi}{\partial w}\right) = 0 \tag{2.86}$$

Eqs. (2.37), with $\Delta\omega$ again set equal to zero, are also applicable. Combination of Eqs. (2.85) with (2.37c) and Eq. (2.86) with (2.37b) leads to

$$\zeta \mathcal{E} = \rho \tag{2.87a}$$

$$\omega_0 \mathcal{Q} = -\Omega \mathcal{E} N \tag{2.87b}$$

Eqs. (2.37b) and (2.37c) may be combined to yield

$$\mathcal{Q}^2 \frac{\partial}{\partial w}\left(\frac{\rho}{\mathcal{Q}}\right) = \Omega \mathcal{E} N \mathcal{Q} + \frac{\partial \phi}{\partial w}(1 - N^2) \tag{2.88}$$

in which Eq. (2.39) has been employed. From Eqs. (2.87), (2.37) and (2.39), one obtains

$$\mathcal{Q}^2 = a^2 N^2 (1 - N^2) / \left[1 + a^2 N^2\right] \frac{\partial N}{\partial w} = -\omega_0 \frac{a\left[1 - N^2\right]}{1 + a^2 N^2} \tag{2.89}$$

$$a = \Omega / \zeta \omega_0 \tag{2.90}$$

Finally, Eq. (2.88) yields

$$\frac{\partial \phi}{\partial w} = \omega_0 a^2 \left\{ \frac{N^2}{1 + (aN)^2} - \frac{1 - N^2}{\left[1 + (aN)^2\right]} \right\} \tag{2.91}$$

Unfortunately, one cannot solve Eq. (2.89) explicitly for the explicit time dependence of N. Solution of Eq. (2.89) merely leads to the inexplicit relation equation for N which has the solution

$$a\omega_0 w = N - (a^2 + 1) \tanh^{-1} N \tag{2.92}$$

For a >> 1 this reduces to Eq. (2.82) as is to be expected.

The "instantaneous" frequency is

$$\omega_{inst} = \omega_0 - \frac{d\phi}{dw} \tag{2.93}$$

For $\mathcal{N} = \pm 1$, i.e., at both ends of the pulse

$$\omega_{inst} = \omega_0 \left[1 - a^2/(1+a^2)\right] \tag{2.94}$$

while at the center of the pulse $\mathcal{N} = 0$ and

$$\omega_{inst} = \omega_0(1+a^2) \tag{2.95}$$

The fractional shift in frequency is $2a^2/(1 + a^2)$. For a picosecond pulse at 1μ, $a \sim 10^{-3}$ and the fractional frequency shift is $\sim 10^6$. The absolute frequency shift is 300 mHz.

The calculation outlined above was subsequently[11] extended to include dispersion in the host medium. The dispersion was treated by standard methods of linear wave propagation. It was found that in the limit of large dispersion, the chirp becomes proportional to the first power of the ratio of optical period to pulse duration rather than to the second power as was found in the previous calculation. As is to be expected, then, this limiting case can be treated in the slowly varying envelope and phase approximation and this formulation is developed below.

The wave equation given in Eq. (2.1) is readily modified to include effects arising from the presence of a host medium. Since the effect of the host is merely to provide an additional contribution to the polarization, one need merely introduce an additional polarization term P_{nr} to describe this nonresonant contribution. The total polarization in Eq. (2.1) is then

$$P = P_r + P_{nr} \tag{2.96}$$

where the first term, P_r, is the resonant polarization resulting from the interaction of the wave with the two-level system suspended in the host medium. The frequency dependence of the nonresonant polarization is conveniently described in terms of a susceptibility $\chi(\omega)$ by writing

$$P_{nr}=\int_{-\infty}^{\infty} \frac{d\omega}{2\pi} e^{-i\omega t} \chi(\omega)E(\omega) \tag{2.97}$$

where $E(\omega)$ is the Fourier transform of the electric field vector

$$E(\omega) = \int_{-\infty}^{\infty} dt e^{i\omega t} E(t) \tag{2.98}$$

In the neighborhood of the carrier frequency ω_o, the susceptibility may be approximated by

$$4\pi\chi(\omega) = a_0 + a_2 (\omega_0/\omega)^2 \tag{2.99}$$

where a_o and a_2 are real. Hence χ is real and $\chi(\omega) = \chi(-\omega)$ which assures the reality of P_{nr}. Note that any absorption associated with an imaginary part of χ is ignored. The nonresonant polarization then satisfies

$$4\pi \frac{\partial P_{nr}}{\partial t} = a_0 \frac{\partial E}{\partial t} - a_2 \omega_0^2 \int_{-\infty}^{t} dt' E(t') \tag{2.100}$$

For an electric field polarized in the Y direction and travelling in the positive X direction, it follows from the Maxwell equations that the associated magnetic field vector is

$$\underset{\sim}{H} = -i\hat{k}\int_{-\infty}^{t} dt' \frac{\partial |\underset{\sim}{E}|}{\partial x} \tag{2.101}$$

where $\hat{k}$ is a unit vector in the Z direction.

Energy conservation is expressed by

$$\nabla\cdot(E\times H)+\frac{1}{2c}\frac{\partial}{\partial t}(E^2+H^2) + \frac{4\pi}{c} E \cdot \frac{\partial P_{nr}}{\partial t} = -\frac{4\pi}{c}\left(\sigma E^2 + \frac{\hbar\omega}{2}\frac{\partial n}{\partial t}\right) \tag{2.102}$$

where Eq. (2.21) has been employed. If one assumes that a steady state pulse is maintained by a balance between ohmic losses and resonant gain, then the right-hand side of Eq. (2.102) will vanish. The left-hand side may be simplified and one finally obtains

$$\underset{\sim}{E}\cdot\left(\frac{1}{c}\frac{\partial \underset{\sim}{E}}{\partial t} - \nabla\times\underset{\sim}{H} + \frac{4\pi}{c}\frac{\partial P_{nr}}{\partial t}\right) = 0 \tag{2.103}$$

If it is assumed that $\underset{\sim}{E}$ is of the form of a steady state pulse with envelope velocity v_e and phase velocity v_p then one may write

$$\underset{\sim}{E} = \hat{j} E_0 \mathcal{E}(t-x/v_p)\cos\left[\omega_0(t-x/v_p) + \phi(t-x/v_e)\right] \tag{2.104}$$

From Eq. (2.101)

$$\nabla\times\underset{\sim}{H} = c\hat{j}\left\{-\frac{1}{v_e}\frac{\partial|E|}{\partial x}+\frac{\omega_0 E_0}{v_e}\left(\frac{1}{v_e}-\frac{1}{v_p}\right)\left(\mathcal{E}_c\sin\Psi-\mathcal{E}_s\cos\Psi\right)\right.$$
$$\left.-\omega_0^2\left(\frac{1}{v_e^2}-\frac{1}{v_p^2}\right)\int_{-\infty}^{t}dt'E\right\} \tag{2.105}$$

where

$$\mathcal{E}_c = \mathcal{E}\cos\phi$$
$$\mathcal{E}_s = \mathcal{E}\sin\phi \tag{2.106}$$

and

$$\psi = \omega_0(t-x/v_p) \tag{2.107}$$

When second harmonic terms are neglected,

$$\frac{\partial}{\partial x}\underset{\sim}{E}\cdot\underset{\sim}{E} = -\frac{1}{v_e^2}\frac{\partial}{\partial t}\underset{\sim}{E}\cdot\underset{\sim}{E} \tag{2.108}$$

and Eq. (2.103) takes the form

$$\frac{1}{2c}\left(1+a_0-\frac{c^2}{v_e^2}\right)\frac{\partial E^2}{\partial t}+\omega_0^2 c\left[\left(\frac{1}{v_e}-\frac{1}{v_p}\right)^2-\frac{a_2}{c^2}\right]\underset{\sim}{E}\cdot\int_{-\infty}^{t}dt'E = 0 \tag{2.109}$$

Since the two terms in this equation have a completely different time dependence, one must require that they vanish separately. This yields

$$\frac{c}{v_e} = \sqrt{1+a_0}$$
$$\frac{c}{v_p} = \sqrt{1+a_0}-\sqrt{a_2} \tag{2.110}$$

Turning now to the wave equation for the medium under consideration, one has

$$\frac{\partial^2\underset{\sim}{E}}{\partial x^2}-\frac{1+a_0}{c^2}\frac{\partial^2\underset{\sim}{E}}{\partial t^2}+\frac{a_2\omega_0^2}{c^2}\underset{\sim}{E} = \frac{4\pi}{c^2}\frac{\partial}{\partial t}\left(\sigma\underset{\sim}{E}+\frac{\partial\underset{\sim}{P_r}}{\partial t}\right) \tag{2.111}$$

With the velocities as determined above, the left-hand side of this equation reduces to a perfect time derivative and one finds

$$\omega_0 A E_0(\mathcal{E}_s\cos\psi-\mathcal{E}_c\sin\psi) = \sigma E+\frac{\partial P_r}{\partial t} \tag{2.112}$$

where

$$2\pi A = -\sqrt{a_2(1+a_0)} \tag{2.113}$$

The resonant polarization is of the form

$$P_n = n_0 \wp \left[-\rho \sin(\psi+\phi) + 2\cos(\psi+\phi) \right] \tag{2.114}$$

where ψ is as defined in Eq. (2.107). Employing the slowly varying envelope approximation,

$$\frac{\partial P_n}{\partial t} = -\omega_0 n_0 \wp \left[\rho \sin(\psi+\phi) + 2\cos(\psi+\phi) \right] \tag{2.115}$$

and Eq. (2.112) yields

$$\begin{aligned} (\zeta\gamma\mathcal{E} - 2)\sin\phi - (\zeta\mathcal{E} - \rho)\cos\phi = 0 \\ (\zeta\mathcal{E} - \rho)\sin\phi + (\zeta\gamma\mathcal{E} - 2)\cos\phi = 0 \end{aligned} \tag{2.116}$$

Two expressions may now be formed for $\tan\varphi$. When they are equated, one finds

$$(\zeta\mathcal{E} - \rho)^2 = -(\gamma\zeta\mathcal{E} - 2)^2 \tag{2.117}$$

where ζ is as defined in Eq. (2.77) and

$$\gamma = \omega_0 A/\sigma \tag{2.118}$$

Since all terms are real, each side of Eq. (2.117) must be zero and hence one obtains

$$\begin{aligned} \rho &= \zeta\mathcal{E} \\ 2 &= \gamma\zeta\mathcal{E} \end{aligned} \tag{2.119}$$

From Eqs. (2.119) it is seen that γ represents the ratio of the in-phase component of polarization to the out of phase component. For a dispersionless system $\gamma = 0$ and hence $2 = 0$. The effects of dispersion may therefore be considered to be large when $\gamma \geq 1$.

From Eq. (2.39)

$$\mathcal{E}^2 = \frac{1 - N^2}{\zeta^2 (1+\gamma^2)} \tag{2.120}$$

and from Eq. (2.37a)

$$\frac{\partial N}{\partial t} = -\frac{\Omega}{\zeta(1+\gamma^2)}(1-N^2) \tag{2.121}$$

The population is again seen to be inverted by the pulse for the solution of Eq. (2.121) is

$$N = -\tanh(t/\tau_p) \tag{2.122}$$

where

$$\tau_p = \zeta(1+\gamma^2)/\Omega \tag{2.123}$$

The pulse shape, which follows from Eq. (2.120) is

$$\mathcal{E} = \frac{1}{\Omega\tau_p}\operatorname{sech} t/\tau_p \tag{2.124}$$

From Eqs. (2.88), (2.119) and (2.120),

$$\frac{\partial\phi}{\partial t} = -\frac{\gamma}{\tau_p}N \tag{2.125}$$

and the "instantaneous" frequency is

$$\omega_{inst} = \omega_0 - \frac{\partial\phi}{\partial t} = \omega_0\left(1 + \frac{\gamma}{\omega_0\tau_p}N\right) \tag{2.126}$$

Hence, for γ comparable to unity, the frequency sweep is proportional to the first power of the ratio of optical period to pulse width.

For large γ it may be easily seen that the population inversion takes place by means of adiabatic rapid passage[35]. Introducing a position vector in a three dimensional ρ, $\mathcal{Q}$, N space according to

$$\underset{\sim}{R} = i\rho + j\mathcal{Q} + kN \tag{2.127}$$

and a vector describing the electric field and the detuning of an individual two-level system by

$$\underset{\sim}{E} \simeq i\mathcal{E} + k\frac{\partial\phi}{\partial t} \tag{2.128}$$

Eqs. (2.37), with f set equal to zero, may be written

$$\frac{d\underset{\sim}{R}}{dt} = \underset{\sim}{E} \times \underset{\sim}{R} \tag{2.129}$$

For large γ, the angle between $\underset{\sim}{R}$ and $\underset{\sim}{E}$ is given by

$$\cos\theta = \frac{R \cdot E}{|R||E|} \xrightarrow[\gamma \gg 1]{} 1 \tag{2.130}$$

Hence the position vector remains collinear with E. As the pulse passes a given two-level system and $\frac{\partial\varphi}{\partial t}$ goes from γ/τ_p to $-\gamma/\tau_p$ the $\hat{k}$ component of R must proceed from 1 to -1.

It is to be expected that future research in the field of ultrashort pulses will place increasing emphasis upon the phase characteristics of such pulses.

2.5 Transformation of Equations for a Two-Level System

It has been found useful to observe that Eq. (2.37) are a set of scalar equations which have exactly the same structure as the Frenet-Serret equations of differential geometry[36]. It is known that the solution to such a set of equations is equivalent to the solution of a Riccati equation[36]. To show this, one first recalls from Eq. (2.39) that an integral of Eqs. (2.37) is

$$N^2 + \rho^2 + \mathcal{Z}^2 = 1 \tag{2.131}$$

Two new functions may now be introduced by writing

$$\frac{N + i\rho}{1 - \mathcal{Z}} = \frac{1 + \mathcal{Z}}{N + i\rho} = \phi \tag{2.132a}$$

$$\frac{N + i\rho}{1 - \mathcal{Z}} \quad \frac{1 + \mathcal{Z}}{N + i\rho} = -\frac{1}{\psi} = \phi^* \tag{2.132b}$$

Equations (2.132) may be inverted to yield

$$N = \frac{1 - \phi\psi}{\phi - \psi} = \frac{2\mathrm{Re}\,\phi}{|\phi|^2 + 1} \tag{2.133a}$$

$$\rho = i\frac{1 + \phi\psi}{\phi - \psi} = \frac{2\mathrm{Im}\,\phi}{|\phi|^2 + 1} \tag{2.133b}$$

$$\mathcal{Z} = \frac{\phi + \psi}{\phi - \psi} = \frac{|\phi|^2 - 1}{|\phi|^2 + 1} \tag{2.133c}$$

Equations governing the time dependence of φ and Ψ are readily deduced by inserting Eqs. (2.133) into Eqs. (2.37). It is found that φ satisfies the Riccati equation

$$\frac{\partial\phi}{\partial\tau} = i\mathcal{E}\phi + \frac{i}{2}\left(f + \frac{\partial\phi}{\partial\tau}\right)(\phi^2 - 1) \tag{2.134}$$

and that Ψ satisfies the same equation.

One may now employ the usual transformation to convert this Riccati equation to a second-order linear equation. If the phase term is neglected the problem is reduced to that of solving the equation

$$\ddot{w} + \frac{1}{4}(f^2+\mathcal{E}^2+2i\dot{\mathcal{E}})w = 0 \tag{2.135}$$

where the dot signifies differentiation with respect to τ. The new dependent variable w is related to φ through the transformations $w = u \exp(-\frac{1}{2}\int_{-\infty}^{\tau} d\tau' \mathcal{E})$ and $\varphi = (2i/f)\, d(\ln u)/d\tau$. From well-known properties of such second-order differential equations, it follows that in general it is impossible to write φ or ψ explicitly in terms of quadratures of $\mathcal{E}$.

Equation (2.135) is particularly instructive since it puts power broadening in evidence and provides an immediate contact with results obtainable from the well-known vector model for describing the response of a two-level system to an external field[37]. We now digress briefly to consider this approach. For a constant envelope $\mathcal{E} = \mathcal{E}_0$, Eq. (2.135) is readily solved in terms of the functions

$$w = \exp\left(\pm \frac{i\tau}{2}\sqrt{f^2+\mathcal{E}_0^2}\right) \tag{2.136}$$

If the population is initially in the lower level and the pulse is turned on at $\tau = 0$, then the proper initial condition for w is readily found to be $\dot{w}(0)/w(0) = i(f - \mathcal{E}_0)/(f^2+\mathcal{E}_0^2)^{\frac{1}{2}}$ and one obtains

$$N = -1+2\cos^2\alpha \sin^2(f\tau/2) \tag{2.137}$$

where

$$\alpha = \tan^{-1}(f/\mathcal{E}_0) \tag{2.138}$$

This constant field result agrees with that obtained from the geometric model. It should be emphasized that although the vector model itself is applied for arbitrarily short pulses, Eq. (2.137) is only applicable if the pulse envelope varies slowly on the time scale Ω^{-1}. For the ultrashort optical pulses under consideration here this condition is violated. An example of a time dependent pulse profile for which Eq. (2.134) is still soluble in closed form is the steady state solution for self-induced transparency, namely

$$\mathcal{E} = 2\,\mathrm{sech}\,\tau \tag{2.139}$$

The solution of Eq. (2.134) when $\mathcal{E}$ has the form given in Eq. (2. 39) and which takes on the velue -1 as $\tau \to -\infty$ may be shown to be

$$\phi = -\frac{f - i\exp(i\sigma/2)}{f - i\exp(-i\sigma/2)} \tag{2.140}$$

where

$$\sigma = \int_{-\infty}^{\tau} d\tau' \mathcal{E} = 4\tan^{-1} e^{\tau} \tag{2.141}$$

Eqs. (2.133) then yield expressions for the response of the system which agree with Eqs. (2.56)

2.6 Specialization to a Soluble Model

Although it is possible to obtain a fairly complete analytical description of steady state pulse propagation in an inhomogeneously broadened medium, other very interesting features of pulse propagation have not thus far been found to yield to any simple analytical treatment. It has been noticed, however, that if inhomogeneous broadening is neglected, the analysis may be pursued much further. Fortunately, it has been found that results predicted on the basis of such a model are preserved to a considerable extent when inhomogeneous broadening is included and the more complete set of equations is investigated by numerical computations[14,53]. Furthermore, the model is not without physical interest in its own right since, as mentioned above, it may be used as an approximate description of optical pulse propagation under conditions of extreme saturation broadening.

The simplification introduced by the assumption of vanishing bandwidth is immediately evident when one recognizes that Eq. (2.134) becomes linear for f = 0. The solution is then

$$\phi = \pm e^{i\sigma} \tag{2.142}$$

where σ is given by Eq. (2.141) or equivalently,

$$\mathcal{E} = \partial\sigma/\partial\tau \tag{2.143}$$

The choice of sign in Eq. (2.142) is again related to the two relevant initial conditions $N(\xi_1 - \infty) = \pm 1$. From Eq. (2.133) there follows

$$N = \pm\cos\sigma \tag{2.144a}$$

$$P = \pm\sin\sigma \tag{2.144b}$$

$$\mathcal{D} = 0 \tag{2.144c}$$

and Eq. (2.35) takes the form

$$\frac{\partial^2\sigma}{\partial\xi\partial\tau} = \pm \sin\sigma \tag{2.145}$$

This nonlinear partial differential equation is the fundamental equation of the model. Fortunately, it has already been studied extensively since it arose long ago in the theory of pseudospherical surfaces, i.e., surfaces of constant negative curvature[38]. More recently, it has arisen in the analysis of many physical problems[39-45].

The general solution of Eq. (2.145) is unknown. However, a variety of particular solutions corresponding to specific pseudospherical surfaces, have been discovered. One rather large class of solutions is expressible in terms of the variables

$$\begin{aligned} u &= a\tau + \xi/a \\ v &= a\tau - \xi/a \end{aligned} \tag{2.146}$$

where a is an arbitrary constant. In terms of these independent variables, Eq. (2.145) takes the form

$$\frac{\partial^2\sigma}{\partial u^2} - \frac{\partial^2\sigma}{\partial v^2} = \pm \sin\sigma \tag{2.147}$$

The above-mentioned solutions are of the form

$$\sigma(u,v) = 4\tan^{-1}\left[F(u)/G(v)\right] \tag{2.148}$$

Substitution of this assumed form into Eq. (2.147) leads to the requirement that F(u) and G(v) satisfy the equations

$$\begin{aligned} F'^2 &= -kF^4 + m^2F^2 + n \\ G'^2 &= kG^4 + (m^2-1)G^2 - n \end{aligned} \tag{2.149}$$

where k, m and n are arbitrary constants. The various psuedospherical surfaces corresponding to such solutions are known as the surfaces of Enneper and have been exhaustively catalogued by R. Steuerwald[46].

Among such solutions are to be found analytical expressions that describe not only the steady state 2π pulse associated with self-induced transparency but also solutions that correspond to a 4π pulse as well as pulse envelopes for which the total pulse area is zero, so-called zero π pulses. As noted previously, the negative part of the envelope in such a pulse is merely the way in which the present model accommodates a phase change of π that could take place in a more complete theory in which the phase term φ of Eq. (2.22) were retained[8,47]. The 4π solution exhibits the pulse breakup phenomenon that has been observed both experimentally[8] and in more complete numerical computations[8,14].

Another, and more general, method of obtaining solutions is to use the fact that Eq. (2.145) is an example of an equation which admits of a Baecklund transformation[48,49]. This transformation theory may be interpreted geometrically as the transformation of a surface which represents a solution of a given partial differential equation into another surface which is the solution to the same or, in some cases, another known equation.

For Eq. (2.145) the transformation equations are[38, 39]

$$\frac{1}{2}\frac{\partial}{\partial\xi}(\sigma_1+\sigma_0)=\pm\frac{1}{a}\sin\left(\frac{\sigma_1-\sigma_0}{2}\right) \tag{2.150a}$$

$$\frac{1}{2}\frac{\partial}{\partial\tau}(\sigma_1-\sigma_0)=a\sin\left(\frac{\sigma_1+\sigma_0}{2}\right) \tag{2.150b}$$

One may easily show that both σ_0 and σ_1 satisfy Eq. (2.145). Hence, from a given solution σ_0 one may obtain a new solution σ_1 which contains not only the constant $\underline{a}$ but also an arbitrary constant of integration. This transformation may be used repeatedly to generate a solution σ_2 from σ_1 etc. For extensive calculations of this sort, it has been found convenient to use a symbolic representation of Eqs. (2.150) in which a transformation from a solution σ_i to a solution σ_j with a constant a_k is represented as shown in Fig. 2. As a first usage of such multiple transformations, one may show quite readily that the four solutions that are related by the transformation depicted in Fig. 3 will satisfy

$$\tan\left(\frac{\sigma_3-\sigma_0}{4}\right)=\frac{a_1+a_2}{a_1-a_2}\tan\left(\frac{\sigma_1-\sigma_2}{4}\right) \tag{2.151}$$

which, quite remarkably, does not involve any quadratures. A simple algebraic manipulation of the eight equations implied by Fig. 3 leads immediately to Eq. (2.151). It will be shown subsequently that this result may be used to construct a 4π pulse as well as a number of different types of zero π pulses.

If $a_1 = a_2$ and the integration constants in σ_1 and σ_2 are different, this relation merely yields

$$\sigma_3=\sigma_0\pm\pi \tag{2.152}$$

When the integration constants are the same, the resulting indeterminate form may be evaluated from the usual Taylor expansion and one finds

$$\tan\left(\frac{\sigma_3-\sigma_0}{4}\right)=\frac{a_1}{2}\left(\frac{\partial\sigma_1}{\partial a_1}+\frac{\partial\sigma_1}{\partial\gamma_1}\frac{\partial\gamma_1}{\partial a_1}\right) \tag{2.153}$$

where γ_1 is the constant of integration arising from the solution of Eqs. (2.150).

It will be shown that the compounding of transformations shown in Fig. 4 yields a 6π pulse. An obvious generalization to obtain a $2n\pi$ pulse and undoubtedly more complicated zero π pulse suggests itself immediately but the subject has not been pursued beyond this point.

All of the above solutions represent modes of propagation that are realizable in an attenuator. It has been found that a solution which applies to a lossless amplifier, the π pulse, is contained within the family of solutions that results from the specification that σ be of the form $\sigma(\xi\tau)$. Such solutions have also been considered within the context of differential geometry[50] and have been used recently in the attenuator case to describe coherent resonance fluorescence[51].

2.6.1 Specific Pulse Profiles

We now turn to a more detailed consideration of the various solutions of Eq. (2.145) that were mentioned above. The results are, of course, meagre in comparison with the complete analytical description of the evolution of arbitrary initial pulse shapes that can be obtained when dealing with linear initial value problems. However, the particular solutions that have been found do exhibit many of the important and interesting features of optical pulse propagation as it has been observed both experimentally and as output from numerical computations.

2.6.1.1 2π Pulse

As has been indicated above, a large number of pulse profiles may be obtained for propagation in an attenuator. Perhaps the most widely known solution of this type is the one related to self-induced transparency. It may be obtained in a number of ways, the simplest being that of assuming a steady state solution of the form $\sigma(t - x/v)$. Such steady state solutions will be discussed subsequently. The solution may also be obtained by noting that $\sigma = 0$ is a solution of Eq. (2.145). This solution may then be used as σ_0 in the Baecklund transformation given by Eqs. (2.150). Choosing the lower sign in the second Eqs. (2.150), as is required for propagation in an attenuator, the two resulting first-order differential equations have the solution

$$\sigma_1 = 4\tan^{-1}e^{\nu} \tag{2.154}$$

where ν is as defined in Eq. (2.146). One constant of integration has been set equal to zero since it merely serves to translate the initial location of the solution along the v axis. The corresponding electric field follows from Eq. (2.143) and one finds

$$\mathcal{E} = 2\alpha\,\mathrm{sech}\,\nu = 2\alpha\,\mathrm{sech}\left[\alpha\Omega(t - x/v)\right] \tag{2.155}$$

where

$$\frac{1}{v} = \frac{1}{c}\left(1 + \frac{\epsilon}{\alpha^2}\right) \tag{2.156}$$

From Eq. (2.155) one sees that $(a\Omega)^{-1}$ determines the width of the pulse envelope. Therefore, setting $a\Omega = \tau_p^{-1}$ where τ_p is the pulse width, the expression for the electric field envelope becomes

$$\frac{E_0 \wp}{\hbar} \mathcal{E} = \frac{2}{\tau_p} \operatorname{sech} (t - x/v)\tau_p \tag{2.157}$$

where

$$\frac{1}{V} = \frac{1}{c} + \alpha' \tau_p^2 = \frac{1}{c}(1 + U_M / U_W) \tag{2.158}$$

α' is as defined in Eq. (2.30) and U_w and U_m are the energy densities of wave and medium respectively. The last form for the velocity given in Eq. (2.158) is particularly instructive and has been derived[52] on simple physical ground by merely equating the average energy of both wave field and medium, $V\tau_p(U_w + U_m)$, to $c\tau_p U_w$ the amount of energy that flows through the volume $V\tau_p$ at the light velocity c. Eqs. (2.157) and (2.158) agree with Eqs. (2.54) and (2.44) in the appropriate limit, namely $g(\Delta\omega) \rightarrow \delta(\Delta\omega)$.

2.6.1.2 4π Pulse

It has been observed both experimentally[8] and from machine computations[8,14] that the combination of field strength and magnitude of dipole moment sufficient to induce two inversions in the population of the two-level system, a so-called 4π pulse, does not propagate as a single pulse but rather separates into two separate 2π pulses. Such pulse separations are also exhibited by the analytical solutions[17,19]. The 4π pulse is obtainable as the function σ_3 in Eq. (2.151) when one chooses $\sigma_0 = 0$. If one chooses the lower sign in Eq. (2.145), as is appropriate for the attenuator, then

$$\sigma_i = 4 \tan^{-1}\left[\exp(\nu_i)\right], \; i = 1,2 \tag{2.159a}$$

where

$$\nu_i = a_i \tau - \xi/a_i \tag{2.159b}$$

The resulting expression for σ_3 may be put in the form

$$\sigma_3 = 4 \tan^{-1}\left[\left(\frac{a_1 + a_2}{a_1 - a_2}\right) \frac{\sinh \frac{1}{2}(\nu_1 - \nu_2)}{\cosh \frac{1}{2}(\nu_1 + \nu_2)}\right] \tag{2.160}$$

For $a_1 > 0$, $a_2 < 0$ the function σ_3 in Eq. (2.160) varies from -2π to 2π as τ proceeds from $-\infty$ to ∞. Since

$$\theta = \frac{E_0}{\hbar}\int_{-\infty}^{\infty} dt\, \mathcal{E} = \sigma(\infty) - \quad (-\infty) \tag{2.161}$$

one may expect that the associated electric field will correspond to a 4π pulse.

Setting $a_1\Omega = \tau_1^{-1}$, $-a_2\Omega = \tau_2^{-1}$ using Eq. (2.143), the electric field is found to be

$$\frac{E_0 \wp}{\hbar}\mathcal{E} = A\,\frac{(2/\tau_1)\,\mathrm{sech}\, x + (2/\tau_2)\,\mathrm{sech}\, Y}{1 - B(\tanh x\, \tanh Y - \mathrm{sech}\, x\, \mathrm{sech}\, Y)} \tag{2.162}$$

where

$$\begin{aligned} A &= (\tau_2^2 - \tau_1^2)/(\tau_2^2 + \tau_1^2) \\ B &= 2\tau_1\tau_2/(\tau_2^2 + \tau_1^2) \\ x &= (t - x/v_1)/\tau_1 \\ Y &= (t - x/v_2)/\tau_2 \end{aligned} \tag{2.163}$$

and the velocities V_1 and V_2 are

$$\begin{aligned} \frac{1}{V_1} &= \frac{1}{C}(1 + \Omega^2\tau_1^2\epsilon) = \frac{1}{C} + \alpha'\tau_1^2 \\ \frac{1}{V_2} &= \frac{1}{C}(1 + \Omega^2\tau_2^2\epsilon) = \frac{1}{C} + \alpha'\tau_2^2 \end{aligned} \tag{2.164}$$

A graph of Eq. (2.162) is shown in Fig. 5. As the pulses become completely separated Eq. (2.162) reduces to

$$\frac{E_0 \wp}{\hbar}\mathcal{E} = \frac{2}{\tau_1}\,\mathrm{sech}(X \pm \beta) + \frac{2}{\tau_2}\,\mathrm{sech}(Y \pm \beta) \tag{2.165}$$

where the upper sign is to be used for $\tau_1 < \tau_2$ and the lower sign for $\tau_1 > \tau_2$ and where

$$\beta = \tanh^{-1} B \tag{2.166}$$

In order to obtain a pulse envelope that begins at $\xi = 0$ with only one peak as a function to time, one must impose the requirement $\partial^2\mathcal{E}/\partial\tau^2 < 0$ at $\xi = \tau = 0$. This condition, along with the requirement $\mathcal{E} > 0$ leads to

$$(1 - r)(1 + r^2 - 3r) > 0\,, \quad r = \tau_1/\tau_2 \tag{2.167}$$

which is equivalent to

$$\tfrac{1}{2}(3 - \sqrt{5}) < \tau_1/\tau_2 < \tfrac{1}{2}(3 + \sqrt{5}) \tag{2.168a}$$

Figure 5 could, of course, be continued back to negative values of ξ to provide an example of the envelope distortion that takes place when an ultrashort pulse overtakes a slower pulse and passes through it.

In addition to the above results for specific pulse profiles, certain conclusions relating to 4π pulses of arbitrary initial shape may also be given. These results are obtained by employing a technique previously applied to the Korteweg de Vries equation(63) which has solutions with many of the same pulse like properties as Eq. (2.145). It will be discussed further in Section 2.6.3.

One begins by noting that Eq. (2.145) possesses the two conservation laws

$$\frac{\partial}{\partial\tau}\ \frac{1}{2}\left(\frac{\partial\sigma}{\partial\xi}\right)^2 + \frac{\partial}{\partial\xi}(1-\cos\sigma) = 0$$

$$\frac{\partial}{\partial\tau}(1-\cos\sigma) + \frac{\partial}{\partial\xi}\left[\frac{1}{2}\left(\frac{\partial\sigma}{\partial\tau}\right)^2\right] = 0 \qquad (2.168b)$$

which follows from Eq. (2.145) after multiplication by $\partial\sigma/\partial\xi$ and $\partial\sigma/\partial\tau$ respectively. Integrating over all ξ and over τ from $\tau = 0$ up to an arbitrary final time one finds

$$\int_{-\infty}^{\infty} d\xi\, \frac{1}{2}\left(\frac{\partial\sigma}{\partial\xi}\right)^2 = 4C_1$$

$$\int_{-\infty}^{\infty} d\xi\,(1-\cos\sigma) = 4C_2 \qquad (2.168c)$$

where c_1 and c_2 are positive constants that are obtained by evaluating Eq. (2.168c) for a given initial form of σ. After the pulses have completely separated one may write

$$\sigma = \sum_{i=1,2} 4\tan^{-1}\left\{\exp\left[a_i(\tau-\tau_i) - \xi/a_i\right]\right\} \qquad (2.168d)$$

Eqs. (2.168c) then yields the paid of algebraic relations

$$a_1^{-1} + a_2^{-1} = C_1$$

$$a_1 + a_2 = C_2 \qquad (2.168e)$$

Introducing the positive quantities $\alpha_1 = a_1$, $\alpha_2 = -a_2$, one finds that the final amplitudes are given by

$$a_{1,2} = \frac{1}{2}\left(C_2 \pm \sqrt{C_2^2 - 4C_2/C_1}\right) \qquad (2.168f)$$

Also, one notes that, since the α_i are real

$$C_1 C_2 > 4 \tag{2.168g}$$

It has been shown[78] that Korteweg de Vries equation satisfies an infinite number of conservation laws. For that equation, the above technique may be extended to treat pulses which evolve into any number of isolated pulses. Thus far, no additional conservation laws have been found for Eq. (2.145) although, as will be shown below, it is known to have solutions that break up into more than two pulses.

2.6.1.3 Zero π Pulses

As mentioned previously, Eq. (2.145) also admits of solutions for which the associated electric field envelope becomes negative. Such solutions cannot be discarded on any physical basis since a negative field envelope merely corresponds to a phase change of π in the carrier wave.

Three different types of zero π pulses have been constructed from the solutions mentioned above. The simplest type is obtained by merely choosing $a_2 > 0$ in the previous solution for the 4π pulse. The electric field envelope in dimensionless form is

$$\mathcal{E} = 2A \frac{a_1 \operatorname{sech} \nu_1 - a_2 \operatorname{sech} \nu_2}{1 - B(\tanh \nu_1 \tanh \nu_2 + \operatorname{sech} \nu_1 \operatorname{sech} \nu_2)} \tag{2.169}$$

where

$$A = (a_1^2 - a_2^2)/(a_1^2 + a_2^2) \tag{2.170}$$

$$B = 2a_1 a_2/(a_1^2 + a_2^2) \tag{2.171}$$

An example of this result is shown in Fig. 6.

In the limit $a_1 = a_2$, Eq. (2.151) becomes indeterminate. In this case, with ν_1 again set equal to zero, one may use Eq. (2.153) and obtain as the second form for a zero π pulse,

$$\sigma = 4 \tan^{-1}(u \operatorname{sech} \nu) \tag{2.172}$$

This yields the field envelope

$$\mathcal{E} = 4a \operatorname{sech} \nu \left(\frac{1 - u \tanh \nu}{1 + u^2 \operatorname{sech}^2 \nu} \right) \tag{2.173}$$

A graph of this result is shown in Fig. 7.

The third, and by far the most interesting type of zero π pulse is obtained by allowing the parameters a_1 and a_2 in Eq. (2.151) to become complex and requiring

$$a_1 = a_2^* = a = \alpha + i\beta \tag{2.174}$$

One then finds

$$\sigma = 4 \tan^{-1} \left\{ \frac{\alpha}{\beta} \frac{\sin q}{\cosh p} \right\} \tag{2.175}$$

where

$$p = \alpha(\tau - \xi/|a|^2) \tag{2.176}$$

and

$$q = \beta(\tau + \xi/|a|^2) \tag{2.177}$$

The electric field envelope is

$$\mathcal{E} = 4\alpha \operatorname{sech} p \left[\frac{\cos q - (\alpha/\beta) \sin q \tanh p}{1 + (\alpha/\beta)^2 \sin^2 q \operatorname{sech}^2 p} \right] \tag{2.178}$$

A graph of this result is shown in Fig. 8.

Unlike the two previous types of zero π pulses, the envelope given in Eq. (2.174) tends to remain as a single localized disturbance. It provides an alternate and more flexible form of self-induced transparency. It has been found[53] from numerical computations that this pulse shape is remarkably insensitive to variations in inhomogeneous broadening.

2.6.1.4 6π Pulse

As mentioned above, the 6π pulse is obtained from the sequence of transformations depicted in Fig. 4. From this diagram, the corresponding analytical expressions are easily seen to be

$$\sigma_f = \sigma_2 + 4\tan^{-1}\left(K_{13}\tan\frac{\sigma_a-\sigma_b}{4}\right) \tag{2.179}$$

where

$$\sigma_2 = 4\tan^{-1}e^{\nu_2}$$

$$\sigma_a = 4\tan^{-1}\left[K_{12}\frac{\sinh\frac{1}{2}(\nu_1-\nu_2)}{\cosh\frac{1}{2}(\nu_1+\nu_2)}\right]$$

$$\sigma_b = 4\tan^{-1}\left[K_{23}\frac{\sinh\frac{1}{2}(\nu_2-\nu_3)}{\cosh\frac{1}{2}(\nu_2+\nu_3)}\right] \tag{2.180}$$

and

$$K_{ij} = (a_i+a_j)/(a_i-a_j) \tag{2.181}$$

One may immediately impose a number of constraints upon the triad of constants a_1, a_2, a_3. In the first place, for the envelope function corresponding to σ_2 to be positive, one must require $a_2 > 0$. One then proceeds to make σ_a a 4π pulse which requires $a_1 < 0$. Also, σ_b is made a zero π pulse which requires $0 < a_3 < a_2$. The three constants a_i may be related to the widths of the three pulses when complete separation has taken place by setting $-a_1\Omega = \tau_1$, $a_2\Omega = \tau_2$, $a_3\Omega = \tau_3$.

As with the 4π pulse, one must impose additional restrictions in order to assume a pulse shape that consists of a single peak at $\xi = 0$. The inequality is much more complicated in this case than in Eqs. (2.167) and has not been analyzed in detail. By a trial-and-error method the case shown in Fig. 9 has been obtained.

2.6.1.5 π Pulse

To describe a π pulse, one must turn to the other completely different class of solutions of Eq. (2.145) that were mentioned above. These are solutions in which the independent variables occur solely in the product form $\xi\tau$. When one sets $Z = \xi\tau$ in Eq. (2.145) it reduces to the ordinary differential equation[54]

$$Z\sigma'' + \sigma' - \sin\sigma = 0 \tag{2.182}$$

where the prime indicates differentiation with respect to Z.

A new dependent variable, w, related to σ by $w = \exp(i\sigma)$, may be shown to satisfy a special case of the equation that defines the third Painleve transcendent[70]. Since the properties of such functions are essentially unknown and tables appear to be unavailable, it seems preferable to resort to a direct numerical integration of

Eq. (2.182). The result of such a numerical solution is shown in Fig. 10 which also includes the result for $\sigma' = (\mathcal{E}/\xi)$ as well as a phase plane diagram of the solution. The example shown in Fig. 10 satisfies the condition $\sigma(0) = 0.1$ as well as $\sigma(0) = \sin\sigma(0)$ which is required for continuity at the origin.

Scaling laws for π pulse propagation may be inferred from these results. Since the abscissa for the pulse envelope is $\xi\tau$, the actual pulse envelope narrows linearly with increasing distance of propagation. Also, since $\mathcal{E} = \xi\sigma'$, the amplitude of the envelope increases linearly with distance. This spatial evolution of the pulse shape is shown explicitely in Fig. 11. Similar results have been obtained from direct numerical analysis[71,16] of the partial differential equations governing optical pulse propagation in a resonant medium. A comparison of Fig. 11 with results presented in Ref. 16 shows that until the signal becomes so large that the linear loss is dominant, neglect of the loss term introduces no significant change in propagation in an amplifier.

The fact that the self-consistent interaction of field and resonant matter should give rise to ringing is not unexpected in view of the known[82] response of an inverted population to a specified spatial mode of the electric field. The ringing may also be inferred from a theorem concerning solutions of Eq. (2.145). It may be shown[79] that there is no function which satisfies Eq. (2.145) and at the same time remains within the interval $0 < \sigma < \pi$

2.6.2 Steady State Solutions

An example of a steady state solution has already been given with the discussion of the 2π pulse. This solution is actually a limiting form of a more general oscillatory solution which is now considered. Similar results for propagation in an inhomogeneously broadened medium have also been reported[27,28,29].

Steady state solutions will be functions of one of the variables defined in Eq. (2.146). Choosing the variable to be v, one readily shows that the conservation laws given by Eqs. (2.38) and (2.39) take the form

$$-\frac{1}{2a^2}\mathcal{E}^2 + N = N_1 \tag{2.183a}$$

$$\rho^2 + N^2 = 1 \tag{2.183b}$$

where N_1 is a constant of integration and the constant a is again $(\Omega\tau_p)^{-1}$. Allowing for a steady state solution in which $\mathcal{E}$ is non-zero when the entire population is in the ground state, one sees from Eq. (2.183b) that the constant N may be less than -1.

From Eq. (2.37a) and (2.183) one readily obtains

$$\left(\frac{dN}{dv}\right)^2 = 2(N-N_1)(1-N^2) \tag{2.184}$$

which shows that N may be expressed in terms of elliptic function.

If $-1<N_1<1$, a solution for which the population varies between N_1 and 1 is given by

$$\int_N^1 \frac{dN}{\sqrt{(N-N_1)(1-N^2)}} = \sqrt{2}\int_v^{v_0} dv \tag{2.185}$$

which leads to[55]

$$N = 1-2k^2 sn^2[(v-v_0),k] \tag{2.186}$$

where $k^2 = \frac{1}{2}(1-N_1)$. From Eq. (2.183a),

$$\mathcal{E} = 2ak\,cn[(v-v_0),k] \tag{2.187}$$

A solution for which $-1<N<N_1$ could also be given, but it requires that a be imaginary. This implies envelope function propagation faster than the light velocity. In the limit $k \to 1$ this solution goes over to one which represents 2π pulse propagation in an amplifier which is unstable.

For $N_1 < -1$ it is seen that $k^2 > 1$. Using the relations[56]

$$\begin{aligned} sn(v,k) &= k^{-1} sn(kv, k^{-1}) \\ cn(v,k) &= dn(kv, k^{-1}) \end{aligned} \tag{2.188}$$

one finds that the population difference and field envelope may be written

$$N = 1-2sn^2[k^{-1}(v-v_0),k] \tag{2.189a}$$

$$\mathcal{E} = 2ak^{-1} dn[k^{-1}(v-v_0),k] \tag{2.189b}$$

where now $k^2 = 2/(1-N_1)$. These latter forms may, of course, be obtained by direct integration of Eq. (2.184). In the limit $N_1 \to -1$ both solutions reduce to that for the 2π pulse in an attenuator.

It has been conjectured[57] that these steady state solutions may be realized in self-pulsing situations.

2.6.3 Relation to the Korteweg-deVries Equation

It has been noted[58] that the hyperbolic secant solution of Eq. (2.145) and the decomposition of pulses into a sequence of such "solitary waves" is very similar to results obtained in recent investigations of the Korteweg-deVries equations[58-63]. In fact, one may show that, for steady state solutions, the square of the envelope function $\mathcal{E}$ satisfies the corresponding steady state Korteweg-deVries equation. This may be seen quite readily by writing $\sigma(\xi,\tau)$ in the form $\sigma(v)$ where $v = \tau - \xi$. A first integral of the resulting equation is readily obtained. The integral satisfying $\mathcal{E}(-\infty) = \sigma(-\infty) = 0$ is

$$\cos\sigma = 1 - \frac{1}{2}\mathcal{E}^2 \tag{2.190}$$

When this result is solved for σ and differentiated, one obtains

$$\frac{1}{4}\left(\frac{du}{dv}\right)^2 = u^2 - \frac{1}{4}u^3 \tag{2.191}$$

where $u \quad \mathcal{E}^2$. Two derivatives of this equation yields

$$4\frac{du}{dv} - 3u\frac{du}{dv} - \frac{d^3u}{dv^3} = 0 \tag{2.192}$$

The substitutions

$$u = \frac{4}{3k}f(x)$$

$$v = \frac{1}{2}k^{1/2}x \tag{2.193}$$

transforms Eq. (2.192) to

$$-kf' + ff' + f''' = 0 \tag{2.194}$$

where the prime indicates differentiation with respect to x. Eq. (2.194) is the steady state form of the Korteweg-deVries equation. The solution that vanishes for large values of x may be written in the form[62]

$$f = 3k\,\mathrm{sech}^2\left(\frac{1}{2}k^{1/2}x\right) \tag{2.195}$$

which is readily shown to be equivalent to the result given in Eq. (2.157). Periodic solutions in terms of elliptic functions have also been given . They are related to the result given in Eq. (2.187) and are referred to as cnoidal waves.

Although the multisoliton and oscillatory[77] solutions of the Korteweg-deVries equation are similar to results obtained above for $2n\pi$ and π pulses respectively, and the criterion given in Eq. (2.167 is similar to one appearing in the breakup of two soliton solutions of the Korteweg-deVries equation[80], to the authors knowledge no quantitative relation between Eq. (2.145) and the time dependent Korteweg-deVries equation has been discovered.

2.6.4 Stability Considerations

When inhomogeneous broadening is present, the stability of the area under the electric field envelope $\mathcal{E}(x,t)$ may be inferred[7,8] from the solution of Eq. (2.68). However, an integration over the frequency of the detuning associated with inhomogeneous broadening is a crucial step in the derivation of this result. In the model being considered here, inhomogeneous broadening is neglected and so one must rely upon other considerations to infer area stability. This is accomplished quite readily by noting that Eq. (2.145) may be written

$$\frac{\partial \mathcal{E}}{\partial x} = \frac{\hbar \alpha'}{\wp} \sin\sigma \tag{2.196}$$

where

$$\sigma(x,t) = \sigma(x,-\infty) + \int_{-\infty}^{t} dt' \mathcal{E}(x,t') \tag{2.197}$$

For a system initially in the lower level, one may take $\sigma(x,-\infty) = -\pi$ for then $N(x,-\infty) = \cos\sigma(x,-\infty) = -1$. For a system initially in the upper level one may assume $\sigma(x,-\infty) = 0$.

For the hyperbolic secant pulse envelope given in Eq. (2.155) $\theta = (\wp/\hbar)\int_{-\infty}^{\infty} dt\,\mathcal{E} = 2\pi$ so that near the trailing edge of this pulse, Eq. (2.196) goes to

$$\frac{\partial \mathcal{E}}{\partial x} = \frac{\hbar}{\wp} \alpha' \sin\left[\begin{pmatrix}-\pi\\0\end{pmatrix} + 2\pi\right] \tag{2.198}$$

where the upper choice is made for the attenuator and the lower choice for the amplifier. Now if there is a perturbation in $\mathcal{E}$ such that the total area θ is greater than 2π, then in an attenuator $\partial\mathcal{E}/\partial x \sim \sin(\pi + \epsilon) < 0$. The field at the trailing edge therefore tends to decrease to recover a total area of 2π. On the other hand, if the perturbation is such that θ is less than 2π, then $\partial\mathcal{E}/\partial x > 0$ and the field at the trailing edge increases. The total area of such a pulse therefore tends to remain at 2π. In the amplifier, the inequalities are reversed and the hyperbolic secant no longer represents a stable pulse envelope. These results are in agreement with those previously obtained[7,8] for the case in which inhomogeneous broadening is included. The above considerations predict only the area stability and leave open the question of perturbations in which the total area remains unchanged. We now take up this topic and show, by exhibiting a Liapunov functional with vanishing derivative, that in the attenuator the pulse shape is stable but not asymptotically stable, i.e., perturbations remain finite.

An appropriate Liapunov functional[64] F(u) is given by

$$F(u) \equiv \int_{-\infty}^{\infty} dv \left[\left(\frac{\partial \sigma}{\partial u} \right)^2 + \left(\frac{\partial \sigma}{\partial v} \right)^2 + 2 (1 - \cos \sigma) \right] \tag{2.199}$$

which is proportional to the total energy residing in field and medium. Differentiation with respect to u and a subsequent partial integration yields

$$\frac{dF}{du} = \int_{-\infty}^{\infty} dv \, \frac{\partial \sigma}{\partial u} \left(\frac{\partial^2 \sigma}{\partial u^2} - \frac{\partial^2 \sigma}{\partial v^2} + \sin \sigma \right) + \frac{\partial \sigma}{\partial u} \, \frac{\partial \sigma}{\partial v} \Bigg|_{v=-\infty}^{v=\infty} \tag{2.200}$$

which vanishes by virtue of Eq. (2.147)(in which the lower sign has been chosen as is appropriate for an attenuator) and the boundary condition that σ represent a pulse and hence $\partial\sigma/\partial u$ and $\partial\sigma/\partial v$ must vanish at $v = \pm\infty$.

Since dF/du is merely zero rather than negative definite, it is not unexpected that a first-order perturbation analysis of Eq. (2.147) will contain a zero eigenvalue. This is readily seen to be the case. Setting $\sigma = \sigma^{(0)}(v) + \sigma^{(1)}(u,v)$, one finds that $\sigma^{(1)}$ satisfies

$$\frac{\partial^2 \sigma^{(1)}}{\partial u^2} - \frac{\partial^2 \sigma^{(1)}}{\partial v^2} - (1 - 2 \operatorname{sech}^2 v) \sigma^{(1)} = 0 \tag{2.201}$$

Expressing $\sigma^{(1)}$ in the form

$$\sigma^{(1)}(u,v) = V(v) e^{su} \tag{2.202}$$

V(v) is found to satisfy the Schroedinger equation

$$V'' + (\lambda - 2 \operatorname{sech}^2 v) V = 0 \tag{2.203}$$

where $\lambda = -(S^2 + 1)$. For $\lambda = -1$ (and hence S = 0) one readily finds[65] V(v) = sechv which is the solution corresponding to the expected zero eigenvalue.

2.7 Inhomogeneous Broadening and Photon Echo

A very extensive analysis of the effects on pulse shapes of both homogeneous and inhomogeneous broadening has been carried out numerically[14,16]. Thus far only the steady state pulse shape has been described analytically when inhomogeneous broadening is present. However, if one foregoes consideration of the actual pulse shapes and confines attention to the area under the envelope of the pulse, then further progress may be made. In particular, it has been shown[24] that a very simple description may be given of the space-time evolution of the photon echoes that may appear behind two

optical pulses as they propagate through a resonant inhomogeneously broadened medium. This was carried out by noting that the area theorem, Eq. (2.68) is still satisfied if the pulses are assumed to be infinitely narrow, i.e., of the form

$$\mathcal{E}(\xi,\tau) = \theta(\xi)\,\delta(\tau) \tag{2.204}$$

where $\delta(\tau)$ is a delta function. The assumption of propagation at the light velocity is consistent with that of zero pulse width according to Eq. (2.57a)

The apparent inconsistency of using a delta function in the slowly varying envelope $\mathcal{E}(\xi,\tau)$ does no violence to the theory. It merely provides a convenient device for obtaining solutions to Eqs. (2.35) to (2.37) in the short pulse limit. We now give a derivation of the area theorem for delta function pulses and show how some of its implications may be readily explored.

The response of the system is governed by the Riccati equation given in Eq. (2.134). Introducing the new complex function $u = u_r + iu_i$ by the definition $\Phi = \exp(iu)$ Eqs. (2.134) and (2.133) become

$$\frac{\partial \mu}{\partial \tau} - i\mathcal{E}\sin\mu = \mathcal{E} \tag{2.205}$$

$$\rho = \operatorname{sech}\mu_i \sin\mu_r \tag{2.206}$$

$$\mathcal{Z} = -\tanh\mu_i \tag{2.207}$$

$$N = \operatorname{sech}\mu_i \cos\mu_r \tag{2.208}$$

Using the form for $\mathcal{E}$ given in Eq. (2.204) and integrating Eq. (2.205) across the singularity at $\tau = 0$, one finds

$$\mu^> - \mu^< = \theta(\xi) \tag{2.209}$$

Since θ is real, u_i is continuous across the pulse and according to Eq. (2.207), $\mathcal{Z}$ is also continuous across the pulse. The change in population is

$$\Delta N = N^> - N^< = \operatorname{sech}\mu_i^< (\cos\mu_r^> - \cos\mu_r^<) \tag{2.210}$$

which may be written as

$$N^> = N^< \cos\theta - \rho^< \sin\theta \tag{2.211}$$

Similarly, Eq. (2.206) yields

$$\rho_> = \rho_< \cos\theta + N_< \sin\theta \tag{2.212}$$

Eqs. (2.211), (2.212) and the continuity of $\mathcal{Q}$ across the pulse may be summarized in the vector form

$$\begin{pmatrix} \rho_> \\ \mathcal{Q}_> \\ N_> \end{pmatrix} = \begin{pmatrix} \cos\theta & 0 & \sin\theta \\ 0 & 1 & 0 \\ -\sin\theta & 0 & \cos\theta \end{pmatrix} \begin{pmatrix} \rho_< \\ \mathcal{Q}_< \\ N_< \end{pmatrix} \tag{2.213}$$

The 3 x 3 matrix represents a rotation about the $\mathcal{Q}$ axis by an angle θ and may be represented symbolically by $R_{\mathcal{Q}}(\theta)$. Considering $(\rho, \mathcal{Q}, N)$ as the three components of a vector P, Eq. (2.213) may be written

$$P_> = R_{\mathcal{Q}}(\theta) P_< \tag{2.214}$$

While the pulse is not acting, the system evolves according to the homogeneous counterpart for Eq. (2.205) which has the solution

$$e^{i\mu} = i\cot\tfrac{1}{2}(f\tau + \alpha) \tag{2.215}$$

where $\alpha = \alpha_r + i\alpha_i$ is a constant of integration. It is now a simple matter to show that

$$\rho(\tau) = \operatorname{sech}\alpha_i \sin(f\tau + \alpha_r) = \rho(\tau_0)\cos f(\tau - \tau_0) + \mathcal{Q}(\tau_0)\sin f(\tau - \tau_0) \tag{2.216a}$$

$$\mathcal{Q}(\tau) = \operatorname{sech}\alpha_i \cos(f\tau + \alpha_r) = \mathcal{Q}(\tau_0)\cos f(\tau - \tau_0) - \rho(\tau_0)\sin f(\tau - \tau_0) \tag{2.216b}$$

$$\eta(\tau) = \tanh\alpha_i = \eta(\tau_0) \tag{2.216c}$$

The matrix representation of this result is

$$\begin{pmatrix} \rho(\tau) \\ \mathcal{Q}(\tau) \\ \eta(\tau) \end{pmatrix} = \begin{pmatrix} \cos f(\tau - \tau_0) & \sin f(\tau - \tau_0) & 0 \\ -\sin f(\tau - \tau_0) & \cos f(\tau - \tau_0) & 0 \\ 0 & 0 & 1 \end{pmatrix} \begin{pmatrix} \rho(\tau_0) \\ \mathcal{Q}(\tau_0) \\ \eta(\tau_0) \end{pmatrix} \tag{2.217}$$

which represents a rotation through an angle $f(\tau - \tau_0)$ about the η axis and may be written

$$P(\tau) = R_\eta(\tau - \tau_0) P(\tau_0) \tag{2.218}$$

If a transverse relaxation time were retained in the analysis, so that between pulses ρ and 2 satisfied

$$\frac{\partial \rho}{\partial \tau} + \frac{1}{\Omega T_2}\rho = f2 \tag{2.219a}$$

$$\frac{\partial 2}{\partial \tau} + \frac{1}{\Omega T_2}2 = 0 \tag{2.219b}$$

then Eqs. (2.218) would be replaced by

$$p(\tau) = e^{-(\tau-\tau_0)/\Omega T_2} R_\eta(\tau-\tau_0) P(\tau_0) \tag{2.220}$$

At a time τ after interaction with a pulse of area θ, the state of a system that was initially in the lower level is given by

$$P(\tau) = R_\eta(\tau) R_x(\theta) P(0) = \begin{pmatrix} -\sin\theta \cos f\tau \\ \sin\theta \sin f\tau \\ -\cos\theta \end{pmatrix} \tag{2.221}$$

Eq. (2.35), with $g(\Delta\omega) = g(0)$ to accommodate all spectral components of the delta function, takes the form

$$\frac{\partial \theta}{\partial \xi}\delta(\tau) = -\pi g(0)\delta(\tau)\sin\theta \tag{2.222}$$

which yields the area theorem in the form

$$\frac{d\theta}{d\xi'} = -\sin\theta \,, \quad \xi' = \pi g(0)\xi \tag{2.223}$$

This scheme may now be used repeatedly to describe the response of the medium to a sequence of pulses. The response due to two pulses of area θ_1 and θ_2 a time T apart (in units of Ω^{-1}) is found to have a contribution at $\tau = 2T$. Evaluating P just beyond this time $\tau = 2T$, one finds

$$P(\tau) = R_\eta(\tau-2T) R_x(\theta_3) R_\eta(T) R_x(\theta_2) R_\eta(T) R_x(\theta_1) P(0) \tag{2.224}$$

Carrying out the indicated multiplications for a system that is initially in the ground state, one obtains

$$\begin{aligned} p(\xi,\tau) = &-\sin\theta_1 \cos f\tau - \sin\theta_2 \cos\theta_1 \cos f(\tau-T) \\ &- \left[\sin\theta_3 \cos\theta_2 \cos\theta_1 - \cos\theta_3 \sin^2(\theta_2/2)\sin\theta_1\right]\cos f(\tau-2T) \end{aligned} \tag{2.225}$$

If a relaxation time T_2 were included, this entire expression would merely be multiplied by $e^{-2T/\Omega T_2}$.

Substituting this result into Eq. (2.35) yields

$$\frac{d\theta_1}{d\xi'} = -\sin\theta_1 \tag{2.226}$$

$$\frac{d\theta_2}{d\xi'} = -\sin\theta_2\cos\theta_1 \tag{2.227}$$

$$\frac{d\theta_3}{d\xi'} = -\sin\theta_3\cos\theta_2\cos\theta_1 + \cos\theta_3\sin^2(\theta_2/2)\sin\theta_1 \tag{2.228}$$

Eqs. (2.226) and (2.227) have solutions

$$\tan\frac{\theta_1}{2} = \exp(-\xi' + \alpha) \tag{2.229}$$

$$\tan\frac{\theta_2}{2} = \beta\,\mathrm{sech}(\xi' - \alpha) = \beta\sin\theta_1 \tag{2.230}$$

where

$$e^{\alpha} = \tan\frac{\theta_1(0)}{2}\,,\ \beta = \tan\frac{\theta_2(0)}{2}\csc\theta_1(0) \tag{2.231}$$

Now, if $\theta_1(0) = \pi/2$, $\theta_2(0) \approx \pi$, the optimum case for photon echo experiments, then $|\beta| \gg 1$ and from the solution for θ_2 one sees that θ_2 remains nearly equal to its initial value until θ_1 decays to a value equal to β^{-1}. Until this final state in the pulse evolution is reached, one may set $\theta_2 = \pi$ in Eq. (2.228). The resulting equation may then be transformed to

$$\frac{d\theta_3}{d\theta_1} + \cos\theta_3 + \cot\theta_1\sin\theta_3 = 0 \tag{2.232}$$

Upon substituting $y = \tan(\theta_3/2)$ this becomes a Riccati equation which may be converted to a second-order linear equation by the substitution $y = -2(du/d\theta)/u$. Setting $k = \sin(\theta_1/2)$ one finally obtains

$$k(k^2-1)u'' + (3k^2-1)u' + ku = 0 \tag{2.233}$$

where the prime indicates differentiation with respect to k. Eq. (2.233) has the solution[66]

$$u = aK(k) + bK(k') \tag{2.234}$$

where K(k) is the complete elliptic integral of modulus k and k' is the complementary modulus. Finally, the solution for θ_3 may be written

$$\tan\frac{\theta_3}{2} = \frac{(k'/k)B(k') - (k/k')B(k)}{K(k) + K(k')} \tag{2.235}$$

where B(k) is a tabulated function[67] related to the complete elliptic integral by

$$B(k) = \frac{1-k^2}{k}\frac{dK}{dk} \tag{2.236}$$

Figure 12 contains a graph of Eq. (2.235) as well as the variations in θ_1 and θ_2. It is seen that the amplitude of the echo increases at a rate approximately equal to that at which the first pulse decreases. This has been observed experimentally[15].

2.8 Level Degeneracy

It has been pointed out[8,18] that pulse propagation under conditions which prevail experimentally may lead to considerably different results from those predicted here since level degeneracy may be present. It has also been shown that level degeneracy has a marked effect on the direction of polarization of the electric field vector of the echo pulse in a photon echo experiment[23]. Thus far, however, only the source term for the echo pulse has been calculated when degeneracy is present. No consideration has as yet been given to the complete problem in which the spatial evolution of the photon echo is followed in the presence of level degeneracy. Hence this latter topic will not be pursued here.

To avoid detailed consideration of specific molecular modes, level degeneracy will merely be expressed in terms of a simple jm scheme. The two states previously denoted by a and b are now characterized by angular momentum quantum numbers j'm' and jm respectively. Additional quantum numbers that would be associated with molecular vibration will commute with angular momentum operators and may be ignored. Each element in the 2 x 2 matrices of Eq.(2.10) now becomes a (2J + 1) x (2J' + 1) submatrix itself with elements $\langle j'm' | \underset{\sim}{P} | jm\rangle$. As is well known[68] transitions in j are restricted to $\Delta j = j' - j = -1, 0, 1$, the three alternatives frequently being referred to as P, Q and R branch transitions respectively. In addition, if the quantization axis is alligned parallel to the electric field polarization vector then only the P_z matrix elements need be calculated. All such matrix elements vanish unless $m' = m$ One then finds that $\mathcal{P}_{mj} = \langle j'm | \underset{\sim}{P} | jm\rangle = K_m \mathcal{P}$ where $\mathcal{P}$ is the largest value of $\mathcal{P}_{mj}$ in each of the three cases and

$$K_m = \sqrt{j^2 - m^2}/j \quad , \Delta j = -1 \tag{2.237a}$$

$$K_m = m/j \quad , \Delta j = 0 \tag{2.237b}$$

$$K_m = \sqrt{(j+1)^2 - m^2}/(j+1), \Delta j = 1 \tag{2.237c}$$

Since the submatrices of $\mathcal{V} = -\underset{\sim}{E} \cdot \underset{\sim}{\mathbb{P}} = -E\,\mathbb{P}_z$ are now diagonal in m, the various pairs of levels designated by different $\underset{\sim}{m}$ values are not coupled by the interaction and may be treated separately.

Hence, for each value of m one may write

$$\ddot{p}_m + \omega_{ab}^2 p_m = -\frac{2\omega_{ab}}{\hbar} \eta_m E |< jm/\mathbb{P}_z/j'm >|^2 \tag{2.238}$$

$$\dot{\eta} = \frac{2E}{\hbar\omega_{ab}} \dot{p}_m \tag{2.239}$$

Assuming that all sublevels of the lower state are equally populated initially,

$$\eta_m = \frac{\eta_0}{2j+1} (< j'm|\rho|jm > - < jm|\rho|jm >) \tag{2.240}$$

The electric field is governed by

$$\frac{\partial \mathcal{E}}{\partial t} + c\frac{\partial \mathcal{E}}{\partial x} = \frac{2\pi\omega_0\eta_0}{E_0} \int_{-\infty}^{\infty} d\Delta\omega g(\Delta\omega) \sum_{m=-j<}^{j<} p_m \tag{2.241}$$

where $j<$ refers to the lesser of j and j'. When this relation is integrated over the duration of the pulse, one obtains, in analogy with the derivation of Eq. (2.68)

$$\frac{d\theta}{dx} = \frac{\alpha}{2(2j+1)} \sum_m k_m \sin(k_m\theta) \tag{2.242}$$

where

$$\theta(x) = \frac{E_0\mu}{\hbar} \int_{-\infty}^{\infty} dt' \mathcal{E}(x,t') \tag{2.243}$$

For transparency to take place it is necessary that the right-hand side of Eq. (2.243) vanish. For Q branch transitions this will be possible for $\theta = 2m\pi$ just as in the nondegenerate case since the various K_m are integrally related. For P and R branch transitions, however, the irrational ratios of the various K_m prevent a simultaneous vanishing of all K_m except in the few cases in which there is only one nonvanishing value of K_m. For P and Q branch transitions this takes place for $J = 0, \frac{1}{2}$.

However, it has been noted[18] that the right-hand side of Eq. (2.243) will also vanish if $\int_{-\infty}^{\infty} dt' \mathcal{E} = 0$. Such zero π pulses should exhibit transparency independently of the values of the K_m. Although profiles of zero π pulses have been described in Section 2.6.1, it should be emphasized that they have been obtained for a simple nondegenerate system and are not directly applicable to the present situation.

For large values of j the summation may be approximated by an integration. Setting $m = j\cos\alpha$, the results quoted in Eqs. (2.237) may be replaced by continuous variable K given by

$$K = \begin{cases} \sin\alpha \ , \ \Delta j = \pm 1 \\ \cos\alpha \ , \ \Delta j = 0 \end{cases} \tag{2.244}$$

For $\Delta j = 0$

$$\frac{1}{2j+1} \sum K_m \sin(K_m\theta) \longrightarrow \frac{1}{2}\int_0^{\pi} d\alpha \sin\alpha \cos\alpha \sin(\theta\cos\alpha)$$

$$= (\sin\theta - \theta\cos\theta)/\theta^2 = j_1(\theta) \tag{2.245}$$

where $j_1(\theta)$ is a spherical Bessel function[72]

$$\frac{1}{2j+1} \sum K_m \sin(K_m\theta) \longrightarrow \frac{1}{2}\int_0^{\pi} d\alpha \sin^2\alpha \sin(\theta\sin\alpha)$$

$$= \frac{\pi}{2}\left[H_0(\theta) - H_1(\theta)/\theta\right] \tag{2.246}$$

where the $H_n(\theta)$ are Struve functions[69].

The two forms for the area theorem in the presence of degeneracy for large j are now obtained by combining Eq. (2.243) with Eqs. (2.246) and (2.247). It is again evident from these results that a zero π pulse should exhibit transparency.

For small θ, the area theorem for Q branch transitions reduces to the small 0 form of Eq. (2.68) when orientational averaging is included.

As in Section 2.6, pulse shapes may be obtained in the limit of extreme saturation broadening. Setting $g(\Delta\omega) = \delta(\Delta\omega)$, Eq. (2.145) then goes over to

$$\frac{\partial^2\sigma}{\partial x \partial t'} = \frac{\alpha'}{2j+1} \sum K_m \sin(K_m\sigma) \tag{2.247}$$

where $t' = t - x/c$ and α' is as defined in Eq. (2.30).

Examples of steady state pulse profiles have been obtained numerically[18]. For Q-branch transition with j = 2, the result may be given in a simple closed form[72]. One obtains

$$\sigma = -4\tan^{-1}(\sqrt{5}\,\mathrm{csch}\; w/\tau) \tag{2.248}$$

where $w = t - x/v$ and

$$\frac{1}{v} = \frac{1}{c} + \frac{\alpha'\tau^2}{2} \tag{2.249}$$

The electric field is

$$\frac{\wp E_0 \mathcal{E}}{\hbar} = \frac{4\sqrt{5}\;\mathrm{sech}\; w/\tau}{\tau(1 + 4\,\mathrm{sech}^2 w/\tau)} \tag{2.250}$$

which is shown in Fig. 13.

Section 3

CERENKOV TYPE RADIATION FROM LIGHT PULSES

3.1 Introduction

Optical rectification in non-linear dielectric media produces a polarization that follows in time the intensity of the optical pulse. The so-called dc polarization has frequency components in the millimeter and submillimeter region of the spectrum, and in general has vector components both longitudinal and transverse to the direction of light propagation. Submillimeter radiation can therefore be generated from picosecond light pulses. A general theory of microwave generation via the dc effect does not exist.

The most important feature of the generation of the microwave field from its source is the fact that the source polarization moves through the crystal at the group velocity of the light pulse , which is approximately c/n, whereas the phase velocity of the free microwave field in the same crystal is usually lower, c/m, where n and m are the optical and microwave indices of refraction. Because of the infrared resonances between the optical and microwave frequencies, m is usually larger than n, so the microwave field moves slower than its source, in close analogy with the Cerenkov radiation from a relativistic electron. The analogy with Cerenkov radiation will be shown to be very close for the microwave field generated by the longitudinal component of the polarization. Our understanding of the microwave generation from light pulses in non-linear media is greatly increased by studying the Cerenkov analog of the problem, viz. the coupling of the source to the free fields of the dielectric. For example, one learns to what extent "phase-matching" is important. A comparison of the induction fields and the radiation fields shows the possibility of greatly increasing the microwave power generation by changing the boundary conditions on the problem in such a way as to couple to the induction fields.

This work deals with the radiation from longitudinal and transverse polarizations in optically isotropic and uniaxial crystals. The physical picture that one associates with these phenomena is a light packet accompanied by a dc polarization radiating microwave power in Cerenkov cones, one cone system at the leading edge of the pulse and another at the trailing edge. The interference between these Cerenkov cones is completely accounted for by Fourier analysing the polarization pulse into its frequency components. The radiated fields at any frequency are proportional to the corresponding Fourier component amplitudes of the equivalent source current. In the same way, the interference between waves originating from different regions in the cross section is exhibited in the Fourier-Bessel transforms of the traverse distribution of source polarization.

The first problem that we treat is that of radiation in an optically isotropic medium. Both longitudinal and transverse polarizations are treated. The theoretical technique is to solve the inhomogeneous differential equations for the field potentials, then derive the actual fields by differentiation of the potentials. The second problem is that of a uniaxial crystal, in which the tensor nature of the dielectric

constant so much complicates the problem that it is easier to deal directly with the field quantities rather than the potentials. The method of analysis here is to resolve the source polarization into a continuous spectrum of plane waves, find the electric field components for the ordinary and extraordinary plane waves of microwave field, then sum them all through integration to find the complete ordinary and extraordinary wave fields.

3.2 Optically Isotropic Media

The microwave field is derived from the vector and scalar potentials $\underset{\sim}{A}$ and ψ:

$$\underset{\sim}{H} = \text{curl } \underset{\sim}{A} \tag{3.1a}$$

$$\underset{\sim}{E} = -\frac{1}{c}\frac{\partial \underset{\sim}{A}}{\partial t} - \text{grad } \psi . \tag{3.1b}$$

The polarization field $\underset{\sim}{P}$ is split into its homogeneous and inhomogeneous parts:

$$\underset{\sim}{P} = \underset{\sim}{P}_H + \underset{\sim}{P}_I \tag{3.2}$$

where

$$\underset{\sim}{P}_H = \frac{(m^2 - 1)}{4\pi}\underset{\sim}{E} , \tag{3.3}$$

and $\underset{\sim}{P}_I$, the inhomogeneous part is the source polarization caused by the dc effect in the non-linear medium. The potential field equations are

$$\nabla^2 A - \frac{m^2}{c^2}\frac{\partial^2 A}{\partial t^2} = -\frac{4\pi}{c}\frac{\partial P_I}{\partial t} \tag{3.4}$$

$$\nabla^2 \psi - \frac{m^2}{c^2}\frac{\partial^2 \psi}{\partial t^2} = \frac{4\pi}{m^2}\,\text{div } \underset{\sim}{P}_I \tag{3.5}$$

$$\text{div } \underset{\sim}{A} + \frac{m^2}{c}\frac{\partial \psi}{\partial t} = 0. \tag{3.6}$$

This last is the gauge condition. Only two of the three equations are independent. We use the first to derive $\underset{\sim}{A}$ from P_I, the third to derive ψ from $\underset{\sim}{A}$, then find $\underset{\sim}{E}$ and $\underset{\sim}{H}$ by differentiation of these potentials. The source of $\underset{\sim}{A}$ is a current density. For Cerenkov radiation from electrons the source current is the actual current due to

motion of the electron, and the right hand side of the wave equation for $\underset{\sim}{A}$ is $\frac{-4\pi \underset{\sim}{J}}{c}$.

The comparison between the Cerenkov radiation from an electron of charge e_1 and that from a longitudinal polarization front of length Λ and face charge Q is easily exhibited. In both cases, let $\hat{z}$ be the direction of the motion of the source. For the electron, the charge density is given by

$$\rho = e_1 \delta(x)\delta(y)\ \delta(z - vt) \tag{3.7}$$

where v is the electron speed. The current density is

$$\underset{\sim}{J} = \rho \underset{\sim}{v} = e_1 v \delta(x)\delta(y)\delta(z - vt)\ \hat{z} \tag{3.8}$$

We use the time convention exp $(-i\omega t)$ throughout, and thus have the Fourier component of current at frequency ω as

$$\underset{\sim\omega}{J} = \hat{z} J_\omega = \frac{e_1 \hat{z}}{2\pi}\ \delta(x)\delta(y) e^{i\omega z/v} \tag{3.9}$$

The vector potential equation is therefore

$$\nabla^2 A_\omega + \frac{m^2 \omega^2}{c^2} A_\omega = \frac{e_1}{\pi c \rho}\ \delta(\rho) e^{i\omega z/v} \tag{3.10}$$

where $\underset{\sim\omega}{A} = (0,\ 0,\ A_\omega)$ and where $\delta(x)\delta(y)$ has been replaced by $\delta(\rho)/2\pi\rho$ in cylindrical coordinates. The polarization front is represented by

$$\underset{\sim I}{P} = Q\left[\tfrac{1}{2} - 1/\pi \tan^{-1}\{(z - vt)/\Lambda\}\right]\ \hat{z}\ \delta(x)\delta(y) \tag{3.11a}$$

Its Fourier component equivalent current is

$$\left(\frac{\partial \underset{\sim I}{P}}{\partial t}\right)_\omega = -i\omega \underset{\sim I\omega}{P} = \hat{z}\ \frac{Q}{2\pi}\ e^{-\Lambda|\omega|/v}\ e^{i\omega z/v}\ \frac{\delta(\rho)}{2\pi\rho} \tag{3.11b}$$

Thus the vector potential wave equation is

$$\left(\nabla^2 + \frac{m^2 \omega^2}{c^2}\right) A_\omega = \frac{4\pi i\omega}{c}\ \underset{\sim I\omega}{P} \tag{3.12a}$$

$$= \frac{Q}{\pi c \rho}\ \delta(\rho) e^{i\omega z/v}\ e^{-\Lambda|\omega|/v} \tag{3.12b}$$

where again $\underset{\sim}{A}_\omega = (0,0,A_\omega)$. The energy radiated per cm of path per unit frequency interval by the electron is

$$\frac{d^2W}{d\omega dz} = \frac{e_1^2}{c^2}\left(1 - \frac{c^2}{m^2v^2}\right)\omega \tag{3.13}$$

Hence, by comparison of the two vector wave equations, the radiation from the advancing polarization front must be given by

$$\frac{d^2W}{d\omega dz} = \frac{Q^2}{c^2}\left(1 - \frac{n^2}{m^2}\right)\omega e^{-2\Lambda\omega/v} \tag{3.14}$$

For a single electron, $e_1 = 4.8 \times 10^{-10}$ esu, and the energy radiated per cm path per cm^{-1} bandwidth is $\sim 5 \times 10^{-28}$ erg. For a picosecond pulse focussed to 10^{12} watts/cm^2 in KDP we have $P_I = 8$ esu in say a square millimeter section, so that $Q = 8 \times 10^{-2}$ esu $= 2 \times 10^8 e_1$. The energy radiated here is now $\sim 2 \times 10^{-11}$ erg per cm path per cm^{-1} bandwidth at wavelengths long compared to Λ and to the cross section dimensions. Admittedly, the energy output in this case is small, but techniques for increased coupling can be found, and the important point is that the equivalent of 10^8 relativistic electrons in a cubic millimeter volume is easy to achieve with picosecond pulses and NLO. The defocussing of light is less serious a problem than Coulomb repulsion and beam collimation in megavolt electronics.

We now proceed with accurate calculations of the field quantities for this Cerenkov type interaction - the weak coupling situation.

Calculation of the Electromagnetic Fields

We want to solve

$$\nabla^2 + \frac{m^2\omega^2}{c^2}\underset{\sim}{A}_\omega = \frac{4\pi i\omega}{c}\underset{\sim}{P}_{I\omega} \tag{3.15}$$

and

$$\nabla\cdot\underset{\sim}{A}_\omega - \frac{i\omega m^2}{c}\psi_\omega = 0 \tag{3.16}$$

for the general polarization pulse;

$$\underset{\sim}{P}_I(\underset{\sim}{r},t) = \hat{p}\,F_1(x,y)\,F_2\left(z - \frac{vt}{n}\right) \tag{3.17}$$

which is derived from a collimated picosecond pulse. Fourier analysis of F_2 gives

$$F_2(z-vt) = \int_{-\infty}^{\infty}\left[G_2(\omega)e^{inz\omega/c}\right]e^{-i\omega t}\,d\omega \tag{3.18}$$

The following quite general form of $F_1(x,y)$, expressed in cylindrical coordinates, will take care of most polarization forms derived from rectification of the mode fields of a laser output:

$$F_1(x,y) \rightarrow F_1(\rho,\phi) = \sum_{\ell} F_\ell(\rho)\, e^{i\ell\phi} \tag{3.19}$$

The vector $\hat{p}$ will have longitudinal and transverse components. Because of the linearity of the problem, we may consider either one component alone and also select one l-component of the transverse polarization distribution. Equation (3.15) now becomes

$$\left(\nabla^2 + \frac{m^2\omega^2}{c^2}\right) A_\omega = \frac{4\pi i\omega}{c} F_\ell(\rho)\, e^{i\ell\phi}\, G_2(\omega)\, e^{in\omega z/c} \tag{3.15a}$$

where A_ψ stands for either of the rectangular components $\underset{\sim}{A}_\psi \cdot \hat{x}$ or $\underset{\sim}{A}_\psi \cdot \hat{z}$ corresponding to transverse or longitudinal polarizations respectively. The obvious method of solving Eq. (3.15a) is to substitute

$$A_\omega = u(\rho)\, e^{i\ell\phi}\, e^{in\omega z/c} \tag{3.20}$$

which yields for the scalar $u(\rho)$ the inhomogeneous Bessel equation

$$B_\ell u \equiv \frac{1}{\rho}\frac{d}{d\rho}\rho\frac{du}{d\rho} + \left(S^2 - \frac{\ell^2}{\rho^2}\right) u = \frac{4\pi i\omega}{c} F_\ell(\rho)\, G_2(\omega) \tag{3.21}$$

where $S^2 = \frac{\omega^2}{c^2}(m^2 - n^2)$ is the square of the transverse k-vector.

The solution u is readily found and will be written down later. For the moment it is instructive to look at the structure of the solution being forced on this problem. The only boundary condition is the radiation condition. Equation (3.20) is consistent with a linear loss (diffraction) balancing the energy generation. The exponential factor $e^{in\omega z/c}$ in Eq. (3.20) is an expression of the translational invariance along $\hat{z}$ of the problem. There is no possibility of exponential growth of the microwave field along z here. The magnitude of $F_e(\rho)$ in Eq. (3.15a) is independent of z, which is an approximation that neglects diffraction of the picosecond light pulse along the path of interest, and neglects absorption of the light pulse. Of course, the microwaves rob the light pulse of some of its energy, and they take their momentum from the crystal directly, and some momentum from the light pulse indirectly via the crystal.

Fields Generated by Longitudinal Polarization

When $\hat{p} = \hat{z}$, the solution of Eqs. (3.20) and (3.21) is $\underset{\sim}{A}_\omega = (0,0,ue^{i\ell\varphi}e^{in\omega z/c})$, whereupon Eq. (3.16) gives $\psi_\omega = \frac{n}{m^2} ue^{i\ell\varphi}e^{in\omega z/c}$. From Eq. (3.1) we therefore obtain

$$\underset{\sim}{E}_\omega = \left\{-\frac{n}{m^2}\frac{du}{d\rho}\hat{\rho} - \frac{i\ell n}{m^2\rho}u\hat{\phi} + \frac{i\omega}{c}\left(1-\frac{n^2}{m^2}\right)u\hat{z}\right\} e^{i(n\omega z/c + \ell\phi)} \tag{3.22a}$$

$$\underset{\sim}{H}_\omega = \left\{\frac{i\ell u}{\rho}\hat{\rho} - \frac{du}{d\rho}\hat{\phi}\right\} e^{i(n\omega z/c + \ell\phi)} \tag{3.22b}$$

The energy radiated is found by integration of the Poynting vector

$$\underset{\sim}{S}(t) = \frac{c}{4\pi}\frac{1}{2}\mathrm{Re}\left\{\underset{\sim}{E}(t)\times\underset{\sim}{\bar{H}}(t)\right\} \tag{3.23}$$

$$\int_{-\infty}^{\infty}\underset{\sim}{S}(t)dt = \frac{c}{4}\mathrm{Re}\left\{\int_{-\infty}^{\infty}(\underset{\sim}{E}_\omega\times\underset{\sim}{\bar{H}}_\omega)d\omega\right\} \tag{3.24}$$

Taking into account the frequencies ω and $-\omega$ simultaneously we calculate the energy radiated per unit frequency interval through a cylinder of 1 cm length coaxial with $\hat{z}$ by integrating the ω-derivative of Eq. (3.24) over the cylinder surface. The result is

$$\frac{d^2W}{d\omega dz} = \int_0^{2\pi}\frac{c}{4}\mathrm{Re}\left\{(E_\omega\times\bar{H}_\omega)_\rho + (E_{-\omega}\times\bar{H}_{-\omega})_\rho\right\}\rho d\phi \tag{3.25}$$

When ρ is large enough for the cylinder to enclose the sources completely, Eq. (3.25) is independent of ρ. From Eq. (3.22),

$$(\underset{\sim}{E}_\omega\times\underset{\sim}{\bar{H}}_\omega)_\rho = \frac{i\omega}{c}\left(1-\frac{n^2}{m^2}\right)u\frac{d\bar{u}}{d\rho} \tag{3.26}$$

and Eq. (3.25) becomes

$$\frac{d^2W}{d\omega dz} = \frac{\omega}{4}\left(1-\frac{n^2}{m^2}\right)2\pi i\rho\left(u\frac{d\bar{u}}{d\rho} - \bar{u}\frac{du}{d\rho}\right) \tag{3.27}$$

This formula is for $F_1(x, y) \sim e^{i\ell\varphi} = \cos\ell\varphi + i\sin\ell\varphi$ wherein the cosine and sine terms radiate independently. If only one is present (e.g. $\cos\ell\varphi$) we have to divide Eq. (3.27) by 2. Note that $\frac{1}{2\pi}\int_0^{2\pi}\cos^2\ell\varphi d\varphi = \frac{1}{2}\mathrm{Re}\{e^{i\ell\varphi}e^{-i\ell\varphi}\}$, except when $\ell = 0$.

Fields Generated by Transverse Polarization

When $\hat{p} = \hat{x}$, the solution of Eqs. (3.20) and (3.21) is

$$\underset{\sim}{A}_\omega = \left(u e^{i\ell\phi} e^{in\omega z/c}, 0, 0\right) \longrightarrow \left(u \cos \ell\phi\, e^{in\omega z/c}, 0, 0\right)$$

$$= u \cos \ell\phi \cos\phi\, e^{in\omega z/c}\hat{\rho} - u \cos\ell\phi \sin\phi\, e^{in\omega z/c}\hat{\phi} \tag{3.28}$$

where the φ-dependence has been written more explicitly. Equation (3.16) gives

$$\psi_\omega = -\frac{ic}{\omega m^2}\left[\frac{du}{d\rho}\cos\ell\phi\cos\phi + \frac{\ell u}{\rho}\sin\ell\phi\sin\phi\right] e^{in\omega z/c} \tag{3.29}$$

Use of Eqs. (3.1) and (3.2) gives the fields $\underset{\sim}{E}_\omega$ and $\underset{\sim}{H}_\omega$ from which one readily obtains

$$\mathrm{Re}\left\{\left(\underset{\sim}{E}_\omega \times \bar{H}_\omega\right)_\rho\right\} \simeq \frac{1}{2}\frac{\omega}{c}\cos^2\ell\phi.i\left(u\frac{d\bar{u}}{d\rho} - \bar{u}\frac{du}{d\rho}\right)\left(\sin^2\phi + \frac{n^2}{m^2}\cos^2\phi\right) \tag{3.30}$$

We have dropped terms in $\underset{\sim}{E}$ and $\underset{\sim}{H}$ that fall off faster than $1/\rho^{\frac{1}{2}}$ because they will not contribute to the radiation field. These induction fields are capable of coupling energy out of the system through microwave structures that come in to within a couple of wavelengths of the source. The presence of such a structure changes the boundary conditions on the problem, so that our equations no longer give the correct expressions for these fields. A simple analogy may be helpful here. A radio frequency choke is a poor radiator because of the small overlap of its fields on the free fields of the vacuum. The same choke coil when used as the primary winding of a transformer is capable of coupling strongly to a transmission line connected to a secondary winding.

The formula for the energy radiated by the transverse polarization as calculated from Eq. (3.25) depends on whether $\ell = 0$, $\ell = 1$, or $\ell > 1$. The result is:

$$\left.\frac{d^2W}{d\omega dz}\right|_{\ell=0} = \frac{\omega}{4}\left(1 + \frac{n^2}{m^2}\right)\pi i\rho\left(u\frac{d\bar{u}}{d\rho} - \bar{u}\frac{du}{d\rho}\right) \tag{3.31a}$$

$$\left.\frac{d^2W}{d\omega dz}\right|_{\ell=1} = \frac{\omega}{4}\left(1 + \frac{3n^2}{m^2}\right)\frac{\pi}{4} i\rho\left(u\frac{d\bar{u}}{d\rho} - \bar{u}\frac{du}{d\rho}\right) \tag{3.31b}$$

$$\left.\frac{d^2W}{d\omega dz}\right|_{\ell>1} = \frac{\omega}{4}\left(1 + \frac{n^2}{m^2}\right)\frac{\pi}{2}\, i\rho\left(u\frac{d\bar{u}}{d\rho} - \bar{u}\frac{du}{d\rho}\right) \tag{3.31c}$$

The Eqs. (3.27)(longitudinal polarization) and (3.31)(transverse polarization) both contain the expression $i\rho\left(u\frac{d\bar{u}}{d\rho} - \bar{u}\frac{du}{d\rho}\right)$ in which u is the function that solves Eq. (3.21)

Evaluation of $i\rho(u \frac{d\bar{u}}{d\rho} - \bar{u} \frac{du}{d\rho})$

The solution of Eq. (3.21) can be found most readily from expression

$$u(\rho) = -\frac{i\omega G_2(\omega)}{c} \int_0^{\rho} g_\ell(\rho/\rho_0) F_\ell(\rho_0) \rho_0 d\rho_0 \tag{3.32}$$

where $g_e(\rho|\rho_o)$ is the Green's function of the problem

$$B_\ell \, g_\ell(\rho/\rho_0) = -\frac{4\pi \delta(\rho-\rho_0)}{\rho} \tag{3.33}$$

The Green's function for Eq. (3.33) is [83]

$$g_\ell(\rho/\rho_0) 2\pi^2 i \, J_\ell(s\rho) H_\ell(s\rho_0) \qquad \rho \le \rho_0 \tag{3.34a}$$

and

$$g_\ell(\rho/\rho_0) 2\pi^2 i J_\ell(s\rho_0) H_\ell(s\rho) \qquad \rho \ge \rho_0 \tag{3.34b}$$

Both expressions (3.34) must be used to express the field inside the source. We need only Eq. (3.34b) for the radiation fields. Combination of Eqs. (3.32) and (3.34b) gives

$$u(\rho) = \frac{2\pi^2 \omega G_2(\omega)}{c} \left[\int_0 \rho_\ell(\rho_0) J_\ell(s\rho_0) \rho_0 d\rho_0 \right] H_\ell^{(1)}(s\rho)$$

$$= \frac{2\pi^2 \omega G_2(\omega)}{c} G^\ell(s) H_\ell^{(1)}(s\rho) \tag{3.35}$$

where we use $G^\ell(s)$ to denote the Fourier-Bessel transform (the expression in square brackets) of the source distribution.

Thus

$$i\rho\left(u \frac{d\bar{u}}{d\rho} - \bar{u} \frac{du}{d\rho}\right) = 4\pi^4 \frac{\omega^2}{c^2} \left|G_2(\omega)\right|^2 \left[G^\ell(s)\right]^2 i\rho \left[H_\ell^{(1)}(s\rho) \frac{d}{d\rho} H_\ell^{(2)}(s\rho) - \text{c.c.}\right]$$

$$= 16\pi^3 \frac{\omega^2}{c^2} \left|G_2(\omega)\right|^2 \left[G^\ell(s)\right]^2 \tag{3.36}$$

Energy Radiated in an Isotropic Medium

Equation (3.36) is now substituted into Eqs. (3.27) and (3.31) with the following results

Longitudinal Polarization:

$$\frac{d^2W}{dzd\omega} = 8\pi^4 \frac{\omega^3}{c^2}\left(1-\frac{n^2}{m^2}\right)\left|G_2(\omega)\right|^2\left[G^{\ell}(s)\right]^2\epsilon_{\ell} \tag{3.37}$$

where

$$\epsilon_{\ell} = 1 \quad \text{for} \quad \ell = 0 \tag{3.37a}$$

and

$$\epsilon_{\ell} = \tfrac{1}{2} \text{ for } \ell = 1, 2, 3, \ldots . \tag{3.37b}$$

Transverse Polarization:

$$\left.\frac{d^2W}{dzd\omega}\right|_{\ell=1} = \pi^4 \frac{\omega^3}{c^2}\left(1+3\frac{n^2}{m^2}\right)\left|G_2(\omega)\right|^2\left[G^{\ell}(s)\right]^2 \tag{3.38a}$$

$$\left.\frac{d^2W}{dzd\omega}\right|_{\ell\neq 1} = 4\pi^4 \frac{\omega^3}{c^2}\left(1+\frac{n^2}{m^2}\right)\left|G^2(\omega)\right|^2\left[G^{\ell}(s)\right]^2\epsilon_{\ell} \tag{3.38b}$$

In the above expressions is the transverse component of the k-vector of the field.

For any actual polarization distribution, one uses the decomposition of Eq. (3.19)$_2$ and sums the Eqs. (3.37), (3.38) over ℓ. Equation (3.37) contains the factor $(1 - \frac{n}{m^2})$ in close analogy with Cerenkov radiation. The transverse polarization case does not have this factor, because the radiated power does not vanish when $m = n$. This is in sharp distinction to the case of Cerenkov radiation from a transverse electric dipole on a relativistic particle. The distinction arises because for the particle the equivalent current sources are always along the direction of motion, and furthermore, the transverse dipole partly transforms to a magnetic dipole at right angles to both the electric dipole and the direction of motion. Such a Lorentz transformation does not enter the NLO case, where the equivalent current source may actually be transverse to the direction of motion.

The case $m = n$ represents a match between the speeds of the optical pulse and the microwaves. In the case of SHG this phase matching causes a large increase in power. The present situation is different, because of the essential role played by diffraction of the microwaves. Since $(1 \pm n^2/m^2)$ is slowly varying in n/m, nothing spectacular happens at or near $n = m$. Transverse and longitudinal polarizations radiate about equally well according to our formulae.

Next we examine the case of an anisotropic medium to see what new features are introduced.

3.3 Optically Anisotropic Media

This method of analysis is more powerful than the one used for isotropic media. In essence, we resolve the polarization pulse into its plane wave components, find the electromagnetic plane wave for each polarization wave component, then add all the resulting plane waves to obtain the total field.

Again we start with

$$\underset{\sim}{P}_I (\underset{\sim}{r},t) = \hat{p} F_1 (x,y)\, F_2 \left(z - \frac{vt}{n}\right) \tag{3.17}$$

The Fourier transform of F_1 is given by

$$F_1(x,y) = \iint_{-\infty}^{\infty} G_1(k_x, k_y)\, e^{i(k_x x + k_y y)}\, dk_x\, dk_y \tag{3.39a}$$

or

$$F_1(\rho,\phi) = \int_0^{\infty} d\kappa\, \kappa \int_0^{2\pi} d\theta \cdot G_1(x,\theta)\, e^{i\kappa\rho\cos(\theta-\phi)} \tag{3.39b}$$

where $x = \rho \cos\varphi$, $y = \rho \sin\varphi$, $k_x = K \cos\theta$, $k_y = K \sin\theta$. The inverse of Eq. (3.39b) gives

$$G_1(\kappa,\theta) = \frac{1}{(2\pi)^2} \int_0^{\infty} d\sigma \cdot \sigma \int_0^{2\pi} d\mu\, F_1(\sigma,\mu)\, e^{-i\kappa\sigma\cos(\theta-\mu)} \tag{3.40a}$$

Again assuming that $F_1(\rho,\varphi) = \Sigma_l F_l(\rho) e^{il\varphi}$

$$G_1(x,\theta) = \frac{1}{(2\pi)^2} \sum_l \int_0^{\infty} d\sigma\, \sigma\, F_l(\sigma) \int_0^{2\pi} d\mu\, e^{-i\kappa\sigma\cos(\theta-\mu) + il\mu} \tag{3.40b}$$

$$= \frac{1}{2\pi} \sum_l e^{il(\theta-\pi/2)} G^l(\kappa) \tag{3.40c}$$

where $G^l(x)$ is the Fourier-Bessel transform defined previously in Eq. (3.35), and

$$F_1(\rho,\phi) = \sum_l \int_0^{\infty} d\kappa\, \kappa \int_0^{2\pi} d\theta\, \frac{1}{2\pi}\, e^{il(\theta-\pi/2)} G^l(\kappa) e^{i\kappa\rho\cos(\theta-\phi) + il\theta} \tag{3.39c}$$

Using Eq. (3.18) to transform F_2 now gives the combined result

$$\underset{\sim}{P}_I (\underset{\sim}{r},t) = \hat{p} \sum_l \frac{e^{-il\pi/2}}{2\pi} \int_{-\infty}^{\infty} d\omega\, G_2(\omega) \int_0^{\infty} d\kappa\, \kappa\, G^l(\kappa) \int d\theta \left\{ e^{-i\omega(t - nz/e}\, e^{i\kappa\rho\cos(\theta-\theta) + i\,\theta} \right\} \tag{3.41}$$

The quantity in curly brackets defines the frequency, wavelength, direction and starting phase of an elementary plane wave component of polarization with amplitude $P_{\omega K} d\omega, K dx, d\sigma$ where

$$p_{\omega\kappa} = \frac{1}{2\pi} e^{-i\ell\pi/2} G_2(\omega) G^{\ell}(\kappa) \tag{3.41a}$$

If such a plane wave gives rise to an electromagnetic wave with one field component (say x) of amplitude and phase $\mathcal{E}_{x\omega K} e^{-i\omega(t - nz/c)} e^{iK\rho \cos(\theta - \varphi) + i\ell\varphi} d\omega K dK d\theta$, the total field component due to the totality of elementary plane waves is given by the integral

$$E_x(\underset{\sim}{r},t) = \sum_{\ell} \int_{-\infty}^{\infty} d\omega \int_0^{\infty} d\kappa\, \kappa \int_0^{2\pi} d\theta \left\{ \left(\mathcal{E}_{x\omega x} / p_{\omega\kappa} \right) p_{\omega\kappa} \frac{1}{2\pi} e^{-i\ell\pi/2} G_2(\omega)\, G^{\ell}(\kappa) \right. \tag{3.42}$$

Our problem reduces to finding the ratios $\mathcal{E}_x/P_{\omega K}$, $\mathcal{E}_y/p_{\omega K}$ and $\mathcal{E}_z/p_{\omega K}$ (where e.g. $\mathcal{E}_x \equiv \mathcal{E}_{x\omega K}$) and integrating Eqs. (3.42) to obtain the electromagnetic field. These ratios are found in the general case by solving the inhomogeneous wave equation. The general solutions can then be specialized to the required uniaxial crystal or biaxial crystal, etc.

Solution of the Inhomogeneous Wave Equation

In the anisotropic medium, the displacement vector is related to the field intensity and the inhomogeneous part of the polarization by

$$\underset{\sim}{D} = \epsilon \cdot \underset{\sim}{E} + 4\pi \underset{\sim}{P}_I \tag{3.43}$$

The wave equation is now

$$\nabla\kappa\nabla\kappa \underset{\sim}{E} + \frac{1}{c^2} \epsilon \cdot \frac{\partial^2 \underset{\sim}{E}}{\partial t^2} = \frac{-4\pi}{c^2} \frac{\partial^2 \underset{\sim}{P}_I}{\partial t^2} \tag{3.44a}$$

Resolved into Fourier components. Equation (3.44a) becomes

$$\mathcal{E}_k \left| \left(\frac{c}{\omega} \right)^2 k^2 \left\{ \hat{e} - \hat{s}(\hat{s} \cdot \hat{e}) \right\} - \epsilon \cdot \hat{e} \right| = 4\pi p_{\omega\kappa} \hat{p} \tag{3.44b}$$

where $\mathcal{E}_k \hat{e} = \underset{\sim}{E}_k$, the Fourier transform of $\underset{\sim}{E}$, and $\underset{\sim}{k} = k\hat{s}$ · A subsidiary condition, coming from $\operatorname{div} \underset{\sim}{D}_k = 0$ is

$$0 = \operatorname{div} \underset{\sim}{D}_k = \underset{\sim}{k} \cdot (\epsilon \cdot \underset{\sim}{E}_k + 4\pi \underset{\sim}{P}_k)$$

$$\therefore \hat{s} \cdot \epsilon \cdot \hat{e} = -4\pi p_{\omega\kappa} \hat{p} \cdot \hat{s} / \mathcal{E}_k \tag{3.45}$$

The inhomogeneous wave equation (3.44b) is solved by the method used by Kleinman[84] in his study on SHG.

$$\hat{e}\,\mathcal{E}_k = \hat{e}_1 E_1 + \hat{e}_2 E_2 + \hat{S} E_3 \tag{3.46}$$

where $\hat{S}$ is the wave normal ($\underset{\sim}{k} = k\hat{S}$), $\hat{e}_1$ is the direction of polarization of the $\underset{\sim}{E}$ field for a free ordinary wave and $\hat{e}_2$ is the direction of polarization for the free extraordinary wave. $\hat{e}_1$, $\hat{e}_2$, and $\hat{S}$ are not orthogonal. When Eq. (3.44b) is resolved along these three directions we obtain

$$\left(\frac{c}{\omega}\right)^2 \left\{-k^2 \hat{s}(\hat{s}\cdot\hat{e}_1)E_1 - k^2\hat{s}(\hat{s}\cdot\hat{e}_2)E_2 + k^2\hat{e}_1 E_1 + k\,\hat{e}_2 E_2\right\}$$

$$-(\epsilon\cdot\hat{e}_1 E_1 + \epsilon\cdot\hat{e}_2 E_2) - \epsilon\cdot\hat{s}\,E_3 = 4\pi p_{\omega\kappa}\hat{p} \tag{3.44c}$$

The quantities $\epsilon \cdot \hat{e}_1$ and $\epsilon \cdot \hat{e}_2$ in Eq. (3.44c) are found by solving the homogeneous wave equations for the ordinary and extraordinary waves respectively. These equations are

$$\left(\frac{c}{\omega}\right)^2 k_{1,2}^2\left\{\hat{e}_{1,2} - \hat{s}(\hat{s}\cdot\hat{e}_{1,2})\right\} - \epsilon\cdot\hat{e}_{1,2} = 0 \tag{3.47}$$

Substituting $\epsilon \cdot \hat{e}_{1,2}$ into Eq. (3.44c) we find

$$\left(\frac{c}{\omega}\right)^2 \left[(k_1^2 - k^2)\left\{\hat{s}(\hat{s}\cdot\hat{e}_1) - \hat{e}_1\right\}E_1 + (k_2^2 - k^2)\left\{\hat{s}(\hat{s}\cdot\hat{e}_2) - \hat{e}_2\right\}E_2\right]$$

$$-\epsilon\cdot\hat{s}\,E_3 = 4\pi p_{\omega\kappa}\hat{p} \tag{3.44d}$$

The scalar product of Eq. (3.44d) with $\hat{S}$ gives

$$E_3 = -4\pi p_{\omega\kappa}(\hat{p}\cdot\hat{s})/(\hat{s}\cdot\epsilon\cdot\hat{s}) \tag{3.48a}$$

which is now substituted into Eq. (3.44d) to give

$$\left(\frac{c}{\omega}\right)^2 (k_1^2 - k^2)\left\{\hat{s}(\hat{s}\cdot\hat{e}_1) - \hat{e}_1\right\}E_1 + \left(\frac{c}{\omega}\right)^2 (k_2^2 - k^2)\left\{\hat{s}(\hat{s}\cdot\hat{e}_2) - \hat{e}_2\right\}E_2$$

$$= 4\pi p_{\omega\kappa}\left[\hat{p} - (\epsilon\cdot\hat{s})(\hat{p}\cdot\hat{s})/(\hat{s}\cdot\epsilon\cdot\hat{s})\right] \tag{3.44e}$$

In anisotropic media the $\underset{\sim}{D}$ vectors of the ordinary and extraordinary waves are polarized in the directions $\hat{d}_1$ and $\hat{d}_2$ respectively, which are both perpendicular to the wave normal $\hat{S}$, and each is perpendicular to the non-corresponding $\hat{e}$ vector

$$\hat{d}_1\cdot\hat{e}_2 = 0 = \hat{d}_2\cdot\hat{e}_1 \tag{3.49}$$

The scalar products of Eq. (3.44e) with $\hat{d}_1$ and $\hat{d}_2$ yield the remaining field components:

$$E_1 = 4\pi \left(\frac{\omega}{c}\right)^2 p_{\omega\kappa}\left[\hat{d}_1\cdot\hat{p} - (\hat{d}_1\cdot\epsilon\cdot\hat{s})(\hat{p}\cdot\hat{s})/(\hat{s}\cdot\epsilon\cdot\hat{s})\right] / (\hat{d}_1\cdot\hat{e}_1)(k^2-k_1^2) \qquad (3.48b)$$

$$E_2 = 4\pi \left(\frac{\omega}{c}\right)^2 p_{\omega\kappa}\left[\hat{d}_2\cdot\hat{p} - (\hat{d}_2\cdot\epsilon\cdot\hat{s})(\hat{p}\cdot\hat{s})/(\hat{s}\cdot\epsilon\cdot\hat{s})/(\hat{d}_2\cdot\hat{e}_2)(k^2-k_2^2)\right. \qquad (3.48c)$$

In equations (3.47) and (3.48), k_1, $_2$ denote the wave vectors for ordinary and extraordinary waves and are given in terms of the phase velocities v_0 and v_ℓ of the ordinary and extraordinary waves belonging to the wave normal $\hat{S}$; i.e., $k_1 = \omega/v_0$, $k_2 = \omega/v_\ell$.

These ratios like $\epsilon_x/p_{\omega x}$ needed for Eq. (3.42) come from Eqs. (3.46) and (3.48) when $\hat{e}_1$, $\hat{e}_2$, and $\hat{S}$ are projected on to the x, y, and z axes. To progress from Eqs. (3.48), we specialize to the case of uniaxial crystals.

Uniaxial Crystals

Before we can use Eq. (3.42), we have to evaluate the various scalar product terms that appear in Eq. (3.48). Assume that the motion of the source polarization is in the direction of a principal axis of the dielectric tensor ϵ. The direction of motion is $\hat{z}$ · $\hat{x}$ and $\hat{y}$ are also principal axis directions. For a uniaxial crystal, $\epsilon_x = \epsilon_y$ makes $\hat{z}$ the optic axis while $\epsilon_y = \epsilon_z$ makes $\hat{x}$ the optic axis. In the first case the source moves along the optic axis with either transverse or longitudinal polarization. The latter of these two possibilities can be solved almost by inspection by looking at the solution for Cerenkov radiation from an electron moving along the optic axis and adjusting the coefficients in a way suggested by comparison of Eqs. (3.13) and (3.37). We will concentrate on the transverse polarization case, for motion along the optic axis. This case is easier to treat, though of perhaps less interest than the case where the motion is perpendicular to the optic axis with the polarization along the optic axis. In this latter case the Cerenkov cones are not circular and the integration over θ in Eq. (3.42) is best omitted so that one can consider the azimuthal distribution of radiated energy.

Figures 14 and 15 depict the ellipsoids of wave normals for uniaxial crystals. The relevent phase velocities v_p corresponding to the wave normal $\hat{S} = (S_x, S_y, S_z)$ are derived from the equation for the normal surface

$$\frac{S_x^2}{v_p^2 - v_x^2} + \frac{S_y^2}{v_p^2 - v_y^2} + \frac{S_z^2}{v_p^2 - v_z^2} = 0 \qquad (3.50)$$

For the source moving along the optic axis (Figure 1), $v_x = v_y = v_0 = c/\sqrt{\epsilon_x}$ and $v_z = v_e = c/\sqrt{\epsilon_z}$. The solutions for v_p are then:

$$v_p = v_0 = c/\sqrt{\epsilon_x} \qquad \text{(ordinary)} \qquad (3.51a)$$

and

$$v_p = v_e = \left(\frac{c^2}{\epsilon_x} \cos^2\beta + \frac{c^2}{\epsilon_z} \sin^2\beta \right)^{1/2} \qquad \text{(extraordinary)} \tag{3.51b}$$

Equations (3.51a) and (3.51b) correspond to a sphere and an ovaloid respectively. Here β is the angle between $\hat{S}$ and $\hat{z}$. For the source moving transverse to the optic axis (Figure 15), $v_x = v_\ell = c/\sqrt{\epsilon_x}$, and $v_y = v_z = v_0 = c/\sqrt{\epsilon_z}$. The phase velocities are

$$v_p = v_0 = c/\sqrt{\epsilon_z} \qquad \text{(ordinary)} \tag{3.52a}$$

$$v_p = v_e = \left[\frac{c^2}{\epsilon_z} \sin^2\beta \cos^2\theta + \frac{c^2}{\epsilon_x} (\sin^2\beta \sin^2\theta + \cos^2\beta) \right]^{1/2} \qquad \text{(extraordinary)} \tag{3.52b}$$

Here θ is the azimuthal angle for the wave normal $\hat{S}$.

We now have sufficient information to evaluate the various unit vectors and the scalar products in Eqs. (3.48). The results for the source moving along the optic are as follows:

$$\begin{aligned}
\hat{a}_1 &= (\sin\theta, -\cos\theta, 0) \\
\hat{a}_2 &= (\cos\beta\cos\theta, \cos\beta\sin\theta, -\sin\beta) \\
\hat{S} &= (\sin\beta\cos\theta, \sin\beta\sin\theta, \cos\beta) \\
\epsilon\cdot\hat{S} &= \epsilon_z(\eta\sin\beta\cos\theta, \eta\sin\beta\sin\theta, \cos\beta);\ \eta = \epsilon_x/\epsilon_z \\
\hat{e}_1 &= \hat{a}_1 \\
\hat{e}_2 &= (\cos^2\beta + \eta^2\sin^2\beta)^{\frac{1}{2}} (\cos\beta\cos\theta, \cos\beta\sin\theta, -\eta\sin\beta) \\
\hat{p} &= \hat{x} \\
\hat{a}_1\cdot\hat{p} &= \sin\theta;\ \hat{a}_2\cdot\hat{p} = \cos\beta\cos\theta;\ \hat{p}\cdot\hat{s} = \sin\beta\cos\theta;\ (\hat{a}_1\cdot\hat{e}_1) = 1 \\
\hat{a}_2\cdot\hat{e}_2 &= (\cos^2\beta + \eta^2\sin^2\beta)^{-\frac{1}{2}} (\cos^2\beta + \eta\sin^2\beta);\ (\hat{a}_1\cdot\epsilon\cdot\hat{S}) = 0 \\
(\hat{a}_2\cdot\epsilon\cdot\hat{S}) &= \epsilon_z(\eta - 1)\sin\beta\cos\beta;\ (\hat{S}\cdot\epsilon\cdot\hat{S}) = (\epsilon_z\cos^2\beta + \eta\sin^2\beta).
\end{aligned} \tag{3.53}$$

The results for the source moving transverse to the optic axis with the polarization along the optic axis are

$$\hat{d}_1 = (1 - \sin^2\beta\cos^2\theta)^{-1/2} (0, -\cos\beta, \sin\beta\sin\theta)$$

$$\hat{d}_2 = (1 - \sin^2\beta\cos^2\theta)^{-1/2} (1 - \sin^2\beta\cos^2\theta, -\sin^2\beta\sin\theta\cos\theta, -\sin\beta\cos\beta\cos\theta)$$

$$\hat{s} = (\sin\beta\cos\theta, \sin\beta\sin\theta, \cos\beta)$$

$$\hat{e}_1 = \hat{d}_1$$

$$\hat{e}_2 = (1 - \sin^2\beta\cos^2\theta)^{-1/2} \left[1 + (\eta^2 - 1)\sin^2\beta\cos^2\theta\right]^{-1/2} (1 - \sin^2\beta\cos^2\theta, -\eta\sin^2\beta\sin\theta\cos\theta, -\eta\sin\beta\cos\beta\cos\theta)$$

$$\epsilon \cdot \hat{s} = \epsilon_z (\eta \sin\beta\cos\theta, \sin\beta\sin\theta, \cos\beta)$$

$$\hat{p} = \hat{x}$$

$$\hat{d}_1 \cdot \hat{p} = 0; \quad \hat{d}_2 \cdot \hat{p} = (1 - \sin^2\beta\cos^2\theta)^{1/2}; \quad \hat{p} \cdot \hat{s} = \sin\beta\cos\theta, \quad d_1 \cdot e_1 = 0;$$

$$\hat{d}_2 \cdot \hat{e}_2 = \left[1 + (\eta^2 - 1)\sin^2\beta\cos^2\theta\right]^{-1/2} \left[1 + (\eta - 1)\sin^2\beta\cos^2\theta\right]; \; (\hat{d}_1 \cdot \epsilon \cdot \hat{s}) = 0;$$

$$(\hat{d}_2 \cdot \epsilon \cdot \hat{s}) = (\eta - 1)\sin\beta\cos\theta(1 - \sin^2\beta\cos^2\theta)^{1/2};$$

$$(\hat{s} \cdot \epsilon \cdot \hat{s}) = \epsilon_z + \epsilon_z(\eta - 1)\sin^2\beta\cos^2\theta \tag{3.54}$$

We are now in a position to combine Eqs. (3.46) and (3.48). The case of motion along the optic axis is treated here. The following substitutions are first made:

$$k^2 = \kappa^2 + n^2\left(\frac{\omega}{c}\right)^2 \qquad \kappa^2 = \left(\frac{\omega}{c}\right)^2 \tau^2$$

$$k^2 - k_1^2 = \left(\frac{\omega}{c}\right)^2(\tau^2 + n^2 - \eta\epsilon_z) \qquad k^2 - k_2^2 = \left(\frac{\omega}{c}\right)^2\left(\tau^2 + n^2 - \frac{\eta\epsilon_z}{\cos^2\beta + \eta\sin^2\beta}\right)$$

$$\sin\beta = \tau/(\tau^2 + n^2)^{1/2} \qquad \cos\beta = n/(\tau^2 + n^2)^{1/2} \tag{3.55}$$

The field components to be substituted into Eq. (3.42) are thus

$$\mathcal{E}_x/4\pi p_{\omega\kappa} = \frac{\sin^2\theta}{\tau^2 + n^2 - \eta\epsilon_z} + \frac{n^2\cos^2\theta}{(\eta\tau^2 + n^2)(\eta\tau^2 + n^2 - \eta\epsilon_z)} + \frac{\tau^2\cos^2\theta}{\epsilon_z(\eta\tau^2 + n^2)} \tag{3.56a}$$

$$\mathcal{E}_y/4\pi p_{\omega\kappa} = \frac{-\sin\theta\cos\theta}{\tau^2 + n^2 - \eta\epsilon_z} + \frac{n^2\cos\theta\sin\theta}{(\eta\tau^2 + n^2)(\eta\tau^2 + n^2 - \eta\epsilon_z)} + \frac{\tau^2\cos\theta\sin\theta}{\epsilon_z(\eta\tau^2 + n^2)} \tag{3.56b}$$

$$\mathcal{E}_z/4\pi p = \frac{-\eta n\tau\cos\theta}{(\eta\tau^2 + n^2)(\eta\tau^2 + n^2 - \eta\epsilon_z)} + \frac{n\tau\cos\theta}{\epsilon_z(\eta\tau^2 + n^2)} \tag{3.56c}$$

The integration over θ is performed first. These integrals are of the form

$$\frac{1}{2\pi}\int_0^{2\pi} C(\theta)\, e^{i\kappa\rho\cos(\theta - \phi) + i\ell(\theta - \pi/2)}\, d\theta$$

where $C(\theta)$ is the $\sin^2\theta$, $\cos^2\theta$, $\sin\theta\cos\theta$, or $\cos\theta$. These all integrate into derivatives of Bessel functions. For example, consider the easiest one with $C(\theta) = \cos\theta$. We substitute $\rho\cos\varphi = x$ and $\rho\sin\varphi = y$. This integral is now

$$\frac{1}{2\pi}\int_0^{2\pi} \cos\theta\; e^{i\kappa(x\cos\theta + y\sin\theta)}\; e^{i\ell(\theta - \pi/2)}\, d\theta$$

Using the well known integral representation of the Bessel function, $J_\ell(\xi) = \frac{i^{-\ell}}{2\pi}\oint e^{i\xi\cos\varphi + in\varphi}d\varphi$, the above integral is obviously a derivative with respect to x of a Bessel function, and in fact is $\frac{1}{i}e^{i\ell\varphi}\frac{x}{\rho}J'_\ell(x\rho)$. The other integrals are only slightly more complicated.

The Eqs. (3.42) for E_x, E_y and E_z in terms of the remaining integrals are now as given below in Eqs. (3.57)

$$E_x = \sum_\ell 4\pi e^{i\ell\phi}\int_{-\infty}^{\infty}d\omega\, e^{-i\omega(t-nz/c)}\left(\frac{\omega}{c}\right)^2 G_2(\omega)\int_0^\infty d\tau\,\tau\, G^\ell\left(\frac{\omega\tau}{c}\right)\Big\{$$
$$\Big\{\frac{-1}{\tau^2+n^2-\eta\epsilon_z}\left[\cos^2\phi\,\frac{J'_\ell(\omega\tau\rho/c)}{(\omega\tau\rho/c)}+\sin^2\phi\,J''_\ell(\omega\tau\rho/c)\right]$$
$$-\frac{n^2}{(\eta\tau^2+n^2)(\eta\tau^2+n^2-\eta\epsilon_z)}\left[\sin^2\phi\,\frac{J'_\ell(\omega\tau\rho/c)}{(\omega\tau\rho/c)}+\cos^2\phi\,J''_\ell(\omega\tau\rho/c)\right]$$
$$-\frac{\tau^2}{\epsilon_z(\eta\tau^2+n^2)}\left[\sin^2\phi\,\frac{J'_\ell(\omega\tau\rho/c)}{(\omega\tau\rho/c)}+\cos\phi\,J''_\ell(\omega\tau\rho/c)\right]\Big\}\qquad(3.57a)$$

$$E_y = \sum_\ell 4\pi e^{i\ell\phi}\int_{-\infty}^{\infty}d\omega\, e^{-i\omega(t-nz/c)}\left(\frac{\omega}{c}\right)^2 G_2(\omega)\int_0^\infty d\tau\,\tau\, G^\ell(\omega\tau/c)\Big\{$$
$$\Big\{\frac{1}{\tau^2+n^2-\eta\epsilon_z}\left[\cos\phi\sin\phi\,\frac{J'_\ell(\omega\tau\rho/c)}{(\omega\tau\rho/c)}-\cos\phi\sin\phi\,J''_\ell(\omega\tau\rho/c)\right]$$
$$+\frac{n^2}{(\eta\tau^2+n^2)(\eta\tau^2+n^2-\eta\epsilon_z)}\left[\cos\phi\sin\phi\,\frac{J'_\ell(\omega\tau\rho/c)}{(\omega\tau\rho/c)}-\cos\phi\sin\phi\,J''_\ell(\omega\tau\rho/c)\right]\qquad(3.57b)$$
$$+\frac{\tau^2}{\epsilon_z(\eta\tau^2+n^2)}\left[\cos\phi\sin\phi\,\frac{J'_\ell(\omega\tau\rho/c)}{(\omega\tau\rho/c)}-\cos\phi\sin\phi\,J''_\ell(\omega\tau\rho/c)\right]\Big\}$$

$$E_z = \sum_\ell 4\pi e^{i\ell\phi}\int_{-\infty}^{\infty}d\omega\, e^{-i\omega(t-nz/c)}\left(\frac{\omega}{c}\right)^2 G_2(\omega)\int_0^\infty d\tau\,\tau\, G^\ell\left(\frac{\omega\tau}{c}\right)\Big\{$$
$$+\frac{\eta\tau}{\epsilon_z(\eta\tau^2+n^2)}\left[-i\cos\phi\,J'_\ell(\omega\tau\rho/c)\right]\Big\}$$
$$\Big\{\frac{\eta n\tau}{(\eta\tau^2+n^2)(\eta\tau^2+n^2-\eta\epsilon_z)}\left[i\cos\phi\,J'_\ell(\omega\tau\rho/c)\right]\qquad(3.57c)$$

We now proceed with the integrals over τ. Quite a few of the integrals can be disposed of immediately. Those that involve a Bessel function divided by ρ have asymptotic forms that go as $\rho^{-3/2}$ and contribute nothing to the radiation field. They are induction field terms. Consider now an integral like

$$\int_0^\infty d\tau\,\tau\, G^\ell\left(\frac{\omega\tau}{c}\right)\cdot\frac{1}{\tau^2+n^2-\eta\epsilon_z}\cdot J''_\ell\left(\frac{\omega}{c}\tau\rho\right)$$

Set $J''_\ell\left(\frac{\omega}{c}\tau\rho\right) = \frac{1}{2}H^{(1)''}_\ell\left(\frac{\omega}{c}\tau\rho\right)+\frac{1}{2}H^{(2)''}_\ell\left(\frac{\omega}{c}\tau\rho\right)$. Replace the integral along the positive real axis by the sum of the two contour integrals shown in Figure16 where $H^{(1)}_\ell{}''$ is integrated along the upper contour and $H^{(2)}_\ell{}''$ along the lower. $H^{(1)}_\ell$ and $H^{(2)}_\ell$ vanish along their respective contours at infinity. The vertical contributions on the two contours cancel as can be shown by using the relation

$iH^{(1)}_{\ell}(ix) = (-1)^{\ell+1} H^{(2)}_{\ell}(-ix)$. Thus the sum of the contour integrals equals the wanted integral. The poles are located at $\tau = \pm\sqrt{\eta(\epsilon_z + i\Delta) - n^2}$. These are in the first and third quadrants. The lower contour integral encloses no poles, thus it vanishes. The upper contour integral is $2\pi i$ times the residue at $\tau = \sqrt{\eta\epsilon_z - n^2}$, and thus $\frac{1}{2}\pi i\, G^{\ell}\left[\frac{\omega}{c}(\eta\epsilon_z - n^2)^{1/2}\right] H_{\ell}^{(1)\prime}\left\{\frac{\omega}{c}(\eta\epsilon_z - n^2)^{1/2}\rho\right\}$. The same technique is used for the other integrals. The contributions from the pole at $\tau = -i(n + i\Delta')/\sqrt{\eta}$ involve the function $H^{(2)}_{\ell}(-i\frac{\omega}{c}\frac{n}{\eta^{\frac{1}{2}}}\rho)$ which falls off exponentially in ρ, and gives no radiation field. The surviving integrals are now:

$$E_x = -2\pi^2 i \sum_{\ell} e^{i\ell\phi} \int_{-\infty}^{\infty} d\omega\, e^{-i\omega(t-nz/c)} \left(\frac{\omega}{c}\right)^2 G_2(\omega) \left[G^{\ell}(k_T^o)\, H_{\ell}^{(1)\prime}(k_T^o\rho) \sin^2\phi + \frac{n^2}{\eta^2\epsilon_z} G^{\ell}(k_T^e)\, H^{(1)\prime}(k_T^e\rho) \cos^2\phi \right]$$

$$E_y = -2\pi^2 i \sum_{\ell} e^{i\ell\phi} \int_{-\infty}^{\infty} d\omega e^{-i\omega(t-nz/c)} \left(\frac{\omega}{c}\right)^2 G_2(\omega) \left[G^{\ell}(k_T^o)\, H_{\ell}^{(1)\prime}(k_T^o\rho) \cos\phi \sin\phi + \frac{n^2}{\eta^2\epsilon_z} G^{\ell}(k_T^e)\, H_{\ell}^{(1)\prime}(k_T^e\rho) \cos\phi \sin\phi \right]$$

$$E_z = -2\pi^2 i \sum_{\ell} e \ldots \qquad (3.58)$$

Here k_T^o and k_T^e are the transverse k vector components for ordinary and extraordinary waves

$$k_T^o = \frac{\omega}{c}(\eta\epsilon_z - n^2)^{1/2} \qquad k_T^e = \frac{\omega}{c}\left(\epsilon_z - \frac{n^2}{\eta}\right)^{1/2} \qquad (3.59)$$

To justify the labelling in Eq. (3.59) we compute the corresponding phase velocities. For the ordinary wave we have

$$k_o^2 = \left(\frac{\omega}{v_o}\right)^2 = n^2\left(\frac{\omega}{c}\right)^2 + (k_T^o)^2 = \left(\frac{\omega}{c}\right)^2\epsilon_x \qquad (3.60)$$

Therefore $v_o = c/\sqrt{\epsilon_x}$, which is correct for the ordinary wave. For the extraordinary wave we have

$$k_e^2 = \left(\frac{\omega}{v_e}\right)^2 = n^2\left(\frac{\omega}{c}\right)^2 + (k_T^e)^2 = \left(\frac{\omega}{c}\right)^2\left[\epsilon_z + n^2\left(1 - \frac{1}{\eta}\right)\right] \qquad (3.61)$$

Let β_e be the angle between $\underline{k}_e$ and $\hat{z}$. Then $\cos^2\beta_e = \frac{n^2}{\epsilon_z + n^2\left(1 - \frac{1}{\eta}\right)}$, which can can be solved for n^2.

$$\frac{N^2 = E\cos^2\beta_e}{1 - (1 - \frac{1}{M})\cos^2\beta_e} \qquad (3.62)$$

Substituting Eq. (3.62) into Eq. (3.61) we get

$$\frac{c^2}{v_e^2} = \frac{\epsilon_z}{1 - \left(1 - \frac{1}{\eta}\right)\cos^2\beta_e} \qquad (3.63a)$$

or

$$\frac{v_e^2}{c^2} = \frac{\cos^2\beta_e}{\epsilon_x} + \frac{\sin^2\beta_e}{\epsilon_z} \tag{3.63b}$$

This is identical to Eq. (3.51b), so our identification of this wave vector with the extraordinary wave is correct.

The Eqs. (3.58) are of the form

$$E_x = \int_{-\infty}^{\infty} \left\{ E_x^{(0)}(\omega) + E_x^{(e)}(\omega) \right\} e^{-i\omega t} d\omega \tag{3.64}$$

with similar expressions for E_y and E_z. The superscripts o and e refer to the ordinary and extraordinary fields and the two fields can be treated separately. The asymptotic expressions for E_x, E_y, and E_z can be written down by using the asymptotic relations:

$$-H_\ell^{(1)\prime}(z) \simeq -iH_\ell^{(1)\prime}(z) \simeq H_\ell^{(1)}(z) \simeq \sqrt{\frac{2}{\pi z}}\, e^{i[z-(\ell+1)\pi/4]} \tag{3.65}$$

The results are:

$$E_x^{(0)}(\omega) = \sum_\ell 2\pi^2 i(\omega/c)^2 G_2(\omega) G^\ell(k_T^0) \left(\frac{2}{\pi k_T^0 \rho}\right)^{1/2} e^{i\left[k_T^0 \rho - (2\ell+1)\pi/4\right]} \sin^2\phi$$

$$E_y^{(0)} \cdots$$

$$E_3^{(0)} \tag{3.66a}$$

and

$$E_x^{(e)}(\omega) = \sum_\ell 2\pi^2 i \frac{n^2}{\eta^2 \epsilon_z} \left(\frac{\omega}{c}\right)^2 G_2(\omega)\, G^\ell(k_T^e) \left(\frac{2}{\pi k_T^e \rho}\right)^{1/2} e^{i[k_T^e \rho - (2\ell+1)\pi/4]} \cos^2\phi\, e^{i\phi}\, e^{i\omega n z/c}$$

$$E_y^{(e)}(\omega) = \sum_\ell 2\pi^2 i \frac{n^2}{\eta^2 \epsilon_z} \left(\frac{\omega}{c}\right)^2 G_2(\omega)\, G^\ell(k_T^e) \left(\frac{2}{\pi k_T^e \rho}\right)^{1/2} e^{i[k_T^e \rho - (2\ell+1)\pi/4]} \cos\phi \sin\phi\, e^{i\ell\phi}\, e^{i\omega n z/c}$$

$$E_z^{(e)}(\omega) = \sum_\ell -2\pi^2 i \frac{n\left(\epsilon_z - \frac{n^2}{\eta}\right)^{1/2}}{\eta \epsilon_z} \left(\frac{\omega}{c}\right)^2 G_2(\omega)\, G^\ell(k_T^e) \left(\frac{2}{\pi k_T^e \rho}\right)^{1/2} e^{i[k_T^e \rho - (2\ell+1)\pi/4]} \cos\phi\, e^{i\ell\phi}\, e^{i\omega n z/c} \tag{3.67a}$$

The cylindrical components are readily found from the rectangular components. The angular factors are as follows

$$E_\rho^{(0)}(\omega) \sim \sin\phi \sin 2\phi\, e^{i\ell\phi}$$

$$E_\phi^{(0)}(\omega) \sim \sin\phi \cos 2\phi\, e^{i\ell\phi} \tag{3.66b}$$

$$E_\rho^{(e)}(\omega) \sim \cos\phi\, e^{i\ell\phi}$$

$$E_\phi^{(e)}(\omega) = 0 \qquad (2.67b)$$

The magnetic field components are obtained from

$$H(\omega) = -i\left(\frac{c}{\omega}\right) \text{curl}\, E(\omega) \qquad (3.68)$$

$$H_\rho^{(0)}(\omega) = -n\, E_\phi^{(0)}(\omega) \qquad H_\phi^{(0)}(\omega) = E_\rho^{(0)}(\omega) \qquad H_z^{(0)}(\omega) = \frac{ck_T^e}{\omega} E_\phi^{(0)}(\omega) \qquad (3.69)$$

$$H_\rho^{(e)}(\omega) = 0 \qquad H_\phi^{(e)}(\omega) = n E_\rho^{(e)}(\omega) - \frac{ck_T^e}{\omega} E_z \qquad H_z^{(e)}(\omega) = 0 \qquad (3.70)$$

Evaluation of the Poynting vectors gives

$$\left[E^{(o)}(\omega) \times \bar{H}^{(o)}(\omega)\right]_\rho = \frac{ck_T^o}{\omega} E_\phi^{(o)} E_\phi^{(o)} = 8\pi^3\left(\frac{\omega}{c}\right)^3 |G_2(\omega)|^2 \left[G^\ell(k_T^o)\right]^2 \frac{1}{\rho} \sin^2\phi\cos^2 2\phi \qquad (3.71a)$$

and

$$\left[E^{(e)}(\omega) \times \bar{H}^{(e)}(\omega)\right]_\rho = \frac{ck_T^e}{\omega} E_z^e \bar{E}_z^e - E_z^e \bar{E}_\rho^e$$

$$= 8\pi^3\left(\frac{\omega}{c}\right)^3 \left|G_2(\omega)\right|^2 \left[G(k_T^o)\right]^2 \frac{1}{\rho} \frac{n^2}{\eta^2\epsilon_z} \cos^2\phi \qquad (3.71b)$$

Integration of the Poynting vector gives the energy radiated. For the ordinary waves we find

$$\frac{d^2W}{d\omega dz} = 2\pi^4 \frac{\omega^3}{c^2} \left|G_2(\omega)\right|^2 \left[G^\ell(k_T^o)\right]^2 \epsilon_\ell \qquad (3.72)$$

where $\epsilon_\ell = 1$ for $\ell = 0$
$= 1/8$ for $\cos\varphi$, $3/8$ for $\sin\varphi$
$= \frac{1}{2}$ for $\ell > 1$,

while for the extraordinary waves the result is

$$\frac{d^2W}{d\omega dz} = 4\pi^4 \frac{\omega^3}{c^2} \left|G_2(\omega)\right|^2 \left[G^\ell(k_T^e)\right]^2 \frac{n^2}{\eta^2\epsilon_z} \epsilon_\ell \qquad (3.73)$$

3.4 Summary

The interesting case that we still have not worked out in detail is that where

the source motion is transverse to the optic axis, with the polarization along the optic axis. This will probably be examined later. The case of motion along the optic axis with longitudinal polarization is less interesting, but the problem can be solved by inspection as noted earlier.

The coupling problem solved here between the NLO source polarization and a microwave field is probably the only one that has been treated anywhere to date. We were able to treat the problem fairly exactly because the microwave field we considered is unguided. The case with different boundary conditions on the microwave field will be more relevant to the submillimeter wave generation problem, and we feel better prepared to look at such cases now that we understand the most elementary one.

Section 4

AN EXTENSION OF TPF TECHNIQUES TO SIMULTANEOUS POWER SPECTRUM AND PHASE STRUCTURE MEASUREMENTS

There is considerable interest in non-linear optical phenomena that modify the amplitude and phase structure of short optical pulses. Some of these phenomena have been discussed extensively in the literature already. such as the self-steepening of light pulses propagating in Kerr-active liquids and the associated self-phase modulation.[85,86] Indirect evidence of the phase-modulation has been inferred from spectral broadening measurements,[87] which show a characteristic spacing[88] between the zeros of the power spectrum of the output pulses. More direct evidence has been obtained by studying the output from a grating pair compressor with and without the Kerr-active liquid in the beam.[89] Evidence of self-steepening processes occurring in a mode-locked laser has been obtained previously in this laboratory.[90] More recently, interest has developed in non-linear modifications to the propagating pulse in the presence of the propagating microwave signal generated by optical rectification,[91] and in simultaneous front and back end shock formation in high power optical pulses.[92]

Much of this interest centers around the possibility of generating optical pulses of $\sim 10^{-14}$ second or shorter duration.[93] The various proposals for 10^{-14} sec pulses involve the addition of phase modulation to the pulse and the subsequent compression of those parts of the pulse that have the appropriate frequency sweep characteristics. using pulse compression techniques similar to those initiated in this laboratory.[94] In this type of investigation, it would be desirable to obtain simultaneous power spectrum, phase structure and intensity profile information on a single pulse before trying to compress it. We have investigated the extent to which such information is obtainable using the well established principles of spectroscopy and the more recent two-photon fluorescence (TPF) technique[95,96] and we are in the process of setting up the equipment to make measurements. We believe that the technique we are developing will come close to extracting the maximum available information from a single pulse measurement. A simplified and very approximate theory of the measurement technique and a description of the experimental equipment follow. When experimental results are obtained, a more precise theory will be developed.

At a fixed point, the optical fields of a pulse vary in time as $A(t)e^{i\phi(t)}$ where the principal term in $\phi(t)$ is $\omega_0 t$. The rate of change of the phase is $\dot{\phi}(t)$, which varies in time if there is phase modulation. One could detect the phase modulation by taking a set of filters in the same region of space tuned to different center frequencies $\omega_1, \omega_2, \omega_3$, etc. with the same bandwidth $\delta\omega$, and observing the sequential responses of these filters as the pulse goes by. This is illustrated in Fig. 17 for a complex phase modulation in a pulse with large time-bandwidth product. The optimum filter bandwidths would depend on the phase and amplitude structure of the pulse, but a feeling for the magnitudes involved can be obtained simply by considering a smooth pulse envelope (e.g., Gaussian) with a linear frequency chirp. The product of the

pulse duration T and the pulse bandwidth ($\Delta\omega/2\pi$) is denoted by N, i.e. $T\Delta\omega/2\pi = N$. Therefore $(T/\sqrt{N})(\Delta\omega/2\pi/\sqrt{N}) = 1$. A filter of bandwidth $(\Delta\omega/2\pi/\sqrt{N})$ has a response time duration of approximately its reciprocal, which in this case is $T/\sqrt{N}$. Hence, by dividing the bandwidth into $\sqrt{N}$ parts, the original pulse duration can be resolved into $\sqrt{N}$ filter responses. The curve $\varphi(t)$ versus t can in this case be drawn with $\sqrt{N}$ resolvable points. At the same time, the power spectrum versus ω can be sketched out with $\sqrt{N}$ resolvable points. We do not expect to be able to do better then this with a single pulse. If m identical pulses could be generated, the effective time-bandwidth product becomes mN, and the phase and power spectrum curves could be drawn with $\sqrt{(mN)}$ resolvable points.

The construction of $\sqrt{N}$ separate filtering devices that could be located in the same region of space looks difficult if one thinks in terms of multilayer film devices, etc. Our approach to the problem is indicated in Figure (18). The laser pulse is analysed in a low resolution spectrometer, and the relative arrival times of different spectral components in the focal plane is measured by "two-photon fluorescence" techniques. The incident beam is expanded in a Galilean telescope, then is diffracted from a ruled grating with 1200 rulings per millimeter. The energy in the light pulse, which was distributed in a disk at right angles to the propagation direction is now distributed in a volume that is canted relative to the general propagation direction. The resolving power at this point, for first order diffraction, equals the number of rulings intercepted by the incident beam. The stepped mirror again distributes the pulse energy into a disk at right angles to the beam direction, although the energy distribution is canted in any local region. (The angle at which the pulse is canted is determined by the angular dispersion caused by the grating.) The resolving power of the spectrometer has now been degraded to the number of rulings in the intercept of Figure (19), while the angular dispersion is left unchanged.

We have constructed an apparatus like that shown in Figure (18). The stepped mirror has about 60 elements, and was made by annealing, grinding, polishing and tilting a stack of microscope slides. The filter bandwidth of this system at any point in the focal plane is about 20 cm^{-1}, and the angular dispersion in the focal plane is about 14 cm^{-1} per millimeter.

At each point in the focal plane there is a filtering property with center frequency that varies linearly across the plane and with filter bandwidth determined by the degraded resolution. The focal plane is in the center of a Rhodamine 6G fluorescent dye cell[97]. One beam is inverted so that the ω_1 versus x characteristic is reversed. For a linearly chirped pulse, the wavepackets would be slewed in the manner illustrated by Figure ( ) as they approach the focal plane. The TPF display of such a chirped pulse would be slewed as illustrated by the shaded region in Figure (20). Denoting the time of arrival of the spectral energy centered around frequency ω by $t(\omega)$ the TPF displays the odd function

$$T(\Delta\omega) = t(\omega_0 + \Delta\omega) - t(\omega_0 - \Delta\omega) = -T(-\Delta\omega) \qquad (4.1)$$

for the phase structure and the spectral function

$$S(\Delta\omega) = \int I(\omega_0 + \Delta\omega;t')\ I(\omega_0 - \Delta\omega;t')dt' \qquad (4.2)$$

where the simulaneous functional dependence on frequency and time is constrained by the time-bandwidth product considerations mentioned earlier.

This new technique for using TPF has the great advantage of being able to present phase structure information over a frequency band that exceeds the bandwidth of the two-photon absorption. By adjusting the relative horizontal positions of the two beams the frequency ω_0 can be placed in the middle of the two-photon absorption band. Since we correlate between $I(\omega_0 + \Delta\omega)$ and $I(\omega_0 - \Delta\omega)$ the sum frequency involved in the TPF is always $(\omega_0 + \Delta\omega) + (\omega_0 - \Delta\omega) = 2\omega_0$ as indicated in Figure (20). So even when $\Delta\omega$ greatly exceeds the two-photon absorption bandwidth, the TPF display is still visible and in fact will show an increasing contrast against the background as $\Delta\omega$ increases.

Figure (21) shows the TPF display produced by directing the output train of pulses from a mode-locked neodymium glass laser through the apparatus. The similarity between this Figure and Figure (20) is preliminary evidence that the technique works. Our aim is to optimize the technique and use it for investigation of nonlinear optical effects that change the phase structure of picosecond pulses.

Section 5

STIMULATED SCATTERING AND NONLINEAR PROPAGATION

5.1 Transient Stimulated Raman Scattering

During the semi-annual report period, a number of experiments on stimulated Raman scattering with picosecond laser pulses have been carried out in collaboration with Dr. R. L. Carman, Dr. F. Shimizu, J. Reintjes and Professor N. Bloembergen of Harvard University*.

The essential difference between stimulated Raman scattering with nanosecond duration pulses from a Q-switched laser and that produced with picosecond pulses from a mode-locked laser lies in the fact that phonons generated in the scattering process require time to build up. The characteristic time associated with this build up is the reciprocal of the spontaneous Raman linewidth. In liquids, for those lines which have been stimulated, the linewidths range from about 0.1 cm^{-1} to 20 cm^{-1}, giving a phonon build up time of 0.5 to 100 psec. Consequently, while the "steady state" can be achieved in stimulated scattering with Q-switched pulses, the scattering produced by mode-locked pulses of picosecond duration must be transient.

More quantitatively, the optical electric field, $E(z,t)$, produces in the molecular vibrators a dipole moment, p, proportional to the molecular polarizability, α, that is,

$$p = \alpha E \tag{5.1}$$

In general, the molecular polarizability is a function of the normal coordinates, q_ℓ, of the various normal vibrational modes of the molecules. Taking for simplicity only a single mode with normal coordinate, q, the polarizability may be expanded to give

$$p = \alpha_o E + \left(\frac{\partial \alpha}{\partial q}\right)_o qE \tag{5.2}$$

The effect of this polarization on the electric field can be found by substituting Eq. (5.2) into Maxwell's equations, remembering that the bulk polarization is just N times the above, where N is the molecular density. In a similar fashion, the electric field also affects the molecular vibration. Let us assume

$$E = E_L(z,t)e^{i(k_L z - \omega_L t)} + E_S(z,t)e^{i(k_S z - \omega_S t)} + c.\,c. \tag{5.3}$$

and

---

* The contributions of the Harvard group supported under NASA Grant NGR22-007-117 and Joint Services Electronics Program Contract N00014-67-A-0298-0006.

$$q = Q(z,t)e^{i(k_{ph}z - \omega_0 t)} + c.\ c. \tag{5.4}$$

where E_L and E_S represent the laser and Stokes fields respectively, $\omega_S = \omega_L - \omega_0$ and $k_{ph} = k_L - k_S$. If laser depletion is neglected, Maxwells' equations yield

$$\frac{-\partial E_S}{\partial z} = i\gamma_1 Q^* E_L \tag{5.5}$$

where

$$\gamma_1 = \frac{2\pi N\omega_S^2}{c^2 k_S}\left(\frac{\partial\alpha}{\partial q}\right)_o \tag{5.6}$$

Similarly from the equation of motion for the molecular vibration

$$\frac{\partial Q^*}{\partial t} + \Gamma Q^* = i\gamma_2 E_S E_L^* \tag{5.7}$$

where t is now the retarded time, Γ is the Raman linewidth and

$$\gamma_2 = \frac{1}{\omega_0\mu_0}\left(\frac{\partial\alpha}{\partial q}\right)_o \tag{5.8}$$

Here μ_0 is the reduced mass for the vibration.

The coupled Eqs. (5.5) and (5.7) can be treated conveniently in two limits. The first is the so called steady state limit where $\frac{\partial Q^*}{\partial t} \ll \Gamma Q^*$. Roughly speaking this corresponds to the case that the laser pulse duration is long compared to the vibrational damping time, $1/\Gamma$. Consequently, the molecular vibrations are able to follow the changes in the optical fields. In this limit

$$E_S(z,t) \propto \exp\left(\frac{\gamma_1\gamma_2}{\Gamma}\ |E_L|^2\ z\right) \tag{5.9}$$

The Stokes wave experiences exponential gain with a gain coefficient

$$g = \frac{\gamma_1\gamma_2}{\Gamma}\ |E_L|^2 \tag{5.10}$$

Since $\gamma_1\gamma_2 \propto \sigma$, the integrated Raman cross section, only lines with both a large cross section and a narrow Raman linewidth will exhibit high gain. It is for this reason that nearly all of the lines stimulated with Q-switched lasers represent symmetric stretching modes.

The transient limit, $\frac{dQ^*}{dt} \gg \Gamma Q^*$, corresponds approximately to the case where the laser pulse is short compared to the reciprocal linewidth. In this case the molecular vibrations cannot follow the envelope of the optical pulses. The general solutions to Eqs. (5.5) and (5.7) were first given by Wang[98]. They have since been discussed in some detail by Carman, Shimizu, Wang and Bloembergen[99]. In the transient limit it is found that near the peak of the laser pulse

$$E_S(z,t) \propto \exp\left(\gamma_1\gamma_2 z \int_{-\infty}^{t} |E_L|^2 \, dt\right)^{\frac{1}{2}} \tag{5.11}$$

The Stokes wave again experiences gain but the gain is considerably less than the under steady state conditions. This is simply a reflection of the fact that the phonon wave has insufficient time to build up to its steady state amplitude.

Of particular importance is the fact that in contrast to the steady state result, Eq.(5.11) shows the transient gain to be independent of the Raman linewidth. To exhibit high gain a Raman line need only have a large cross section. On this basis stimulated Raman scattering with picosecond laser pulses would be expected to occur in different lines and in a wider variety of materials than with Q-switched laser pulses. This prediction has found verification in our most recent experimental work[100,101].

Also of interest is the unusual time and distance dependence indicated in Eq. (5.11). The Stokes gain is seen to reach a maximum after the peak of the laser pulse. This is a consequence of the continuing build up of phonon wave amplitude. This continuing build up results not only in a delay in the Stokes pulse emission but also results in a Stokes pulse width which is critically dependent on the detailed time evolution of the laser pulse. If the laser pulse has sharp leading and trailing edges, such as for example, in a square pulse, the Stokes pulse will be dramatically sharpened as the result of the high gain occurring at the trailing edge of the laser pulse. If the laser pulse has a long precursor or a long trailing edge, the Stokes pulse can be considerably longer than the laser pulse. For a Gaussian laser pulse shape, the laser and Stokes pulses should have about the same duration[99].

5.2 Experimental Results - Liquids

Transient stimulated Raman scattering has been observed at United Aircraft in both liquids and gases using a mode-locked ruby laser. Attempts have also been made at the McKay Laboratory by the Harvard group to observe stimulated Raman scattering with a mode-locked neodymium laser. They have been able to reproduce many of the results with the liquids using a frequency doubled beam but have had no success without frequency doubling and have been unable to reproduce any of the results in the gases.

With the mode-locked ruby laser stimulated Raman scattering was observed in all the liquids tried. These included liquids like carbon tetrachloride, water, methanol, ethanol, propanol and acetic acid where stimulated scattering is obtained only with difficulty with Q-switched pulses. Stimulated scattering was also observed in the more usual Raman materials like benzene, chlorobenzene, carbon disulfide and acetone. In all cases, the scattering could be observed with a collimated input beam. Sample cell lengths of 25, 50 and 75 cm were used.

Figure (22)shows a laser pulse train and the corresponding Stokes pulse train for carbon tetrachloride. It is not yet understood why the Stokes pulse train peaks early in the laser train and falls off rapidly toward the middle and end. The forward to backward Stokes emission ratio was measured and was found to be greater than 1000:1, the limit of measurability in that experiment. This confirms the traveling wave nature of the scattering. In addition, the gain in the backward direction was measured by reflecting the forward emitted Stokes radiation back through the liquid cell. There was negligible gain. This result indicates that any background intensity upon which the mode-locked pulses are superimposed must be at least 1000 times less intense than the picosecond pulses themselves. This information is quite important in studying traveling wave interactions, such as the present one.

Of all the liquids tested, carbon tetrachloride showed the greatest energy conversion. Up to 20% of the 0.5 J energy in the laser pulse train was converted to Stokes energy. The relatively high conversion allowed a Stokes pulse width measurement by the two photon absorption-fluorescence technique. Rhodamine 6G in ethanol was found to be a suitable material for that purpose. Figure(22) shows the result. It can be seen that the Stokes pulse duration is comparable to the laser pulse duration (5-10 psec). The fact that the two pulse widths are about comparable lends support to the notion that the laser pulse shape is Gaussian[102]. The spectral width of the first Stokes and of the laser line were also comparable.

Spectra were taken of the outputs of a number of liquids. All showed considerable generation of Stokes in several orders but, curiously, very little anti-Stokes generation. The Stokes line in carbon tetrachloride and chlorobenzene was found to be a doublet, in contrast with the results with Q-switched lasers where a single shift of 459 cm^{-1} is reported. The doublet may arise because of the two isotopes of the chlorine. In methanol, two separate lines are observed, one at 2833 cm^{-1} corresponding to a C-H Stretching mode and one at 2941 cm^{-1} corresponding a symmetrical CH_3 bending mode. Figure (23) illustrates both the spontaneous and stimulated scattering with bending mode. The transient nature of the scattering process contributes heavily toward allowing stimulated scattering in this rather broad line to be observed.

Near and far field patterns have also been taken with many of the liquids. The far field patterns indicate a Stokes beam divergence of from 3 to 10 mrad depending on the liquid used. This is to be compared with a laser beam divergence of about 1 mrad. The anti-Stokes far field patterns show an emission principally in the forward direction but also in phase matched cones. The near field photographs indicate Stokes emission both from the whole beam and from small filaments in the case of long cells. With short cells emission is observed only from the filaments, indicating that as in

the case with Q-switched lasers the threshold for Raman scattering in the liquids is determined by self-trapping and not by the Raman effect itself. The sharp threshold for the trapping and Stokes generation is shown very clearly in Figure (24) . Dielectric reflectors were used to vary the laser intensity without changing the near field pattern.

Figure (25) shows self-trapping in methanol as observed at the laser wavelength, at the Stokes wavelength and at the anti-Stokes wavelength. Although the filaments are very pronounced in the Stokes and anti-Stokes photographs they do not show up in the laser photographs. Instead one observes a number of small dark areas about the same size as the Stokes filaments, suggesting that once the laser light is trapped it is nearly completely converted to Stokes and anti-Stokes. The size of the Stokes filaments varies widely depending on the material. They range from about a 5 μ diameter (resolution limited) in carbon disulfide, to about a 100 μ diameter in water. There is also a considerable range in size in any given material. In methanol, for example, the Stokes filaments run from 5 - 40 μ. Curiously, the anti-Stokes filaments vary much less in size and are generally quite small. In methanol nearly all have the resolution limited 5 μ diameter. More curious still is the fact that each of the anti-Stokes filaments is surrounded by from 1 to 6 concentric and nearly equally spaced rings of anti-Stokes light. The diameter of the first ring varies from filament to filament. The formation of these rings is believed to be related to the so called class II anti-Stokes observed in self-trapping liquids with Q-switched lasers[103].

One interesting and practical result of the self-focusing study is the fact that focusing the laser beam inhibits self-trapping. This is shown in Figure (26) where the results with a collimated beam are contrasted with those with the laser beam focused by a 50 cm focal length lens into the center of the cell. The near field photograph taken at the end of the cell shows little evidence of trapping in the latter case. This is true not only for acetic acid but for all of the low Kerr constant liquids. Recent experimental results indicate that some filamentation still does occur but it only exists over a short length near the focus of the lens. Consequently, if a high quality Stokes beam is required it is best obtained by focusing the laser into the liquid cell and recollimating afterward. The reason trapping is inhibited in the focused beam is not completely clear at the present time, but it is likely associated with the decrease in laser intensity per unit solid angle. Similar inhibition of self-focusing in focused beams has been observed by other workers[104].

5.3 Experimental Results - Gases

Recently a considerable effort has been devoted to transient stimulated Raman scattering in gases. Transient conditions are easily achieved by virtue of the fact that the linewidths are relatively narrow, even at the high pressures required to reach threshold. To observe stimulated scattering, a test cell 54 cm long was pressurized with the sample gas. The output from the mode-locked ruby laser was then focused into the center of the cell with a 50 cm focal length lens. The spectra of the stimulated scattering from gases in the cell were recorded on Kodak 1N plates using a Jarrell-Ash 75-152 Spectrograph. The experimental results for stimulated

vibrational scattering are summarized in Table I, which lists all the gases tried. The number and variety of gases in which stimulated Raman scattering has been observed stands in strong contrast to previous work with Q-switched lasers, where successful results were obtained only with methane, hydrogen and deuterium[105-108]. In other gases competition with Brillouin scattering prevented the build up of stimulated Raman scattering[106]. Transient excitation with picosecond laser pulses not only allows the stimulation of large cross section, broad lines but also very effectively discriminates against the more slowly responding Brillouin scattering.

Of all the gases examined, the largest conversion efficiencies occurred for CH_4 and SF_6. In both cases, more than twenty precent of the total incident laser energy was converted to Stokes energy. In CH_4 stimulated scattering could be produced without focusing. Stimulated vibrational scattering in a collimated beam could also be generated in SF_6, N_2 and CO_2 by telescoping down the incident ruby laser beam with a 2 power Galilean telescope.[2] Nearly all of the conversion takes place in the early pulses of the train, as is shown in Figures (27a) and (27b) for SF_6. Up to seventy percent of the energy in these initial pulses could be converted to Stokes energy as verified by the depletion of the incident laser in Figure(27a) and by direct energy measurements. The reason for the decrease in conversion towards the end of the train is not clear, but it may represent a saturation of the vibrational population. Another possibility is the build up of slower thermal or acoustic perturbations such as discussed by Pohl[109], and observed recently by one of the present authors[110].

In the case of CO_2, O_2 and N_2O, stimulated pure rotational and rotational-vibrational Raman scattering could also be produced if the incident ruby beam is circularly polarized[108]. With Q-switched lasers only hydrogen and deuterium have shown stimulated rotational scattering[107,108]. In N_2O, which has the largest rotational cross section of the three gases, both first and second order rotational and rotational-vibrational Stokes lines are excited. Evidence of rotational scattering is also seen in propylene. Figure(28)shows pure rotational Raman spectra and corresponding densitometer traces for CO_2 and O_2. In CO_2 the lines S(12) through S(24) have been stimulated, while in O_2, S(5) through S(13) have been stimulated. The line shifts observed agree within experimental error with those reported for the spontaneous spectra[111]. In the case of N_2O, the narrowness of the line spacing in comparison to the linewidths precludes an accurated identification of the stimulated lines. The observed rotational scattering spans the region from S(13) to S(20) in both orders.

Often the rotational lines observed are broadened and skewed from line center or even split into several components. This is believed to be the result of an optical Stark effect. Neglecting any permanent molecular dipole moments, the Stark shift for circularly polarized light is to lowest order in perturbation theory

$$\Delta W = \frac{4\pi}{3}\frac{\gamma I}{c}\frac{J(J+1) - 3m^2}{(2J-1)(2J+3)} \qquad (5.12)$$

where the z-axis has been chosen in the direction of propagation. Here γ is the anisotropic part of the polarizibility tensor and I is the incident intensity. Using( ), one may readily confirm that the shifts are an appreciable fraction of the total rotational

energy for the J-levels involved, and that the splitting in the rotational shifts for the different m-states is of the order of a few reciprocal centimeters, in qualitative agreement with the splitting observed. In gases, where rotational freedom is preserved, the Stark shifts are also responsible for the observed Kerr effect. For $\gamma > 0$ in Eq. (5.12), the lowest energy states are $m = \pm J$, corresponding to molecular rotation in the plane of the electric field. This is equivalent to classical alignment. Further evidence of the importance of the optical Stark effect in the transient regime is provided by the observation of self-trapping in a collimated beam in the most anisotropic gases, CO_2 and N_2O. This is clearly seen in the near field patterns shown in Figure (29).

If linearly polarized light is used in an attempt to observe stimulated rotational Raman scattering, one sees instead a broad wing shaded to the Stokes side on both the ruby line and on the vibration Stokes line. Similar results are found in the case of Rayleigh wing scattering[112]. Explanations for the difference in behavior with circular and linearly polarized light have been given by Herman[113] and by Chiao and Godine[114]. The sense of circular polarization of the stimulated first rotational and rotational-vibrational lines is always reversed from that of the incident laser light. The same situation is found in the stimulated rotational scattering from hydrogen[108] and in Rayleigh wing scattering[112]. These experimental results are in agreement with theoretical predictions giving a forward gain ratio for the opposite to same sense of polarization of 6:1, if the anti-Stokes coupling is ignored[108] and 6:0, if this coupling is taken into account[114]. The second rotational and rotational-vibrational Stokes lines observed in N_2O are polarized in the same sense as the laser light, and, therefore, in the opposite sense as the first rotational Stokes lines, as expected from the sequential nature of the higher order Stokes production (Figure 30).

5.4 Vibrational Decay Time Measurements

During stimulated Raman scattering not only is the Stokes wave amplified but so also is the phonon wave. For every Stokes photon produced, an excited vibrational quantum is also created. Stimulated Raman scattering is, therefore, a convenient way of generating a non-equilibrium population distribution. The short time scale of the present experiments makes transient stimulated Raman scattering a useful tool for the study of gas kinetics. A major area of application is in chemical laser diagnostics. These standard techniques often cannot give the desired relaxation rates under conditions pertinent to chemical laser operating conditions. Shock tube analysis is often useful but high temperatures and pressures are required. With electrical excitation ionized species and electrons are necessarily generated. In stimulated Raman scattering only the excited Raman active vibrational state is populated. Experiments can be run at room temperature or below if desired. High pressure is required for the Raman oscillator. If the relaxation rate is linear with pressure, then the results may be extrapolated. If not linear, then a low pressure Raman amplifier may be used in conjunction with a high pressure Raman oscillator. The gas properties would then be studied in the amplifier.

The simplest type of measurement would be a fluorescence measurement. Such a measurement could be used to determine the vibrational decay rate in HF as shown in Figure(31). Other candidates are the terminal laser levels in CO_2 and N_2O and the first vibrational level in CO. Preliminary experiments are now under way in HF.

A more general though more difficult technique for determining vibrational decay rate is shown in Figure(32). Here one monitors the excited state population by detecting spontaneous anti-Stokes scattering produced by a second high intensity light source, possibly another laser. Prior to the arrival of the mode-locked pulse train and the generation of stimulated Stokes light little or no spontaneous anti-Stokes light would be observed due to the absence of excited state population. The anti-Stokes intensity would build up with the creation of vibrational population during the mode-locked pulse train and would decay afterward with the decay rate to be determined. This double Raman technique has been used with a Q-switched ruby laser to determine the vibrational decay time in hydrogen gas at room temperature[115]. With transient stimulated Raman scattering, this technique can be used to make measurements in a host of different gases, including all of those listed in Table I.

Section 6

ORGANIC DYE LASERS

6.1 Simple, High Intensity, Short Pulse Flashlamps

Electrical discharge flashlamps capable of emitting intense light pulses of very short duration are required in a variety of applications, including photochemical studies and laser excitation. Special annular lamps[116,117,118] have been found particularly useful in such applications but often require considerable care in construction and are not readily adapted irradiation of irregularly shaped samples. Some performance characteristics are reported here for high intensity short pulse lamps which are easily constructed and can be formed to efficiently irradiate various sample configurations.

A number of linear cylindrical ablating wall[119,120] lamps were constructed as shown in Fig.(33a), using quartz tubing of 1 mm wall thickness for all lamp envelopes. The semi-flexible plastic (or rubber) tubes shown absorbed mechanical shocks associated with the lamp discharge and effectively prevented damage at the ends of the lamp. The wire electrodes were soldered or spot welded to the inside walls of the metal sleeves, which provided the necessary external electrical contacts. Tungsten, copper, aluminum, and stainless steel electrodes were tested and all were found to give similar results. Performance was also essentially unchanged when the lamps were bent into various forms for irradiation of irregularly shaped samples, as in Fig.(36b)

To enhance the light pulse risetime and to minimize the internal explosive shock associated with the intense short duration discharges, the lamps were continuously evacuated. A small continuous air leak was provided in the pumping line to maintain residual gas pressure high enough (typically 1 to 3 torr) to ensure rapid reproducible discharge initiation, but low enough to minimize explosive lamp failures. No significant changes were observed when gases such as argon, helium, xenon, nitrogen, and CO_2 were substituted for air in the lamps. This is consistent with the idea that the discharge was carried primarily be ablation products from the quartz walls while the residual low pressure gas served only to facilitate discharge initiation.

Electrical energy storage for the lamp was provided by low inductance capacitors (Maxwell Laboratories, Series M) which were connected to the lamps through a triggered spark gap (EG&G, Model GP-142) as shown in Fig.(34). To minimize pulse risetimes, all electrical connections in the discharge circuit were made as short as possible. In some cases several lamps were connected in parallel with another, and all were discharged simultaneously (measured delay between lamps, less than 0.05 μsec) through the spark gap.

Each lamp was tested to destruction to determine the explosion energy, i.e. the discharge energy above which the lamp would fail within one or a few shots. The failure mode in these tests was always that of violent explosion near the center of the lamp envelope.

After determination of the explosion energy for a given lamp, an identical lamp was fired at approximately seventy percent of the explosion energy and the light pulse risetime, duration, and peak intensity were recorded, using an S-4 photodiode and an oscilloscope with a total instrumental response time shorter than 2.5 nsec.

Operation of a lamp at energies higher than seventy percent of the explosion energy generally resulted in increased light pulse fall times without substantially increasing the peak intensity. Risetimes were somewhat shorter at energies near the explosion limit, but lamp life was greatly reduced from the several hundred shots often obtained at seventy percent of the explosion energy.

Performance characteristics typical of the lamps tested are presented in Table II. As expected, the light pulse risetimes (10% to 90%) were shortest for the smallest capacitors used, due to their relatively low inductance. Risetimes were also dependent to some extent on lamp geometry, generally increasing significantly for long thin lamps whose inductance contributed excessively to overall circuit inductance, and for large diameter lamps in which wall ablation apparently developed slowly due to the large free channel available to the discharge. Data for lamps exhibiting risetimes in excess of a microsecond are not included in Table I since conventional gas filled lamps can often be used in applications where longer risetimes are permissible.

Pulse widths (between half intensity points) were generally greatest for lamps of large energy handling capability and tended to be smallest for lamps of small diameter in which emitting atoms were apparently quickly deexcited by wall collisions. Peak light intensity and energy handling capability were found to increase with increasing lamp dimensions and in fact were quite simple related to the projected area (length times diameter) of the lamps, as shown in Fig.(35). The simplicity of the approximate empirical relations of Fig.(35) makes it possible to quickly compare energy handling capabilities and maximum light intensities for various lamp configurations. It should be recognized however that extrapolation of these results to lamps of very large diameter or length may not be justified.

The two righthand columns in Table I represent quantities roughly indicative of the total light emitted (the product of half power pulse width by peak light intensity) and of the rate of rise of light intensity (the ratio of peak light intensity to light pulse risetime). The latter quantity may be useful in characterizing lamps designed for certain applications, such as organic dye laser excitation, where fast rising intense light pulses are required.[17]

Measurements using a ballistic thermopile in conjunction with various filters indicated that the lamps used in these tests radiated more than twenty percent of the electrical input energy into the 2000 to 6000 Å spectral region, with more than three fourths of the radiation falling in the 2000 to 4000 Å range. These measurements, combined with the results of several tests performed to estimate lamp emissivity,

suggest that within this spectral range the lamps emit essentially as blackbody radiators with temperatures in the 20,000 to 30,000 °K range. The corresponding steradiancy at peak intensity in the 2000 to 4000 Å spectral range would thus be typically a few hundred watt/(cm^2. steradian. Å).

As a practical test for lamps of the type described above, five lamps 200 mm long with 3 mm bores were placed alongside a 10 mm dia by 200 mm long quartz cell containing a 10^{-4} molar solution of either rhodamine 6G or 7-diethylamino-4-methyl coumarin in ethanol. Broadband mirrors of 100 percent and 33 percent reflectivity, respectively, were placed at either end of the cell and aligned perpendicular to the cell axis. When all lamps were simultaneously fired in parallel through the spark gap, using a total stored electrical energy of about 700 J, laser oscillation ensued at the expected wavelengths of about 5700 Å for the rhodamine and 4600 Å for the coumarin dye. Typical oscillographs of the lamp pulse and of the coumarin laser output are shown in Fig.(36) The laser output energy emitted through the 33 percent mirror was about one joule in each case, being somewhat higher for the rhodamine dye. This represents one of the highest output energies reported to date for organic dye lasers of this type and demonstrates one practical application of the above described lamps.

6.2 Ultra Fast Flashlamps for Dye Lasers

Since the development of dye lasers two different approaches to the problem of pumping the dyes have been pursued. Laser pumping was first demonstrated in infrared emitting dyes using a Q-switched ruby laser[121]. With frequency doubling this technique was then extended to visible and near UV emitting dyes[122]. More recently, the pulsed nitrogen laser has been used with great success to pump a wide variety of dyes over the UV, visible and near IR regions of the spectrum[123,124]. The fast risetimes achievable with laser pumping avoid the problem presented by singlet to triplet crossover and result in a relatively high conversion efficiency. Flashlamp pumping was first demonstrated in 1967 by Sorokin and Lankard[125]. The most successful flashlamps to date are those of Furumoto and Ceccon,[126] who have achieved lasing in many of the dyes which can be pumped with laser pumping. Flashlamps offer the advantage of broadband pumping and generally higher output energies. Considering that the pumping is a one step process, the overall efficiency is often higher. The principal disadvantage of flashlamps is that fast risetimes have not been achieved so that triplet quenching limits the number of dyes which can be made to lase. A flashlamp with a risetime of 5-10 nanoseconds and an energy handling capability of a few joules would offer all the advantages of both methods of pumping. During the semi-annual report period an experimental effort to devise such a lamp was initiated.

For the initial efforts storage in high voltage, barium titirate "doorknob" capacitors was tried. These are commonly available in a 500 picofarad capacitance and a 20 or 30 kV operating voltage. The 30 kV capacitors have a self-resonant frequency of about 50 Mc, while the 20 kV capacitors have a 60 Mc self-resonant frequency. Two types of discharges were tried, an unconfined discharge in air or

nitrogen, and a capillary discharge in nitrogen. The results with a test fixture holding three (3) of the 30 kV capacitors are shown in Fig. (37). These photographs represent an input energy of about 3/4 joule at 33 kV in each case. For the open arc 1.2 cm diameter ball electrodes, separated by 1.5 cm were used. The light output has a 10 nsec risetime and a width at half-maximum of 35 nsec. This is about the risetime expected considering the 30 Mc self-resonant frequency for the test fixture. With the capillary discharge the light output had a risetime of 18 nsec and a width at half-maximum of 70 nsec. The peak light output is about the same. The arc was 1.5 cm long and confined to the inside of a 1 mm bore quartz capillary tube with a 0.5 mm wall thickness. A pressure of 3 atm of N_2 was necessary to hold off the 33 kV firing voltage; however, the light output and risetime were found to be fairly insensitive to pressure over a range of from 1 to 4 atm. A parallel trigger was used to fire the lamp. The slower risetime of the capillary lamp is believed due to the formation of a hotter, smaller diameter and, therefore, higher inductance arc. The greater integrated light output in the capillary lamp attributes to the hotter discharge. Similar results have been found by other workers with somewhat slower discharges[127].

The open air arc was coupled with a dye cell in an effort to produce lasing in an ethanol solution of rhodamine 6G. In fact, lasing was obtained even with only a 30 percent output reflector. However, the lasing was very erratic due principally to the very erratic behavior of the open arc in the presence of a near by ground plane. Attempts to correct this problem were unsuccessful.

As a result of these experiments a mylar insulated 30 kV strip line capacitor storing two (2) joules is under construction. The erratic behavior of the open arc discharge in the presence of the dye cell mandates the use of capillary lamps. To reduce the circuit inductance several of these will be used in parallel in a scheme similar to that in the 700 joule flashlamp array described in Section 6.1.

6.3 Mode-Locked, Flashlamp Pumped Coumarin Dye Laser at 4600 Å

Experiments during this period have resulted in what is believed to be the first mode-locking of a flashlamp pumped dye laser operating in the blue region of the spectrum. Dyes suitable for passive mode-locking of such lasers are difficult to find, due to the extremely large absorption cross sections required. However, the technique of intracavity modulation at the longitudinal mode difference frequency[128] is readily applied to mode-locking the relatively long duration, high intensity output pulses typical of these lasers.

The laser used in these experiments consisted of 100 percent and 33 percent reflectors spaced by 160 cm, with a 20 cm by 1 cm dia quartz cell centered between the reflectors and filled with a 10^{-4} molar solution of 7-diethylamino-4-methyl coumarin in ethanol. The dye solution flowed through the cell at a rate of about one liter per minute and was excited by means of five specially constructed linear flashlamps, of the type described in Section 6.1, symmetrically placed alongside the cell. The lamps were fired simultaneously through a triggered spark gap from a 3.6 microfarad

capacitor charged to 20 kV. The resulting flash was characterized by a half-intensity duration of a few microseconds and a risetime of several hundred nanoseconds.

An acoustically driven fused quartz block was located in the laser cavity close to the 100 percent reflector and periodically diffracted a few percent of the laser radiation out of the cavity by virtue of the acoustic standing wave in the block.[128] When the periodicity of the diffraction was made equal to the 11 nsec round trip transit time of radiation in the laser cavity, the 4600 Å laser output seen through the 33 percent reflector exhibited the mode-locked characteristics shown in Fig.(38).

6.4 Superradiant Traveling Wave Dye Laser

In recent years a number of dye solutions have been made to lase with either flashlamp or laser pumping. One striking characteristic of many of these dyes is the very high gain which can easily be obtained. Neumann and Hercher[129] have recently demonstrated lasing in a laser pumped rhodamine 6G solution a millimeter thick with cavity mirrors having a reflectivity of only a few percent. Experiments such as this suggest that with a solution thickness of a few centimeters and with a somewhat higher pumping density, superradiant emission should be observed.

Of particular interest is the case of pumping with picosecond duration pulses from a mode-locked laser. The dye inversion is then a wave traveling with a velocity equal to that for a pump pulse. This situation parallels that in Shipman's traveling wave nitrogen laser.[130] Superradiant traveling wave emission has been observed from several polymethine cyanine dyes pumped by a mode-locked ruby laser. This technique offers greater simplicity and ease than the more usual mode-locking technique[131] for generating short dye laser pulses.

The experimental apparatus for observing traveling wave dye laser emission is shown in Fig.(39a). Excitation of the dye was accomplished with a mode-locked ruby laser[132] which produces a train of pulses each having a duration of from 2 to 5 psec and a peak power of up to about 5 GW. A beam divergence of 1 mrad is typical for this laser. The test cell containing the dye is 2 cm thick and is wedged so that the windows make an angle of about 10° to each other. The length of the cell was chosen to be sufficiently long that stimulated emission could be achieved with a moderate dye concentration, yet the cell was short enough that stimulated Raman scattering in the solvent (methanol) was negligible. For photoelectric detection and for the far field photographs, Corning CS-7-69 filters were used to separate the dye emission from the ruby pump light. At full intensity a slight leakage of ruby light through these filters does occur but this is small compared to the dye laser emission. The additional filtering provided by the presence of the dye in the test cell reduces this leakage to below detectability.

A superradiant traveling wave emission was observed for three dyes, cryptocyanine, DDI (1, 1'-diethyl-2,2'-dicarbocyanine iodide) and DTTC (3,3'-Diethylthiatricarbocyanine

iodide) each dissolved in methanol. The results for DTTC are representative. With this dye the emission occurs in a 130 to 180 Å wide band centered at from 7920 Å to 8080 Å depending on the dye concentration. Maximum output occurs with a concentration giving a band center at 7980 Å. At this concentration the low level transmission at 6943 Å through the 2 cm test cell corresponds to an optical density of 6.0. More than 90 percent of the incident pump light is absorbed.

The output from the dye (Fig. 39b) occurs as a train of pulses which follows more or less the overall shape of the incident pump pulse train. Far field photographs such as that in Fig.(39c)show that the emission takes place in a narrow beam with an angular divergence of about 15 mrad. As in the case of pumping with a Q-switched laser,(133) the direction of polarization of the output beam is the same as that in the pump beam. With 1 joule of pump energy the total energy emitted in the forward direction is generally from 10 to 30 mJ. The forward to backward emission ratio was measured photoelectrically and was found to be about 100:1, thus confirming the traveling wave nature of the device.

An attempt was made to measure the pulse width directly by the two photon absorption-fluorescence technique. This was not successful. However, the pulse width can be inferred from other measurements. The high forward to backward emission ratio indicates that the fluorescence decay time and, therefore, the pulse duration, must be less than the 90 psec transit time through the cell. One indication of how much less is given by the fact that, if the entrance window of the dye cell is sufficiently thin, an emission occurs not only in the forward direction but alos in the direction normal to the outside face of this window. This emission arises due to the amplification of fluorescence radiation generated near the window, which travels through the window and is reflected back at the glass to air interface. The resultant emission is shown in Fig.(39d),where a window 1.5 mm thick was used. With a window twice as thick, as was the case in Fig.(39d),only a faint emission in the direction of the window normal is observed even with the entrance face nearly perpendicular to the pump beam. This indicates an appreciable decay of gain in a time equal to the difference in the round trip transit times for the two windows. That is to say, the pulse duration must be on the order of 15 psec or less.

That such short pulses are to be expected can easily be shown. In the frame of reference moving with the emitted pulses the growth of the energy density, W, per unit frequency interval per unit solid angle follows the relation(134)

$$\frac{d}{dt}W(z,t) - h\nu S(\nu)\bar{B}\Delta N(z,t) = h\nu S(\nu)\bar{A}N_2(z,t) \qquad (6.1)$$

where $S(\nu)$ is the lineshape function, $\bar{A}$ and $\bar{B}$ are the Einstein A and B coefficients per unit solid angle for given polarization and N_2 and ΔN are the excited state population and inversion in the dye, respectively. Saturation effects are ignored in Eq. (6.1). In general N_2 and ΔN are functions both of position, z, in the moving frame and of time, t. However, if the difference in group velocities of the emitted

dye laser pulse and the incident pump pulse is ignored, N_2 and ΔN are not explicitly dependent on time and Eq. (6.1) can be readily integrated.

The results are shown in Fig.(40) for an excited state population of the form

$$N_2(t_o) = N(e^{-t_o/\tau_f} - e^{-t_o/\tau_r}) \qquad (6.2)$$

Here the position, z, has been replaced by $t_o = z/v$, where v is the common group velocity. For the polymethine cyanine dyes, a fluorescence decay time of $\tau_f = 50$ psec would seem to be a reasonable estimate from the present experiments. The population risetime would be the longer of the pump pulse duration or the Franck-Condon time[135] for the dye. A value of $\tau_r = 2$ psec, corresponding roughly to the pump pulse duration, was chosen.

From Fig. 21 it can be seen that a fairly modest gain will give a substantial pulse sharpening initially. However, once the dye laser pulse duration becomes comparable to the pumping pulse duration, or more accurately, to the inversion risetime, a considerable increase in gain is required to achieve even a slight decrease in pulse duration. If the dye laser emission builds up to the point that the gain saturates, then there may be an additional pulse sharpening due to the nonlinear amplification.[136]

Although this technique has been demonstrated only for a single class of dyes all emitting in the infrared region of the spectrum, it should be possible to obtain visible region emission in other dyes by pumping with the second harmonic of either a mode-locked ruby or neodymium laser. However, the longer lifetimes of most of the other common laser dyes would necessitate a very high gain or possibly strong saturation in order to obtain picosecond pulse durations.

Section 7

OTHER AREAS OF INVESTIGATION

7.1 Stimulated Emission from Laser Produced Plasmas

The possibility of obtaining coherent radiation from laser produced plasmas is of great interest and some preliminary experimental and theoretical investigations of this possibility have been carried out. The production of ultraviolet radiation by laser action is hampered by the very fast spontaneous population decay which typifies this region of the spectrum. For efficient excitation, the pumping source must have a rise time comparable to or less than the spontaneous decay time. Conventional optical and electrical pumping sources are capable of rise times in the nanosecond region. A thousandfold improvement in this figure can be achieved through the use of picosecond laser pulses. The most general scheme for pumping would be the production of a plasma by laser induced breakdown in the material which is to lase. The inversion could then be achieved by the same mechanisms as in the more usual electrical discharge lasers, although the electronic temperatures are much higher in the present case.

Some general considerations are treated here and applied to the possibility of obtaining emission from the 3371 Å line in nitrogen and from metal vapors. The consideration can be extended to shorter wave lengths. Some experimental observations of fluorescence from metal vapors are also presented.

The gain coefficient for an inverted lossless medium is

$$\alpha = \frac{h\upsilon B g(\Delta\upsilon)}{c} \Delta N \tag{7.1}$$

where B is the Einstein B coefficient, $g(\Delta\upsilon)$ is a linewidth function and ΔN, the inversion. It is convenient to define a gain cross section, σ, such that

$$\sigma = \frac{\alpha}{\Delta N} = \frac{h\upsilon B g(\Delta\upsilon)}{c} . \tag{7.2}$$

In many of the low pressure, high temperature superradiant lasers which have been made to operate, doppler broadening is the most important line broadening mechanism. For the purposes of discussion, let us temporarily assume that this is so in our case also. Then at line center

$$g(\Delta\upsilon = 0) = 2\left(\frac{\ell n 2}{\pi}\right)^{\frac{1}{2}} \frac{1}{\Delta\upsilon_D} \tag{7.3}$$

where $\Delta\upsilon_D$ is the doppler width (FWHM). This gives

$$\sigma \cong 0.94 \frac{h\upsilon}{c} \frac{B}{\Delta\upsilon_D} = 0.94 \frac{h\upsilon}{c} \frac{B}{A} \frac{A}{\Delta\upsilon_D} \tag{7.4}$$

where A is the Einstein A coefficient. This yields

$$\sigma = \frac{0.94}{8\pi}\lambda^2 \frac{A}{\Delta\upsilon_D} \approx 1.2 \times 10^{-2}\lambda^2\left(\frac{A}{\Delta\upsilon_D}\right) \tag{7.5}$$

Since A is the reciprocal of the radiative decay time, all of the quantities in the above relation are measurable.

In a high density plasma of the kind produced by laser induced breakdown, the predominant optical losses are due to free-free absorption[137]. The loss coefficient is given by the celebrated formula

$$K = 3.1 \times 10^{-31} \frac{Z^3 N^2 g}{T^{\frac{3}{2}}(h\upsilon)^2} \tag{7.6}$$

where Z is the degree of ionization, N is the ion density, T is the plasma temperature, $h\upsilon$ is the photon energy in ev, and

$$g = 0.55 \ln\left[\frac{2.4 \times 10^3 T}{Z^{\frac{4}{3}} N^{\frac{1}{3}}}\right] \tag{7.7}$$

The total power gain coefficient is

$$G = \sigma - K = Nf\sigma - 3.1 \times 10^{-31} \frac{Z^3 N^2 g}{T^{\frac{3}{2}}(h\upsilon)^2} \tag{7.8}$$

where $f = \frac{\Delta N}{N}$.

Laser generated plasmas in gases typically have high plasma temperatures and a high degree of ionization. The values $T = 5 \times 10^5\ ^\circ K$ and $Z = 5$ are representative of the conditions which might be achieved. The free-free losses for such a plasma are indicated in Fig.(41) as a function of wavelength and of pressure. It has been assumed that the ion density is equal to the particle density.

For the 3371 Å line, the doppler width is $\Delta\upsilon_D \approx 8.5 \times 10^{10}\ sec^{-1}$ at $5 \times 10^5\ ^\circ K$. The radiative decay time for this line is 40 nsec, giving $A = 2.5 \times 10^7\ sec^{-1}$.[138] These values give for the line center gain cross section

$$\sigma = 1.25 \times 10^{-14}\ cm^2. \tag{7.9}$$

From this, and the free-free absorption given in Fig.(41), the gain coefficient can be calculated as a function of the pressure and of the fractional inversion, f. The result is shown in Fig.(42). For $f > 10^{-3}$ superradiant emission will occur in a 1 cm path length. On the other hand, if the fractional inversion is less than $f \approx 10^{-5}$, the net gain will always be negative so that oscillation will be impossible. It should be noted that from our estimated cross section and the measured gain coefficient, the fractional inversion achieved in a conventional nitrogen discharge laser is calculated to be $f \approx 6 \times 10^{-5}$.

To estimate gain for a UV line we assume that the dipole moment of the 3371 Å line in nitrogen is representative. If the principal broadening mechanism is doppler broadening (probably not a very good assumption), then the gain cross section is the same, namely $\sigma = 1.25 \times 10^{-14}$ cm^2. The most important effect of decreasing the wavelength is to decrease the free-free absorption (see Fig. 41). The net gain coefficient vs wavelength and pressure is shown in Fig.(43) for $f = 10^{-4}$. The peak gain is seen to increase and move to higher pressure with decreasing wavelength.

In recent years superradiant emission has been observed in metal vapors such as those of lead, copper, zinc, cadmium and manganese. Excited vapors of such metals can be produced by focussing a laser beam onto a surface of the solid. To our knowledge a definitive study of the conditions existing in such a plasma has been made only for carbon.(139) The pertinent parameters are $T \approx 10^5$ °K, $N \approx 10^{19}$ and $3 \leq Z \leq 6$. For want of better data, we shall take $T = 10^5$ °K, $N = 10^{19}$, $Z = 5$ for the metals. The overall gain coefficient is then

$$G = 10^{19} f\sigma - 1.1 \times 10^{10} \lambda^2. \qquad (7.10)$$

For copper vapor $A = 1.3 \times 10^6$ sec^{-1} and $\sigma = 8 \times 10^{-15}$ cm^2 at 10^5 °K. Similarly for lead $A = 2.2 \times 10^6$ sec^{-1} and $\sigma = 7.2 \times 10^{-14}$ at 10^5 °K. The net gain coefficient for copper and lead are plotted as a function of f and λ in Figs.(44) and(45) Again a fraction inversion of 10^{-4} to 10^{-3} is needed for superradiant emission.

The calculations outlined above are very rough. Nevertheless, the results are sufficiently encouraging that an experimental effort has been undertaken to observe stimulated emission in laser produced plasmas. The experimental apparatus is shown in Fig.(46). In the initial experiments, the mode-locked ruby laser beam was focussed with a cylindrical lens onto the target and no resonator was used. The samples included copper, lead, zinc and cadmium. The visible region emission was observed with a fast S-4 photodiode looking down the axis of the cylindrical plasma. It was hoped that the gain might be high to observe superradiant emission. Although such was not the case, a number of interesting results were obtained.

A strong fluorescence was observed for all of the samples. The results for copper are representative (Fig. 47). The fluorescence takes place in a number of lines including the 5105 Å and 5782 Å lines which are superradiant in a pulsed discharge. The overall fluorescence emission begins near the peak of the mode-locked ruby laser pulse train and builds up until the end of the train at which time it then decays with an 80 nsec decay time. Two observations are of particular importance. The first is that the fluorescence rises with a subnanosecond (diode limited) time constant after each laser pulse, indicating that the fast pumping rates can be achieved by this technique. The second observation is that overall fluorescence emission increases with increasing power density at the target with a fixed ruby laser output. This indicates that the ruby laser should be focussed into as small a volume as possible.

It is planned that further experiments in this area will be conducted. These experiments have been deferred awaiting the completion of a 10 joule, subnanosecond pulse neodymium laser facility that is under construction at this laboratory.

7.? Nonlinear Propagation Effects

When an intense light wave propagates through a Kerr active liquid, the intensity dependent index of refraction can lead to a variety of effects such as self-focusing, self-phase modulation and steepening and alteration of the state of polarization of the wave. During this period, consideration has been given to the latter effect and several conclusions have been reached. It has been known for some time that when an elliptically polarized wave propagates through such a liquid, the orientation of the axis of the ellipse are rotated by an amount proportional to the product of the fields along the major and the minor axis and the distance traveled (Reference 137). This effect has been used to measure some of the nonlinear coefficients of the liquid (Reference 138). A somewhat more general approach to this effect has been carried out and it has been concluded that linear polarization is an unstable mode of propagation in such a liquid while circular polarization is a neutrally stable mode. The analysis has also been extended to the case where an additional linear birefringence, such as could be produced by an external electric field, is present. This investigation is still in progress; an outline of the method of approach and some of the main results is given below. A more detailed discussion will be reported upon completion of the analysis.

We consider the propagation of an optical pulse in a liquid having an anisotropic molecular polarizability. For the present, we will assume that the molecular reorientation time, τ, is short compared to the duration of the pulse. For typical liquids such as CS_2 and $C_6H_5NO_2$, τ is a few picoseconds to about 30 picoseconds. In this case we find that the polarization in the liquid can be written as

$$\bar{P} = \epsilon\bar{E} + g(I)\bar{E} + \bar{P}_a = \bar{P}_{LIN} + \bar{P}_{NL} \qquad \epsilon\bar{E} = \bar{P}_{LIN} \tag{7.1}$$

Here the first term represents the ordinary linear polarizability, the second term an intensity dependent but isotropic polarizability and the third term an anisotropic polarizability. We write the optical field as $\mathcal{E}_0 \hat{\mathcal{E}} e^{i(kz-\omega t)}$ and allow for the presence of a dc field E. The direction of propagation will be taken as the +z axis and the direction of the dc field will define the +x axis. The anisotropic part of the polarizability may then be expressed as

$$P_a = a \begin{bmatrix} a & b \\ -b & 0 \end{bmatrix} E \tag{7.12}$$

with $a = E^2$ and $b = \frac{1}{2}(\mathcal{E}_y \mathcal{E}_x^* - \mathcal{E}_x \mathcal{E}_y^*)$. The fields may be calculated from the usual slowly varying envelope approximation,

$$\frac{\partial \mathcal{E}}{\partial z} = i \frac{2\pi k}{\epsilon} P_{NL} e^{-ikz} \tag{7.13}$$

Substitution of Eqs. (7.11) and (7.12) into Eq. (7.13) yields a set of two coupled equations in $\mathcal{E}_x$ and $\mathcal{E}_y$. It is convenient to write

$$\mathcal{E}_{x,y} = \mathcal{E}_{ox,oy} e^{i\phi_{x,y}(z)} \tag{7.14}$$

Equating the real and imaginary parts of Eq. (7.13) gives four equations for $\mathcal{E}_{ox}$, $\mathcal{E}_{oy}$, ϕ_x and ϕ_y. One integral follows immediately, i.e., $|\mathcal{E}_{ox}|^2 + |\mathcal{E}_{oy}|^2 =$ constant as would be expected since the material is lossless. We may then write

$$\mathcal{E}_{ox} = I^{\frac{1}{2}} \cos\theta$$
$$\mathcal{E}_{oy} = I^{\frac{1}{2}} \sin\theta \tag{7.15}$$

Finally, solving for $\psi = \phi_y - \phi_x$ we find that the isotropic part of the nonlinear polarization drops out and we obtain two equations for θ and ψ.

$$\frac{d\theta}{dz} = \dot{\theta} = \gamma I \cos\theta \sin\theta \sin 2\psi \tag{7.16}$$

$$\frac{d\psi}{dz} = \dot{\psi} = \gamma_0 + \gamma I(\cos 2\psi - 1)\cos 2\theta$$

where $\gamma = \frac{\pi k \gamma}{4\epsilon}$, $\gamma_0 = \frac{\pi k \gamma}{\epsilon} E^2$

These two equations describe completely the state of polarization of the wave as it propagates. The isotropic part of the nonlinear response does not enter because it does not change the state of polarization.

Equations(7.16) do not lead to a direct solution for $\theta(Z)$ and $\phi(Z)$however, it is possible to find a solution for ϕ as a function of θ. We find

$$\sin^2\phi = \left[\frac{2\gamma_0}{\gamma I}(\cos 2\theta - \cos 2\theta_0) + \sin^2\phi_0 \sin^2 2\theta_0\right]\left[\sin^2 2\theta\right]^{-1} \qquad (7.17)$$

Here θ_0 and ϕ_0 are constants that are determined by the initial conditions of polarization. This equation yields trajectories of ϕ vs θ, the sense of traversal of these being determined by Equation (7.16). These are plotted schematically in Figure(48)for the case $\gamma_0 = 0$ and Figure(49) for $\gamma_0 \neq 0$. For the case $\gamma_0 = 0$, the curves are the the usual rotating polarization ellipse. The points $\sin\phi = \pm 1$, $\theta = \pm \pi/4$ are the two senses of circular polarization. They are neutrally stable, as they are surrounded by the trajectories. The case of linear polarization, $\phi = 0$, θ arbitrary is seen to be unstable as all trajectories diverge from this line. The case $\gamma_0 \neq 0$ corresponds to the presence of a linear birefringence. Here the trajectories split into two classes depending on the initial conditions and the intensity. One type is similar to the case $\gamma_0 = 0$ and corresponds to a rotating (and distorted) elliptical polarization. The other corresponds, for example, to an initial linear polarization at an angle θ. The polarization then becomes elliptical, rotates and becomes more circular. After passing through the circular state, the polarization continues to rotate with increasing ellipticity until it becomes linear at $-\theta$. In the degenerate case $I = 0$, these trajectories simply become θ = constant, $\phi = \gamma_0 Z$ as may be seen directly from Eqs. (7.16). This is just the induced birefringence and the phase difference between x and y components increases linearly with distance. The trajectories on a plot of ϕ vs θ are two vertical lines at $\pm\theta$.

It is anticipated that further work will be carried out in the analysis of these polarization effects. Analytical solutions for $\theta(Z)$ and $\phi(Z)$ have been obtained and will be discussed in a later report. It would also be of interest to extend this analysis to nonlinear materials with a more complicated spatial symmetry, i.e., nonlinear crystals such as calcite. It is expected that these nonlinear polarization effects will be important in the propagation of high power pulses in dielectric media, particularly in the polarization effects in self-trapped filaments.

REFERENCES

1. DeMaria, A. J., D. A. Stetser and W. H. Glenn, Jr., Science 156, 1557 (1967).

2. Magyar, G., Nature 218, 16 (1968).

3. Bellman, R., G. Birnbaum and W. G. Wagner, J. Appl. Phys. 34, 780 (1963).

4. Frantz, L. M. and J. S. Nodvik, J. Appl. Phys. 34, 2346 (1963).

5. Basov, N. G., R. V. Ambartsumyan, V. S. Zuev, P. G. Kryukov and V. S. Letokhov, Soviet Physics JETP 23, 16 (1966).

6. McCall, S. L. and E. L. Hahn, Bull. Am. Phys. Soc. 10, 1189 (1965).

7. McCall, S. L. and E. L. Hahn, Phys. Rev. Letters 18, 908 (1967).

8. McCall, S. L. and E. L. Hahn, Phys. Rev. 183, 457 (1969).

9. Arecchi, F. T. and R. Bonifacio, IEEE J. Quant. Elect. 1, 169 (1965).

10. Armstrong, J. and E. Courtens, IEEE J. Quant. Elect. 4, 411 (1968).

11. Armstrong, J. and E. Courtens, IEEE J. Quant. Elect 5, 249 (1969).

12. Tang, C. L. and B. D. Silverman, in Physics of Quantum Electronics, edited by P. L. Kelley, B. Lax and P. E. Tannenwald (McGraw-Hill Book Co., Inc., New York, 1966) p. 280.

13. Wittke, J. P. and P. J. Warter, J. Appl. Phys. 35, 1668 (1964).

14. Hopf, F. A. and M. O. Scully, Phys. Rev. 179, 399 (1969).

15. Patel, C. K. N. and R. E. Slusher, Phys. Rev. Letters 19, 1019 (1967).

16. Icsevgi, A. and W. E. Lamb, Jr., Phys. Rev. 185, 517 (1969).

17. Lamb, G. L.,Jr., Phys. Letters 25A, 181 (1967).

18. Rhodes, C. K. A. Szoke and A. Javan, Phys. Rev. Letters 21, 1151 (1968).

19. Lamb, G. L.,Jr., in In Honor of Philip M. Morse, edited by H. Feshbach and K. V. Ingard (M.I.T. Press, 1969) p. 83.

20. Abella, I. D., N. A. Kurnit and S. R. Hartmann, Phys. Rev. 141, 391 (1965).

21. Compaan, A., L. Q. Lambert and I. D. Abella, Phys. Rev. Letters 20, 1089 (1968).

REFERENCES
(Continued)

22. Patel, C. K. N. and R. E. Slusher, Phys. Rev. Letters 20, 1087 (1968).

23. Gordon, J. P., C. H. Wang, C. K. N. Patel, R. E. Slusher and W. J. Tomlinson, Phys. Rev. 179, 294 (1969).

24. Lamb, G. L. Jr., Phys. Letters 28A, 548 (1969).

25. Lamb, W. E. Jr., in Proceedings of the International School of Physics "Enrico Fermi", Course XXXI, edited by P. A. Miles (Academic Press, Inc., New York, 1964), Phys. Rev. 134, A1429 (1964).

26. Karplus, R. and J. Schwinger, Phys. Rev. 73, 1020 (1948).

27. Arecchi, F. T., V. DeGiorgio and C. G. Someda, Phys. Letters 27A, 588 (1968).

28. Crisp, M. D., Phys. Rev. Letters 22, 820 (1969).

29. Eberly, J. H., Phys. Rev. Letters 22,760 (1969).

30. The form of the theorem required is given in G. N. Watson Theory of Bessel Functions, 2nd Edition, p 382,(Cambridge University Press, London (1962)): If f (r) is a continuous function of r when r > 0, such that

$$\int_0^\infty dr f(r) e^{-r^2 t} = 0$$

for all sufficiently large positive values of t, then f(r) is identically zero.

31. Abramowitz, M. and I. A. Stegun, Handbook of Mathematical Functions, (U. S. Government Printing Office, 1964).

32. Courtens, E. and A. Szoke, Phys. Letters 28A, 296 (1968).

33. Treacy, E. B. Phys. Letters, 28A, 34 (1968).

34. Treacy, E. B.,Appl. Phys. Letters 14, 112 (1969).

35. Treacy, E. B., Phys. Letters 27A, 421 (1968).

36. Eisenhart, L. P., A Treatise on the Differential Geometry of Curves and Surfaces, (Dover, New York, 1960), Section 13.

37. Rabi, I. I., N. F. Ramsey and J. Schwinger, Rev. Mod. Phys. 26, 167 (1954).

38. Reference 36, pp. 280 - 290.

39. Seeger, A., H. Donth and A. Kochendoerfer, Z. Physik 134, 173 (1953).

REFERENCES
(Continued)

40. Skyrme, T. H. R., Proc. Roy. Soc. (London) A262, 237 (1961).

41. Perring, J. K. and T. H. R. Skyrme, Nucl. Phys. 31, 550 (1962).

42. Enz, H., Phys. Rev. 131, 1392 (1963).

43. Josephenson, B. D., Advan. Phys. 14, 419 (1965).

44. Lebwehl, P. and M. J. Stephen, Phys. Rev. 163, 376 (1967).

45. Scott, A. C., Am. J. Phys. 37, 52 (1969).

46. Steuerwald, R. Abhandlungen der Bayerische Akad. Wiss (Muenchen)40, 1 (1936).

47. Patel, C. K. N, and R. E. Slusher (to be published).

48. Forsyth, A. R., Theory of Differential Equations (Dover, New York, 1959), Vo. VI, Chap. 21, and additional references are cited therein.

49. Clairin, M. J., Annales de Toulouse 2e Ser. 5, 437 (1903).

50. Ameler, M. H., Math. Annalen 130, 234 (1955).

51. Burnham, D. C. and R. Y. Chiao (to be published).

52. Courtens, E., Phys. Rev. Letters 21, 3 (1968).

53. Hopf, F. A., G. L. Lamb, Jr., C. K. Rhodes and M. O. Scully (to be published).

54. Lamb, G. L., Jr., Phys. Letters 29A, 507 (1969).

55. Byrd, P. F. and M. D. Friedman, Handbook of Elliptic Integrals (Springer Verlag, Berlin, 1954) p. 79.

56. Magnus, W. and F. Oberhettinger, Formulas and Theorems for the Special Functions of Mathematical Physics (Chelsea, New York, 1954) 2nd Edition, p. 105.

57. Risken, H. and K. Nummedal, J. Appl. Phys. 39, 4662 (1968).

58. Arecchi, F. T., G. L. Massorini and P. Schwendimann, Rivista del Nuevo Cimento 1, 181 (1969).

59. Zabusky, N. J. and M. D. Kruskal, Phys. Rev. Letters 15, 240 (1965).

60. Washimi, H. and T. Taniuti, Phys. Rev. Letters 17, 996 (1966).

REFERENCES
(Continued)

61. Gardner, G. S., J. M. Greene, M. D. Kruskal and R. M. Miura, Phys. Rev. Letters 19, 1095 (1967).

62. Lax, P. D., Comms. Pure and Appl. Math. 21, 467 (1968).

63. Karpman, V. I. and V. P. Sokolov, Soviet Physics JETP 27, 839 (1968).

64. Hahn, W., Stability of Motion (Springer Verlag, New York, 1967) p. 213.

65. Morse, P. M. and H. Feshbach, Methods of Theoretical Physics (McGraw-Hill Book Co., New York, 1953) Vol. I, pp 734 and 768, Vol. II, p 1651.

66. Kamke, E., Differtialgleichungen Loesungsmethoden und Leosungen Band I (Chelsea, New York, 3rd Edition, 1959) p. 483.

67. Jahnke, E. and F. Emde, Tables of Functions (Dover, 1945) 4th Edition, p. 82.

68. Condon, E. U. and G. H. Shortley, The Theory of Atomic Spectra (Cambridge, 1957) p. 63.

69. Reference 31, p 496.

70. Ince, E. L., Ordinary Differential Equations (Dover, 1956) p. 345.

71. Bonifacio, R. and L. M. Narducci, Lett. al Nuovo Cimento 1, 671 (1969).

72. Schiff, L. I., Quantum Mechanics (McGraw-Hill Book Co., New York, 1949) p. 77.

73. Poluektov, I. A. and Yu. M. Popov, JETP Letters 9, 330 (1969).

74. Dicke, R. H., Phys. Rev. 93, 99 (1954).

75. VanVleck, J. H., Phys. Rev. 24, 330 (1924), esp. footnote 25. Reprinted in Sources of Quantum Mechanics, B. L. Van der Walrden, editor, (Dover, 1968).

76. Zambusky, N. J. in Nonlinear Partial Differential Equations (Academic Press, New York, 1967) edited by W. F. Ames, pp. 233 - 258.

77. Berezin, Yu. A. and V. I. Karpman, JETP 24, 1049 (1967).

78. Miura, R. M., C. S. Gardner and M. Kruskal, J. Math. Phys 9, 1204 (1968).

79. Blaschke, W., Vorlesungen uber Differentialgeometric, Vol. I, 14th Edition, (Berlin, 1945) p. 206.

REFERENCES
(Continued)

80. Lax, P. D., Comm. on Pure and Appl. Math 21, 467 (1968).

81. Seeger, A. Theorie der Gitterfehlstellen in Handbuch der Physik, Vol. VII, Part 1, p. 566.

82. Buley, E. R. and F. W. Cummings, Phys. Rev. 134, A1454 (1964).

83. Morse, P. M. and H. Feshbach, Methods of Theoretical Physics, (McGraw-Hill Book Co., New York, 1953) p. 827.

84. Kleinman, D. A., Phys. Rev. 128, 1761 - 1775 (1962).

85. DeMartini, F., Townes, C.H., Gustafson, T.K. and Kelley, P.L., Phys Rev. 164, 312 (1967).

86. Gustafson, T.K., Taran, J.P., Haus, H.A., Lifsitz, J.R. and Kelley, P.L., Phys. Rev. 177, 306 (1969).

87. Shimizu, Fujio, Phys. Rev. Letters 19, 1097 (1967).

88. Cheung, A.C., Rank, D.M., Chiao, R.Y. and Townes, C.H., Phys. Rev. Letters 20, 786 (1968).

89. Laubereau, A., Phys. Letters 29A, 539 (1969).

90. Treacy, E.B., Appl. Phys. Letters 14, 112 (1969).

91. Kelley, P.L., et al., Conference on Non-Linear Optics held in Chania, Crete (1969).

92. Knight, W. and Peterson, G.A., "Light Pulse Propagation in a Non-Linear Dispersive Medium", United Aircraft Research Laboratories,(unpublished).

93. See for example Fisher, R.A., Kelley, P.L. and Gustafson, T.K., Appl. Phys Letters 14, 140 (1969) and Reference 7.

94. Treacy, E.B., Phys. Letters 28A, 34 (1968).

95. Giordmaine, J. A., Rentzepis, P. M., Shapiro, S. L. and Wecht, K. W. Appl. Phys. Letters 11, 216 (1967).

96. Rentzepis, P. M. and M. A. Duguay, Appl. Phys. Letters 11, 218 (1967).

97. DeMaria, A. J., W. H. Glenn, M. J. Brienza and M. E. Mack, Proc. IEEE 57, 2 (1969). This reference describes the use of Rhodamine 6G for TPF measurements.

REFERENCES
(Continued)

98. Wang, C. S ., Phys. Rev. 182, 482 (1969).

99. Carman, R. L., F. Shimizu, C. S. Wang and N. Bloembergen, to be published.

100. Carman, R. L., M. E. Mack, F. Shimizu and N. Bloembergen, Phys. Rev. Letters 23, 1327 (1969).

101. Mack, M. E., R. L. Carman, J. Reintjes and N. Bloembergen, Appl. Phys. Letters 16, 209 (1970).

102. Hacken, H. and M. Pauthier, J. Quant. Elec. 5, 454 (1968).

103. Garmire, E., Phys. Letters 17, 251 (1965).

104. Minck, R. W.,R. W. Terhune and C. C. Wang, Appl. Optics 5, 1595 - 1612 (1966).

105. Minck, R. W., R. W. Terhune and W. G. Rado, Appl. Phys. Letters 3, 181 (1963).

106. Hagenlocker, E. E., R. W. Minck and G. Rado, Phys. Rev. 154, 226 (1967).

107. Bloembergen, N., G. Bret, P. Lallemand, A. Pine and P. Simova, IEEE J. Quant. Elec. 3, 197 (1967).

108. Minck, R. W., E. E. Hagenlocker and W. G. Rado, Phys. Rev. Letters 17, 229 (1966).

109. Pohl, D., Phys. Rev. Letters 23, 711 (1969).

110. Mack, M. E., Second Conference on the Laser, Annals of the New York Academy of Science 168, 419 (1970).

111. Herzberg, G., Spectra of Diatomic Molecules, (Van Nostrand, New Jersey, 1950); G. Herzberg, Infrared and Raman Spectra, (Van Nostrand, New Jersey, 1945).

112. Foltz, N. D., C. W. Cho, D. H. Rank and T. A. Wiggins, Phys. Rev. 165, 396 (1968).

113. Herman, R. M., Phys. Rev. 164, 200 (1967).

114. Chiao, R. Y. and J. Godine, Phys. Rev., to be published.

115. DeMartini, F. and J. Ducuing, Phys. Rev. Letters 17, 117 (1966).

116. Claesson, S. and Lidqvist, L., Arkiv Kemi 12, 1 (1957).

117. Sorokin, P.S., Lankard, J.R., Hammond, E.C. and Morruzi, V.L., IBM J. Res. Develop. 11, 130 (1967).

REFERENCES
(Continued)

118. Furamoto, H. and H. Ceccon, Presented at IEEE Convension on Laser Engineering and Applications, Washington, D. C., May 1969.

119. Anderson, J. A., Astrophys. J. 75, 394 (1932).

120. Goldstein, R. and F. N. Mastrup, IEEE J. Quant.Elect. QE-3, 529 (1967).

121. Sorokin, P. P. and J. R. Lankard, IBM J. Research & Develop. 10, 162 (1966).

122. Sorokin, P. P., J. R. Lankard, E. C. Hammond and V. L. Morrizzi, IBM J. Research and Develop. 11, 130 (1967).

123. Myer, J. A., C. L. Johnson, E. Kierstead, R. D. Sharma and I. Itzkan, Appl. Phys. Letters 16, 3 (1970).

124. Broida, H. P. and S. C. Haydon, Appl. Phys. Letters 16, 142 (1970).

125. Sorokin, P. P. and J. R. Lankard, IBM J. Research & Develop. 11, 148 (1967).

126. Furumoto, H. and H. Ceccon, Appl. Optics 8, 1613 (1969); J. Appl. Phys. 40, 4204 (1969).

127. Fungel, F. B. A., High Speed Pulse Technology II, Chapter 5b, p. 71, (Academic Press, New York, 1965).

128. Hargrove, L. E., R. L. Fork and M. A. Pollack, Appl. Phys. Letters 5, 4-5,(1964).

129 Neumann, G. and M. Hercher, 1969 IEEE Conference on Laser Engineering and Applications, Paper 3.7.

130. Shipman, J. D., Appl. Phys. Letters 10, 3 (1967).

131. Glenn, W. H., M. J. Brienza and A. J. DeMaria, Appl. Phys. Letters 12, 54 (1968).

132. Mack, M. E., J. Quant. Elect. 4, 1015 (1968).

133. Sorokin, P. P., J. R. Lankard, E. C. Hammond, V. L. Morruzi, IBM J. Research & Develop. 11, 130 (1967).

134. Birnbaum, G., Optical Masers, (Academic Press, New York, 1964), p. 32.

135. Pine, A. S., J. Appl. Phys. 39, 106 (1968).

136. Basov, N. G., R. V. Ambartsumyan, V. S. Zuev, P. G. Kryukov, and V. S. Letokhov, Soviet Physics JETP-23, 16 (1966).

REFERENCES
(Continued)

137. Maker, P. D. and R. W. Terhune, Phys. Rev. 137, A801 (1965).

138. Maker, P. D. and R. W. Terhune, Phys. Rev. 12, 507 (1964).

139. Ginsberg, V. L., Doke. Akad. Nauk 56, 253 (1947).

PUBLICATIONS AND PRESENTATIONS

The following is a list of the publications and major presentations for which partial or complete support can be attributed to the present contract.

Treacy, E. B.,Chirped Optical Pulses, Annals of the New York Academy of Sciences 168, 400 - 418, 1970.

Mack, M. E., Stimulated Thermal Rayleigh Scattering with Picosecond Pulses, Annals of the New York Academy of Sciences, 419 - 436, 1970.

Treacy, E. B., Measurement of Phase Structure in Picosecond Pulses, Seminar presented at the University of Rochester, Department of Physics, December 8, 1969.

Mack, M. E., R. L. Carman, F. Shimizu, and N. Bloembergen, Forward Picosecond Stokes Pulse Generation in Transient Stimulated Raman Scattering, Phys. Rev. Letters 23, 1327 (1969).

Mack, M. E., Superradient Traveling Wave Dye Laser, Appl. Phys. Letters 15, 166 (1969).

Glenn, W. H., Picosecond Laser Pulses, Seminar presented at the Summer School in Quantum Electronics, University of Colorado, Boulder, Colorado, August 14, 1969; Picosecond Laser Pulses, Am. Phys. Soc. DEAP Meeting, Washington, D. C., May 2, 1969.

Treacy, E. B., Lectures on mode-locked lasers, measurement of picosecond pulses and optical adiabatic inversion presented at the Physics of Quantum Electronics Summer School, Flagstaff, Arizona, June, 1969.

Mack, M. E. and E. B. Treacy, Nonlinear Effects in the Propagation of Picosecond Pulses, Spring Meeting of the New England Section of the American Physical Society, Storrs, Connecticut, April 12, 1969.

Treacy, E. B. and A. J. DeMaria, Adiabatic Inversion of SF_6 in the Infrared, Spring Meeting of the New England Section of the American Physical Society, Storrs, Connecticut, April 12, 1969.

Mack, M. E., R. L. Carman, J. Rientjes and N. Bloembergen, Transient Stimulated Rotational and Vibrational Scattering in Gases, Appl. Phys. Letters 16, 209, (1970).

Ferrar, C. M., Simple, High Intensity, Short Pulse Flashlamps, Rev. Sci. Instr. 40, 1436 - 1438 (1969).

Ferrar, C. M., Mode-Locked, Flashlamp Pumped Coumarin Dye Laser at 4600 Å, IEEE J. Quant. Elect QE-5, 550 (1969).

PUBLICATIONS AND PRESENTATIONS
(Continued)

Lamb, G. L. Jr., P. Pulse Propagation in a Lossless Amplifier, Phys. Letters 29A, 507 (1969).

Mack, M. E. and E. B. Treacy, A Nonlinear Image Contrast Amplifier, IEEE J. Quant. Elect. QE-5, 382 - 383 (1969).

Treacy, E. B. and A. J. DeMaria, Adiabatic Inversion in the Infrared, Phys. Letters 29A, 369 - 370 (1969).

Table I - Vibration Raman Lines Stimulated

	GAS	PRESSURE (atm.)	OBSERVED STIMULATED SHIFTS (cm^{-1})	CORRESPONDING SPONTANEOUS SHIFTS (cm^{-1})	DESIGNATION
N_2	Nitrogen	55-100	2330	2330.7	ν_0
O_2	Oxygen	50-100	1550	1554.7	ν_0
CO_2	Carbon Dioxide	20- 50	1385	1388.3	ν_1
N_2O	Nitrous Oxide	50	1282	1285.0	ν_1
			774	775	ν_1
SF_6	Sulfur Hexafluoride	15- 20	1551	1550	$2\nu_1$
			2323	2325	$3\nu_1$
CH_4	Methane	80-100	2916	2914.2	ν_1
C_2H_4	Ethylene	55	1344	1342.4	ν_3
C_3H_6	Propylene	90	~ 2920	2924(liq.)	ν_4
HCl	Hydrogen Chloride	35	2883	2886.0	ν_0
HBr	Hydrogen Bromide	20	2558	2558	ν_0

Table II - Performance Characteristics for Various Lamps

Lamp Size, Bore x Length (mm)	Projected Area (mm^2)	Capacitance (mfd)	Rise Time, T_R (μsec)	Pulse Duration $T_{\frac{1}{2}}$ (μsec)	Relative Peak Intensity, I	Explosion Energy (Joules)	$I \times T_{\frac{1}{2}}$	$I \div T_R$
1 x 90	90	.22	.17	0.6	.08	53	.05	0.5
3 x 35	105	.22	.20	0.6	.10	51	.06	0.5
3 x 70	210	.22	.15	1.7	.23	110	0.4	1.5
3 x 120	360	1.8	.25	2.0	.29	230	0.6	1.2
5 x 130	650	1.8	.25	3.5	.56	440	2.0	2.2
8 x 100	800	3.6	.80	4.0	.61	520	2.4	0.8
6 x 135	810	1.8	.35	4.8	.65	440	3.1	1.9
Four Parallel								
3 x 90	1080	1.8	.30	3.6	.68	565	2.5	2.3
Two Parallel								
3 x 200	1200	1.8	.25	3.3	.75	565	2.5	3.0
5 x 280	1400	3.6	.45	7.0	.82	870	5.7	1.8
11 x 150	1650	3.6	.80	8.0	.83	795	6.6	1.0
Two Parallel								
5 x 200	2000	3.6	.40	7.8	.96	955	7.5	2.4
5 x 400	2000	3.6	.45	11.0	.89	1120	9.8	2.0
Four Parallel								
3 x 200	2400	3.6	.35	6.0	1.00	1200	6.0	2.9

J920479-21

FIG. 1

DIAGRAM OF AREA THEOREM FOR ULTRASHORT PULSES

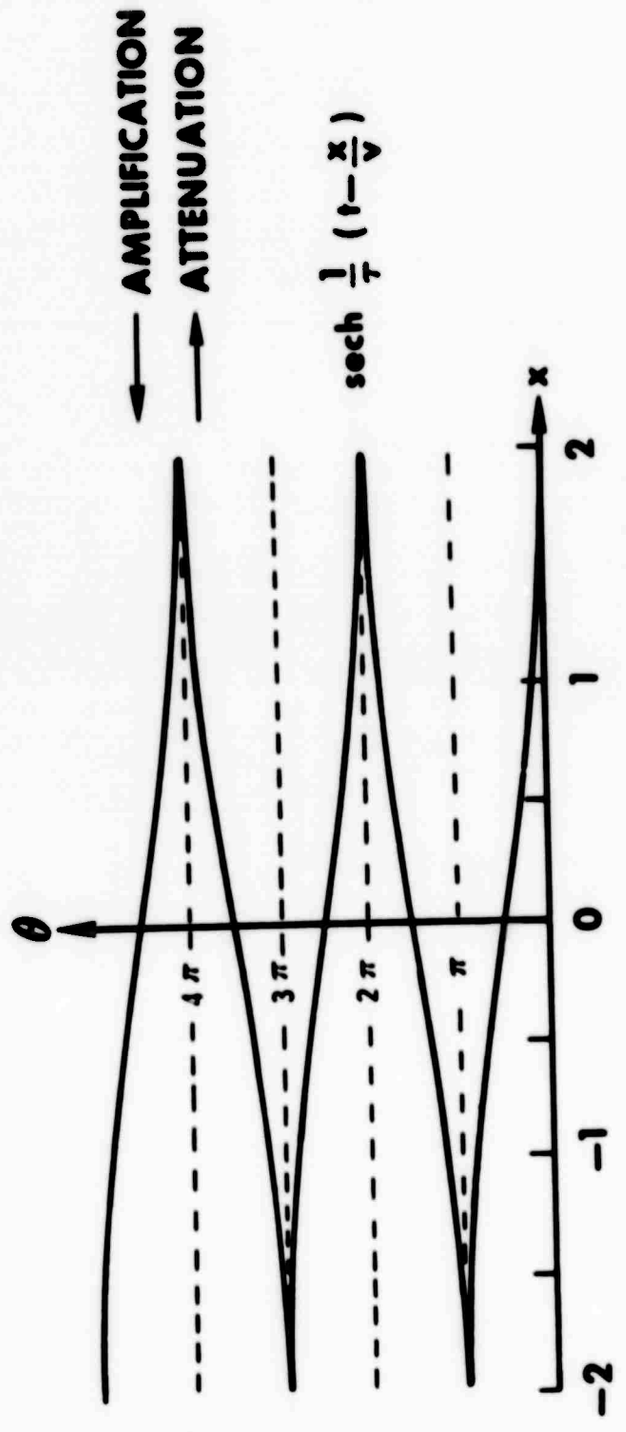

SCHEMATIC REPRESENTATION FOR THE BAECKLUND TRANSFORMATION GIVEN BY EQ. (2-37)

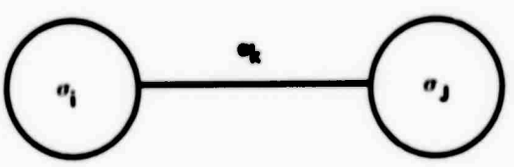

DIAGRAM FOR SEQUENCE OF TRANSFORMATIONS GIVING 4/7 PULSE

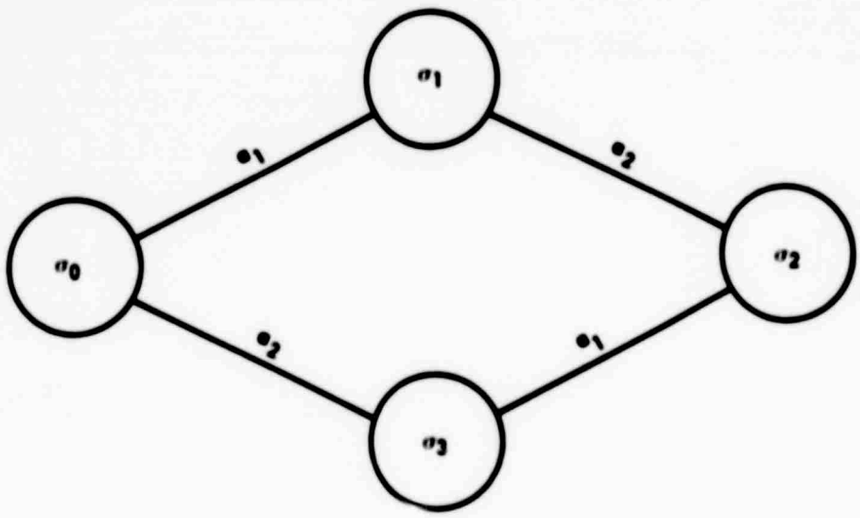

J920479-21

FIG. 4

DIAGRAM FOR SEQUENCE OF TRANSFORMATIONS GIVING 6/7 PULSE

J920479-21

FIG. 5

PROPAGATION OF A 4π PULSE IN AN ABSORBING MEDIUM

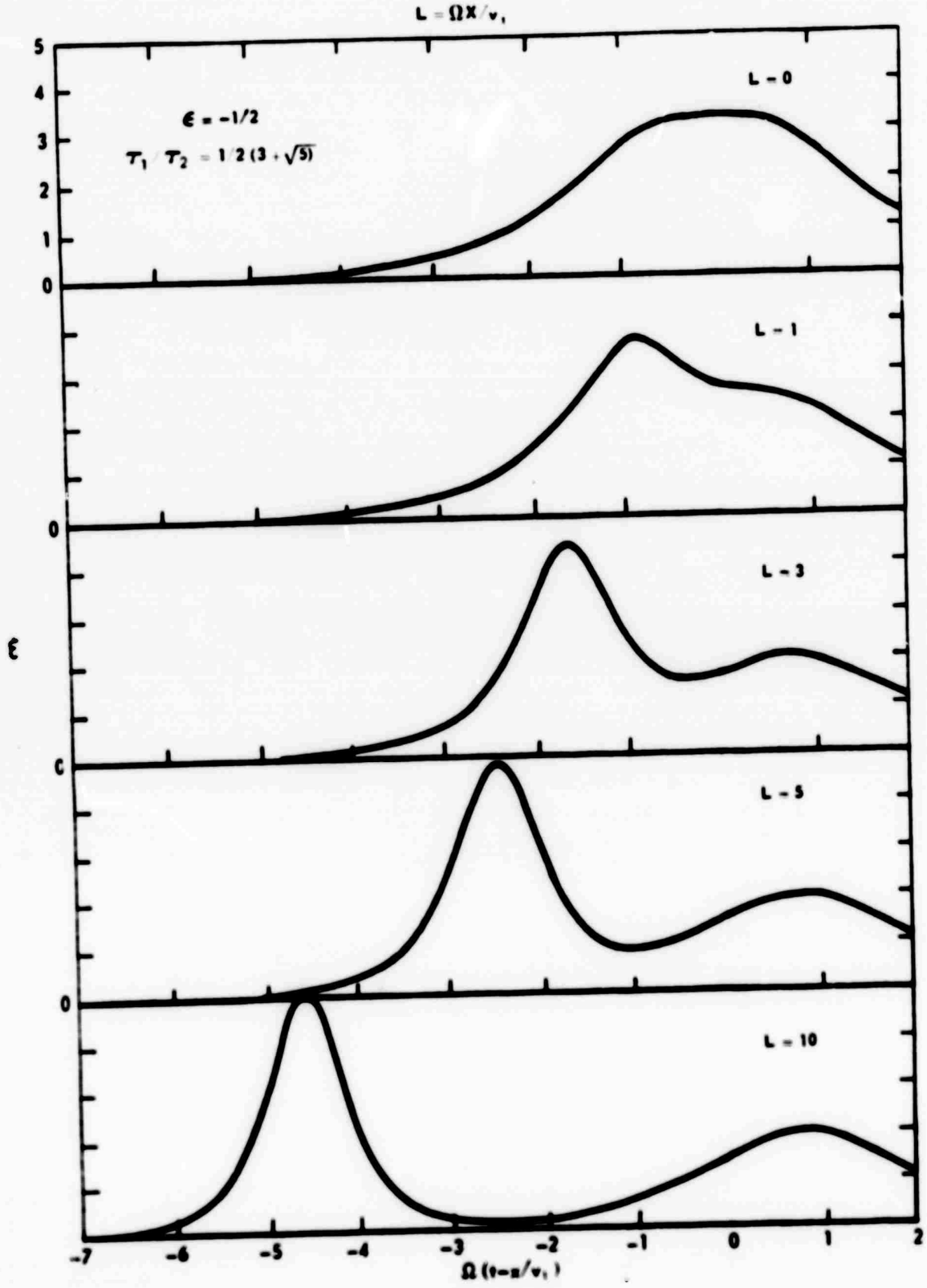

FIG. 6

FIRST TYPE OF ZERO π - PULSE

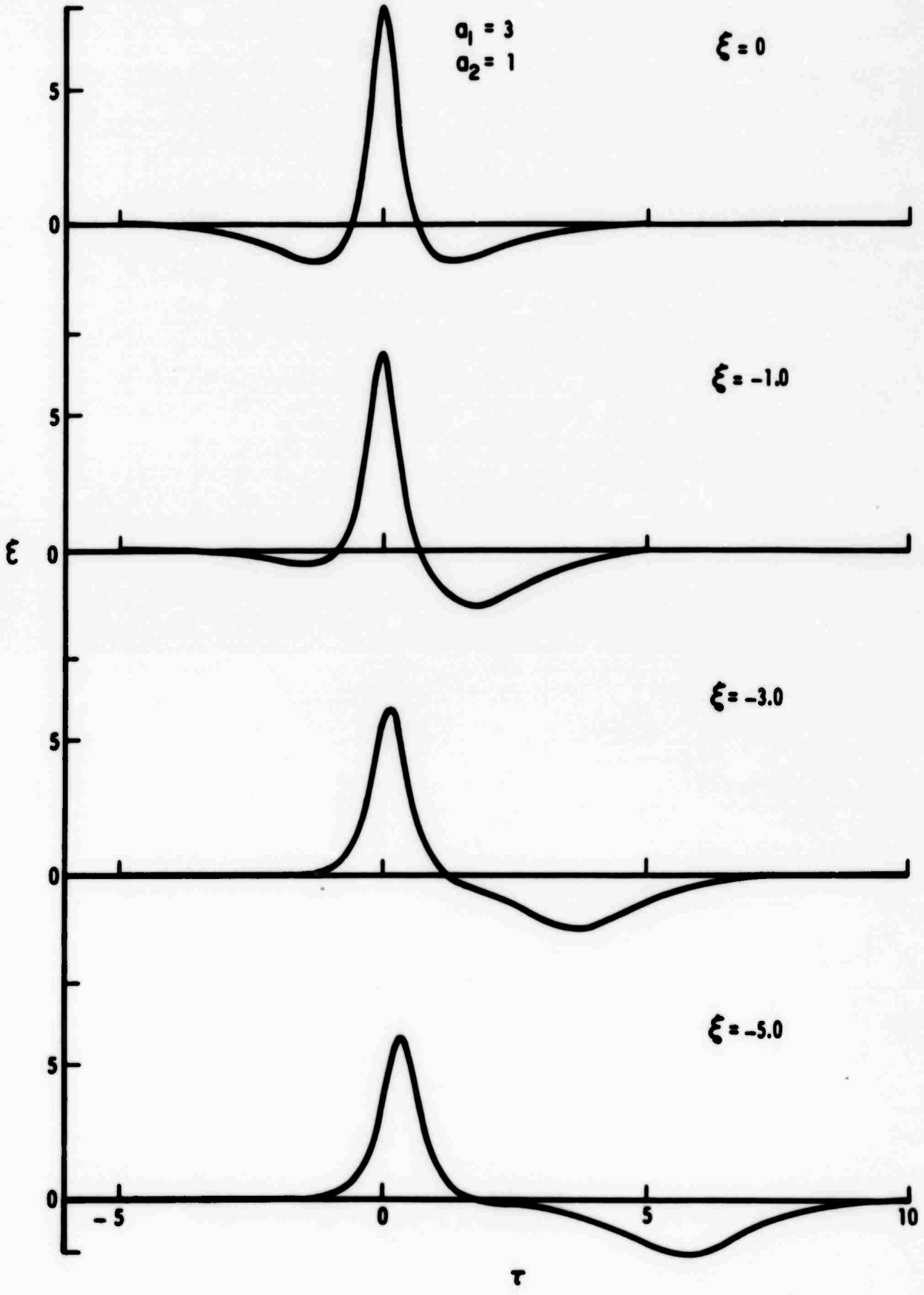

J920479-21

FIG. 7

SECOND TYPE OF ZERO π – PULSE

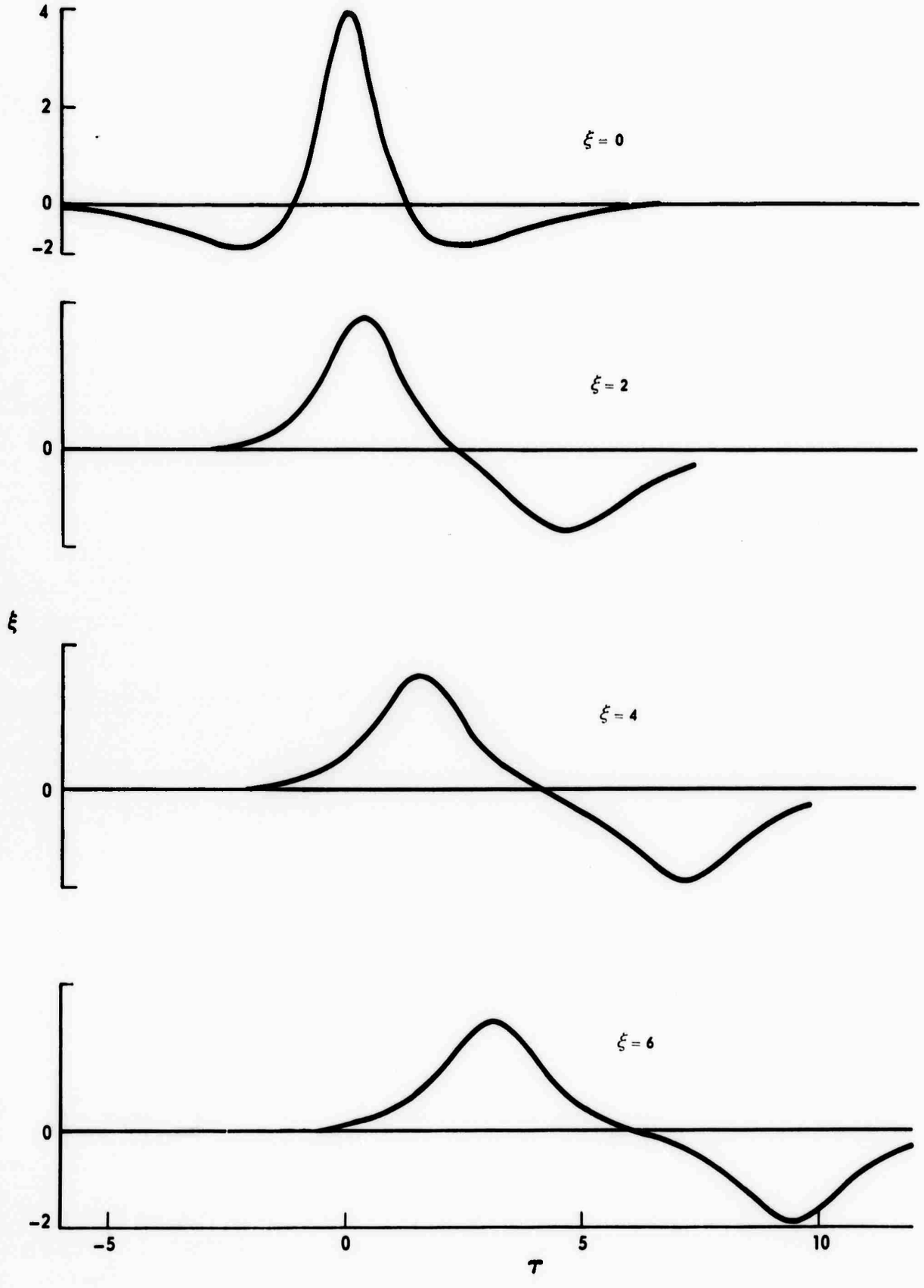

J920479-21

FIG. 8

THIRD TYPE OF π - PULSE

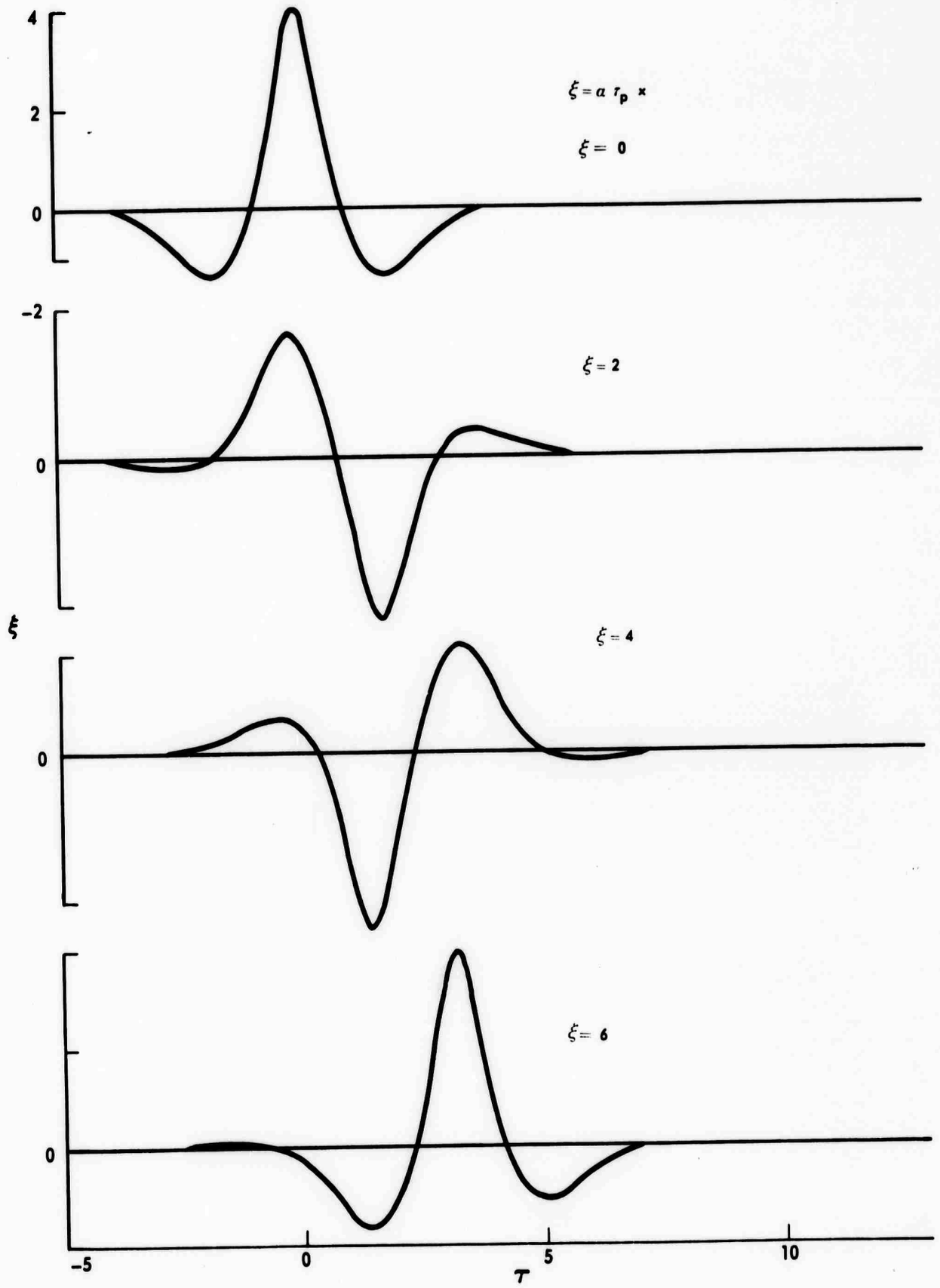

FIG. 9

BREAKUP OF 6π PULSE AS DERIVED FROM SEQUENCE OF TRANSFORMATIONS SHOWN IN FIG. 4

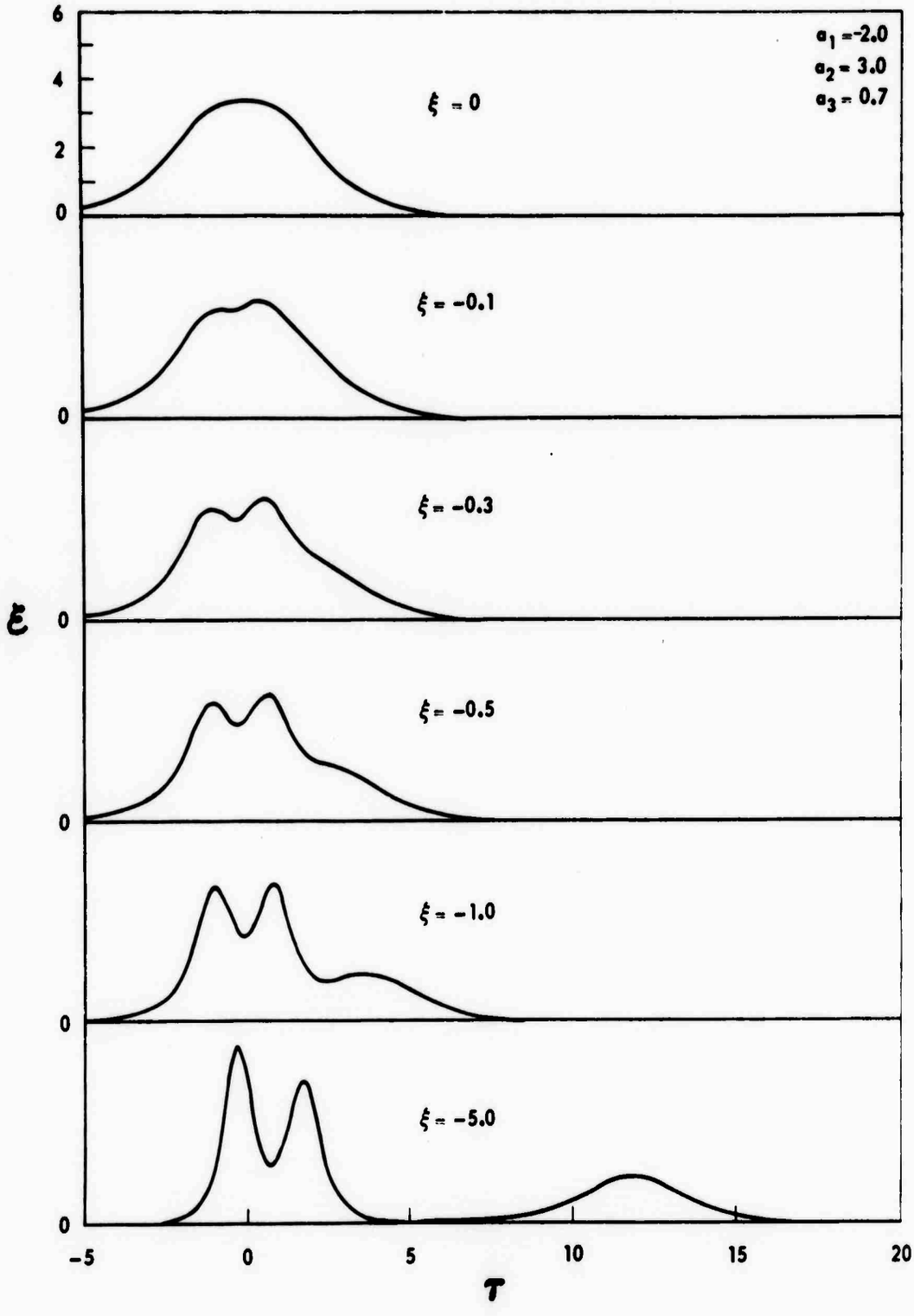

π – PULSE IN A LOSSLESS AMPLIFIER

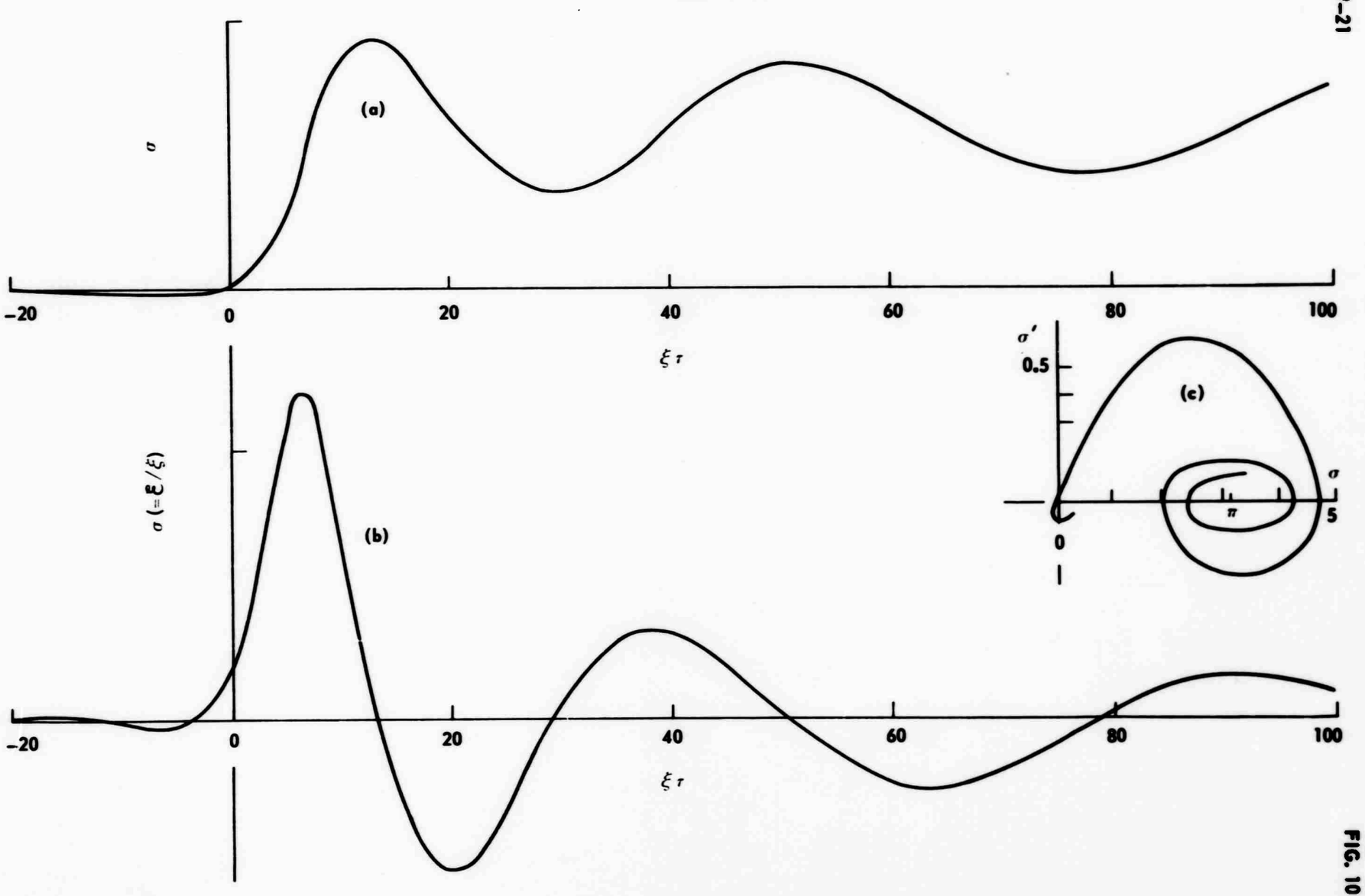

FIG. 10

J920479-21

FIG. 11

PROPAGATION OF π – PULSE IN AMPLIFIER

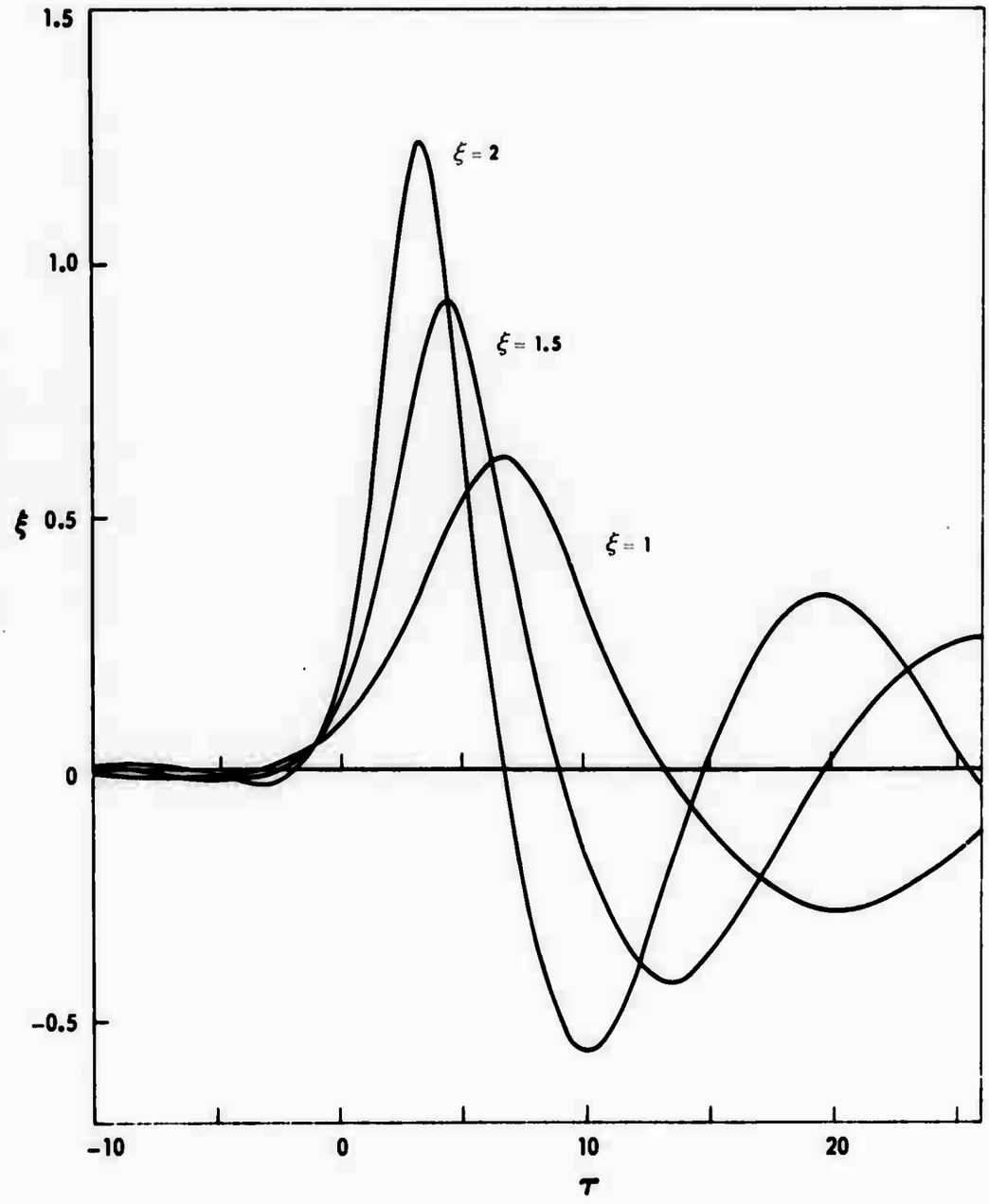

J920479-21

FIG. 12

SPATIAL DEVELOPMENT OF PHOTON ECHO

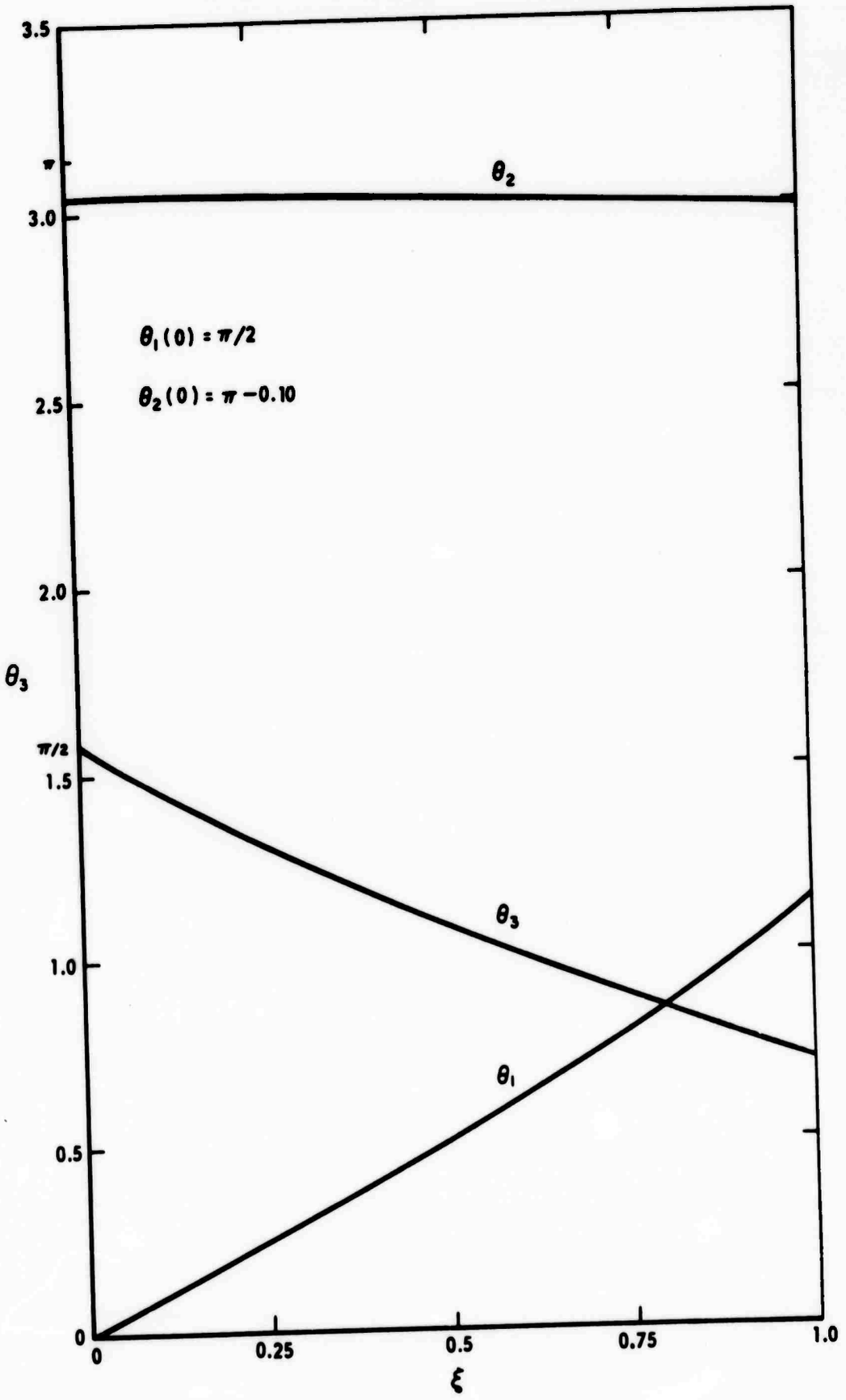

FIG. 13

PULSE PROFILE INCLUDING LEVEL DEGENERACY–Q(2) TRANSITION

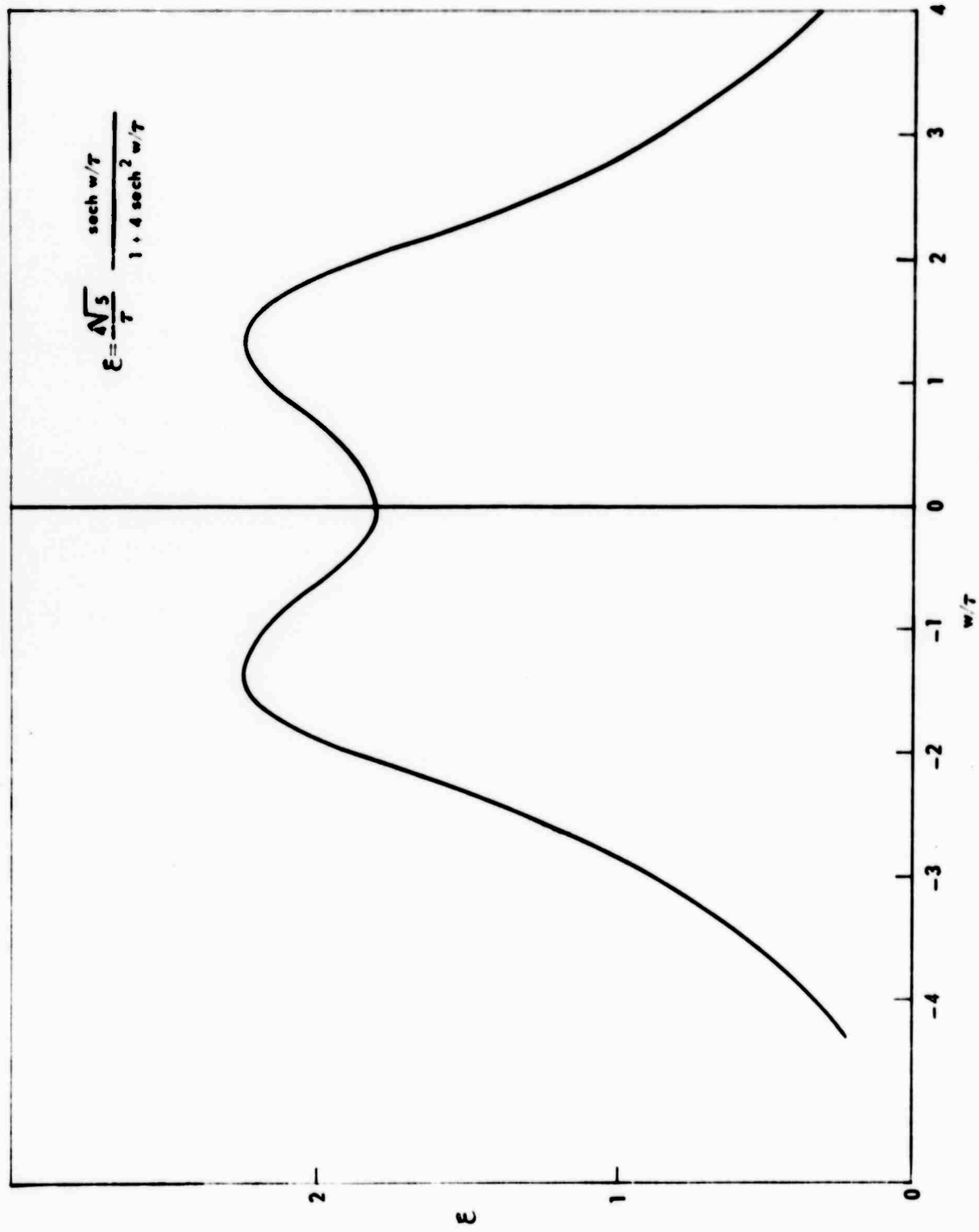

SOURCE MOVING ALONG OPTIC AXIS

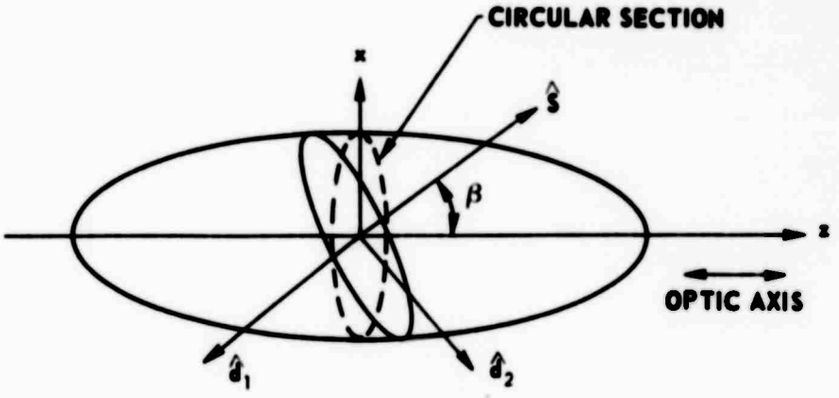

$\hat{d}_1 \perp \hat{S}$

$\hat{d}_1 \perp \hat{z}$

$\hat{S} \times \hat{d}_1 = \hat{d}_2$

$$\frac{x^2 + y^2}{\epsilon_x} + \frac{z^2}{\epsilon_z} = 1$$

a) UNIAXIAL NEGATIVE

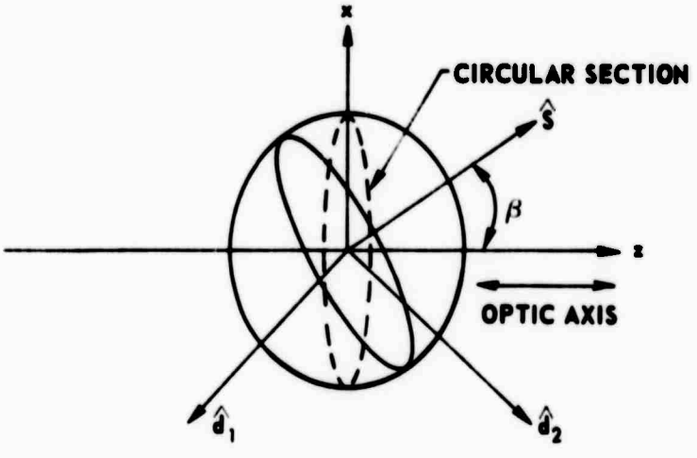

b) UNIAXIAL POSITIVE

SOURCE MOVING TRANSVERSE TO OPTIC AXIS

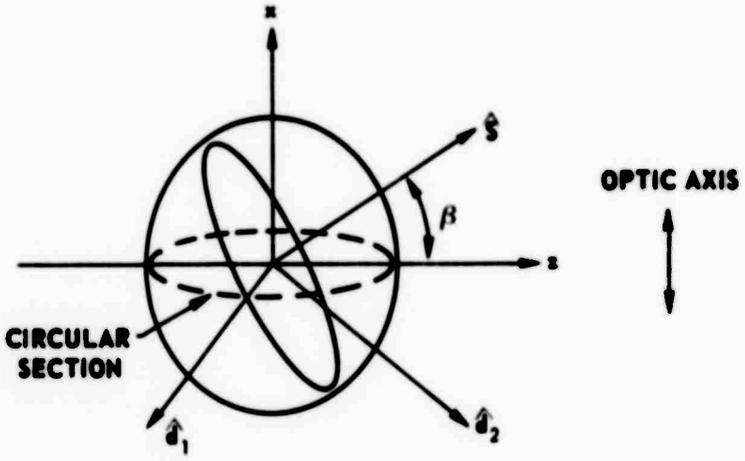

$\hat{d}_1 \perp \hat{s}$

$\hat{d}_1 \perp \hat{x}$

$\hat{s} \times \hat{d}_1 = \hat{d}_2$

$$\frac{x^2}{\epsilon_x} + \frac{y^2 + z^2}{\epsilon_z} = 1$$

a) UNIAXIAL NEGATIVE

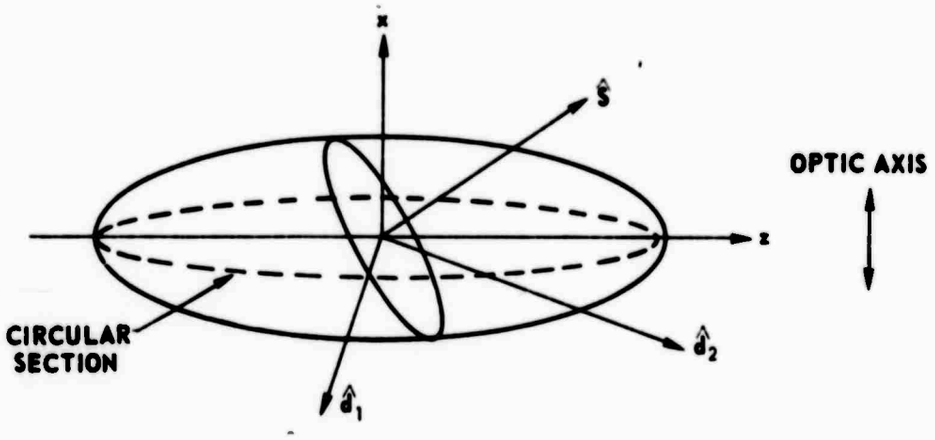

b) UNIAXIAL POSITIVE

FIG. 16

CONTOURS OF INTEGRATION USED FOR EVALUATION OF

$$\int_0^\infty d\tau \left\{ \frac{f(\tau)\, J_i'\left(\frac{\omega}{c}\tau\rho\right)}{\tau^2 \cdot n^2 - \eta'^2_z} \right\}$$

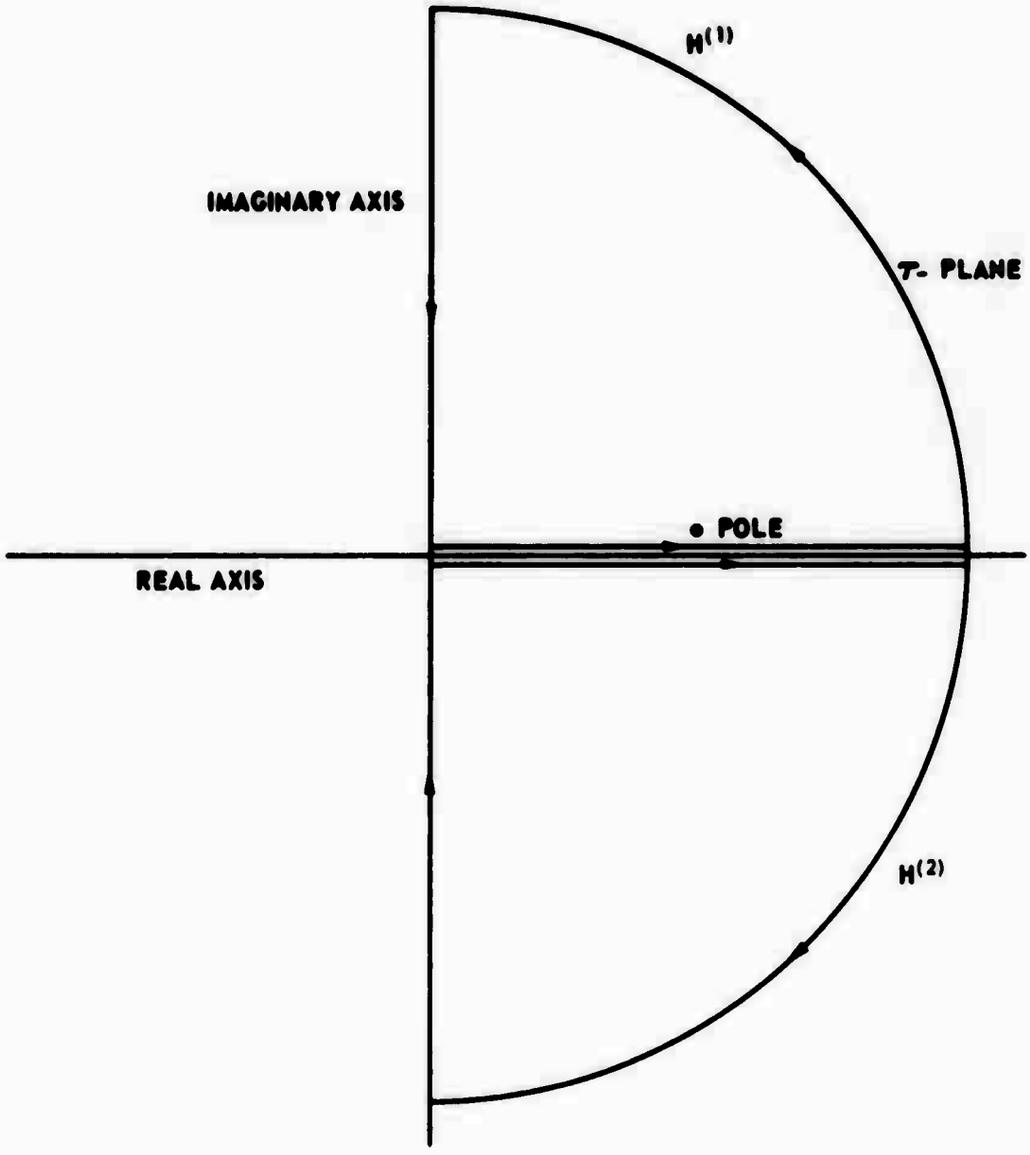

RESPONSE TIMES OF VARIOUS FILTERS FOR A COMPLEX PHASE MODULATED PULSE WITH LARGE TIME - BANDWIDTH PRODUCT

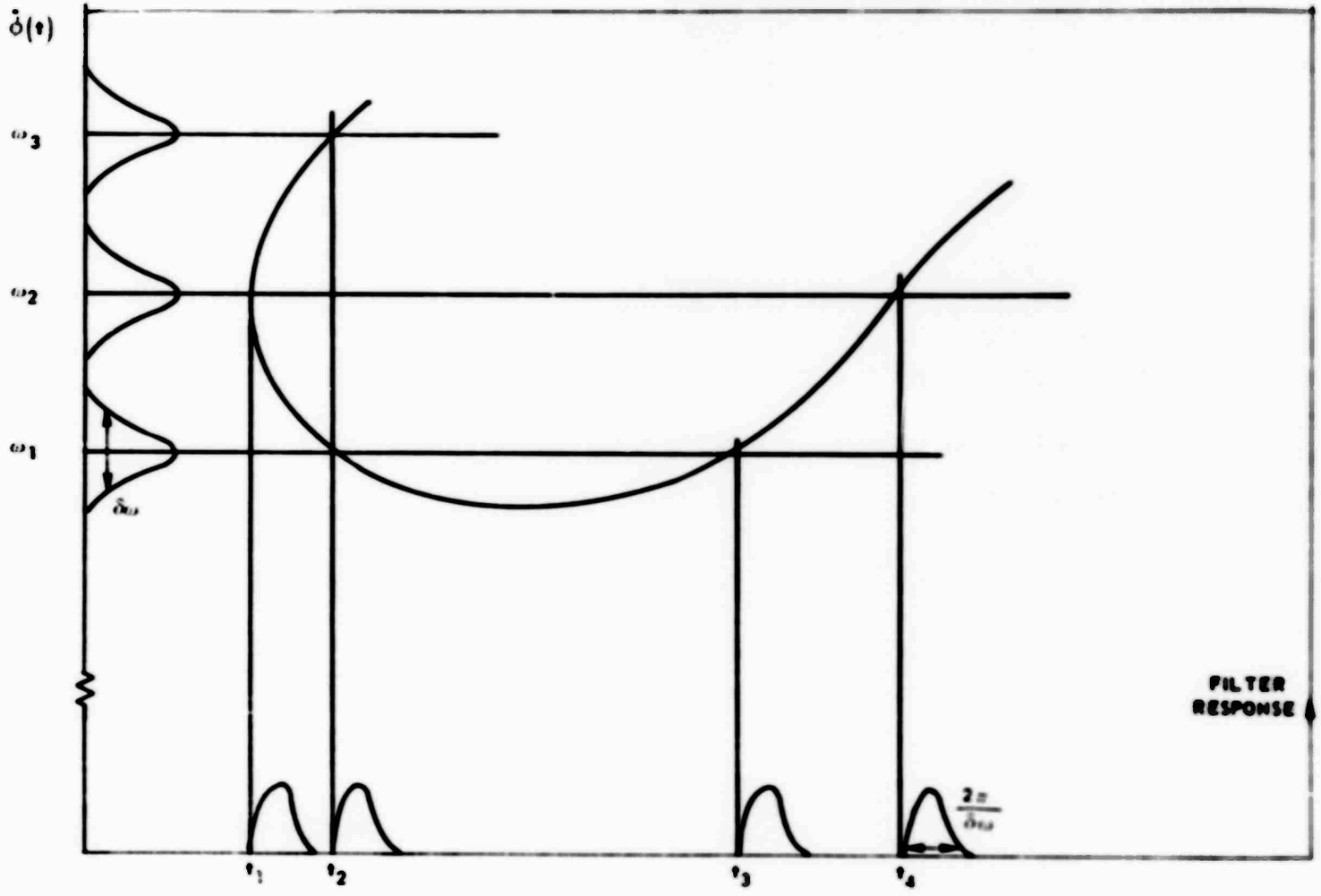

FIG. 17

J920479-21

FIG. 18

APPARATUS FOR MEASURING CHIRP CHARACTERISTICS

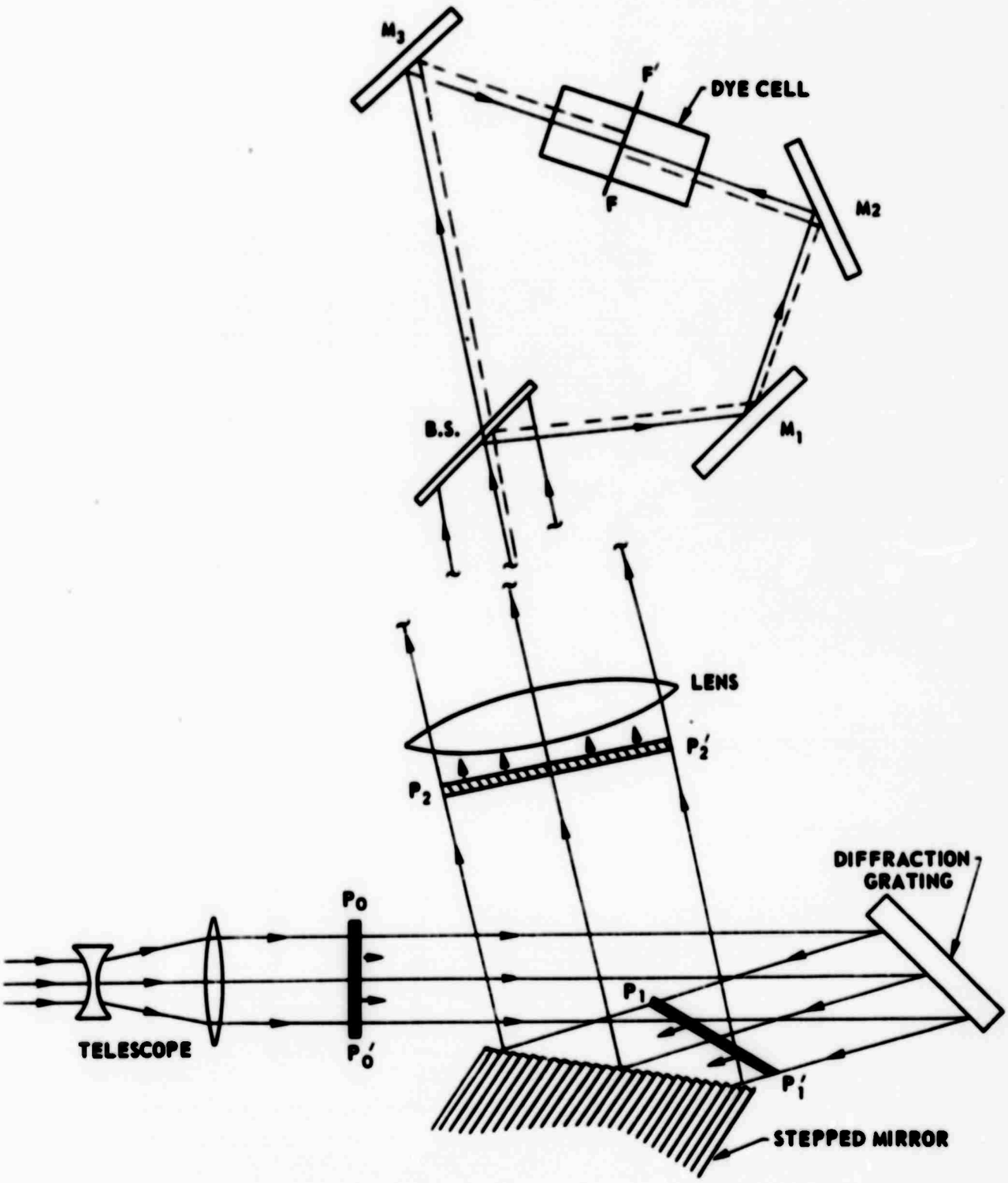

J920479-21

FIG. 19

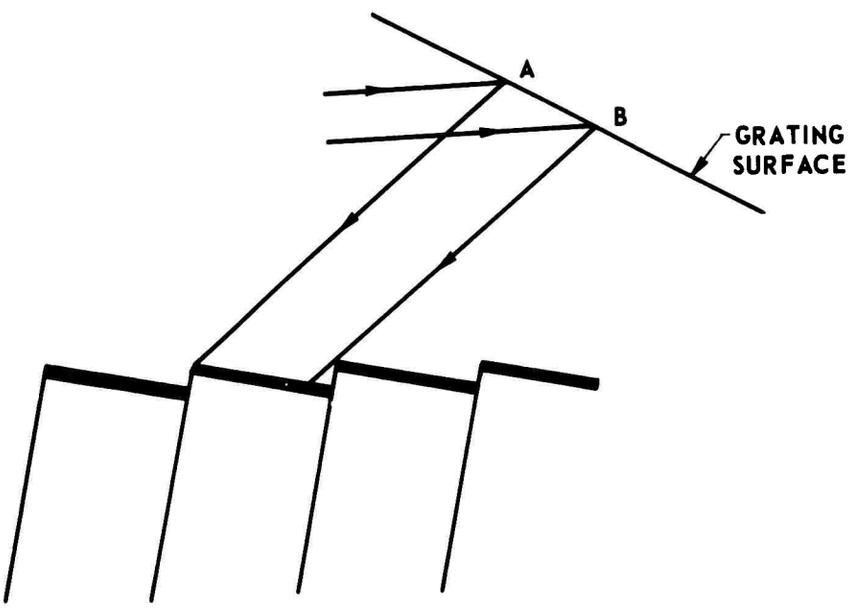

$$\text{RESOLVING POWER} = m\frac{AB}{d}$$

J920479-21

FIG. 20

CANTED TPF DISPLAY OF A PULSE WITH POSITIVE LINEAR FREQUENCY SWEEP

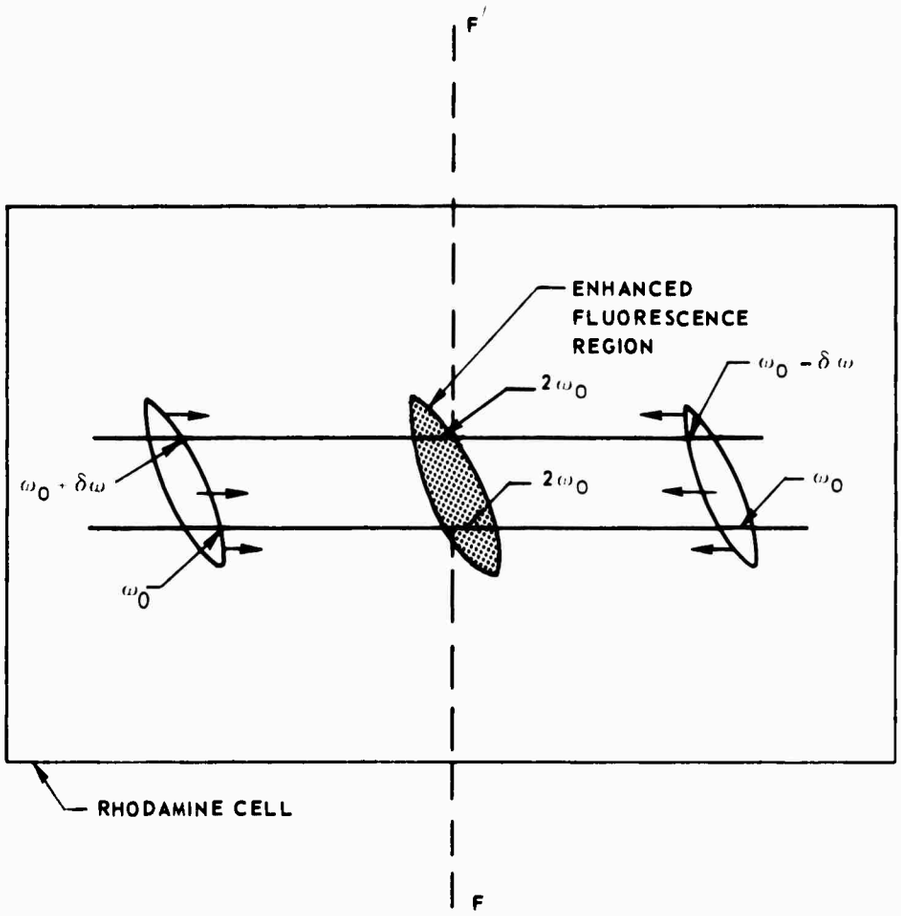

J920479-21

FIG. 21

TWO-PHOTON ABSORPTION-FLUORESCENCE DISPLAY OF CHIRP

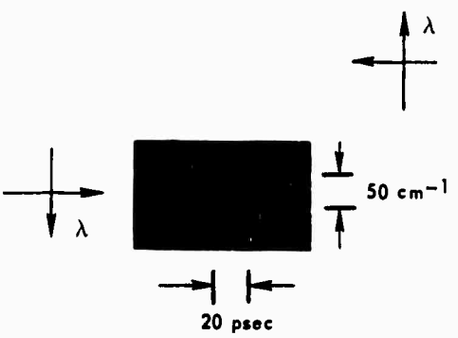

J920479-21

FIG. 22

STIMULATED RAMAN SCATTERING IN CCl_4

a) INTERLEAVED STOKES AND LASER PULSE TRAINS. THE FIRST PULSE IN EACH PAIR IS THE LASER PULSE

b) TWO-PHOTON ABSORPTION-FLUORESCENCE STOKES PULSE WIDTH MEASUREMENT

c) TWO-PHOTON ABSORPTION-FLUORESCENCE STOKES PULSE WIDTH MEASUREMENT

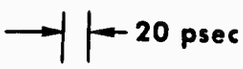

J920479-21

FIG. 23

RAMAN SCATTERING IN METHANOL

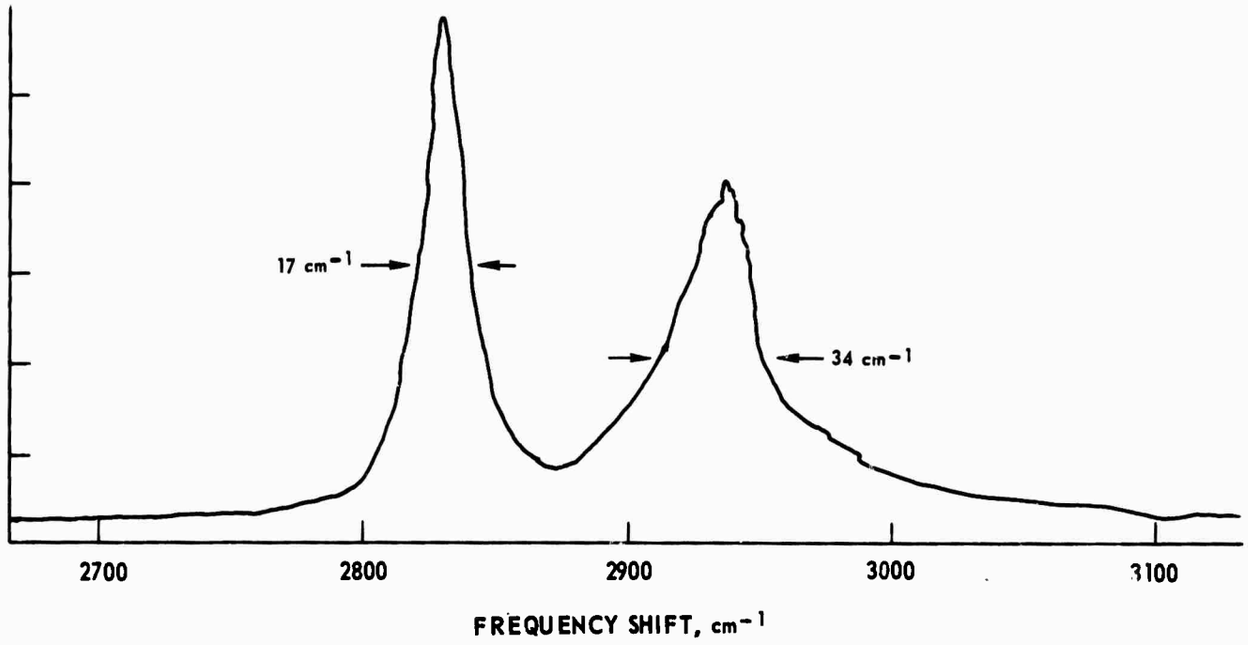

a) SPONTANEOUS SPECTRUM

b) STIMULATED SPECTRUM IN THE BENDING MODE

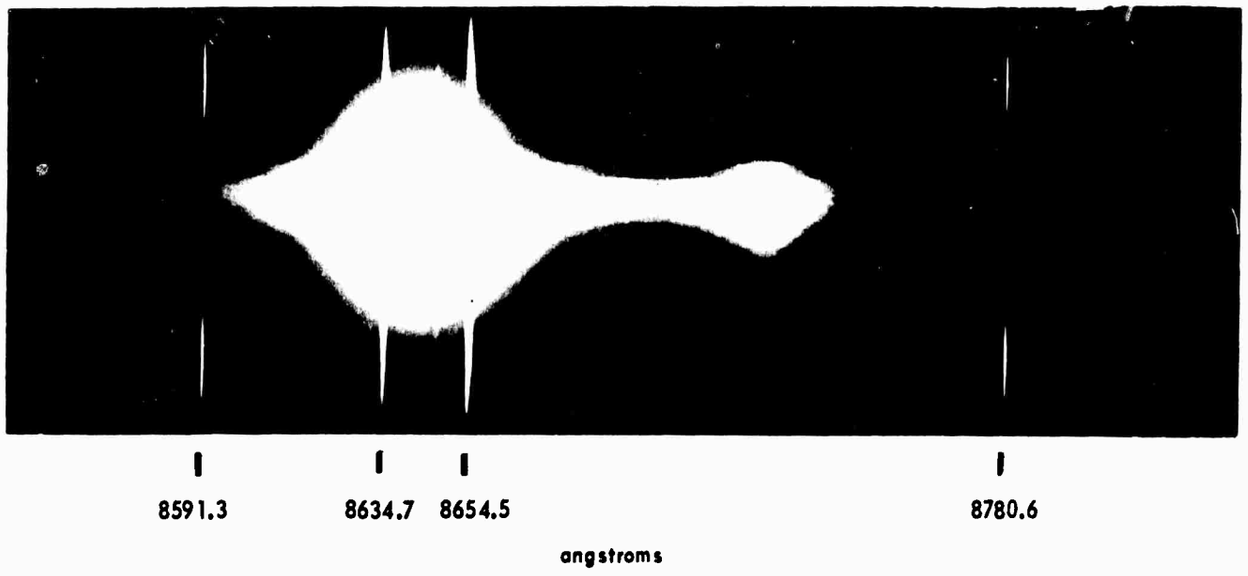

SELF-TRAPPING IN METHANOL - STOKES LIGHT

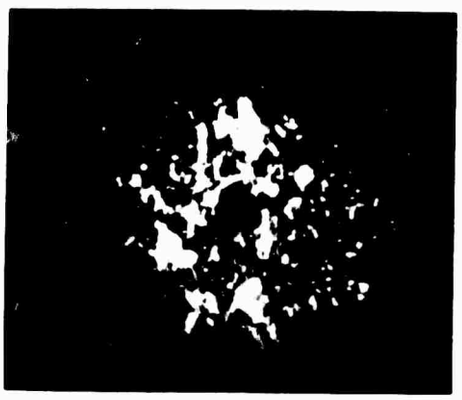

a) FULL LASER INTENSITY (100%)

b) 70%

c) 50%

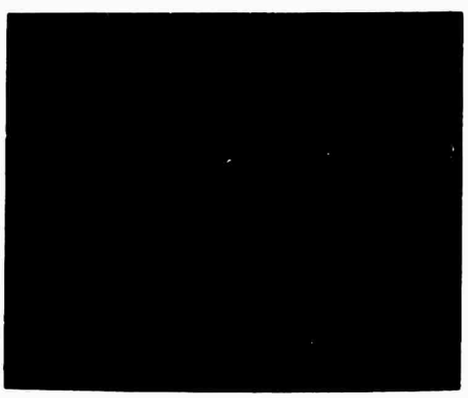

d) 30%

SELF-TRAPPING IN METHANOL

a) LASER

b) STOKES

c) ANTI-STOKES

SELF-TRAPPING IN ACETIC ACID-STOKES LIGHT

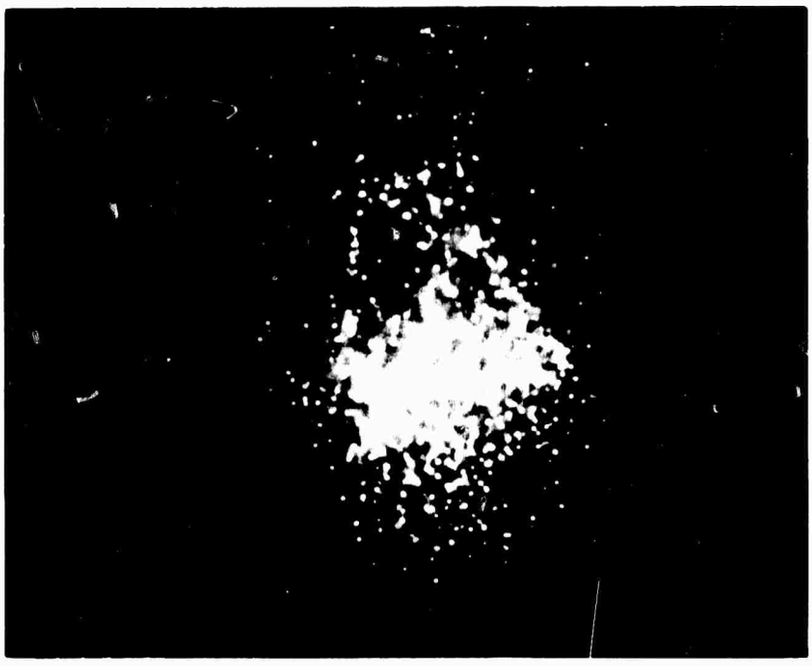

a) COLLIMATED BEAM

b) FOCUSED BEAM

STIMULATED VIBRATIONAL SCATTERING IN SF_6

a) LASER – INCIDENT AND TRANSMITTED

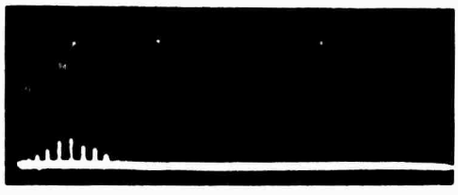

b) STOKES

STIMULATED PURE ROTATIONAL RAMAN SCATTERING

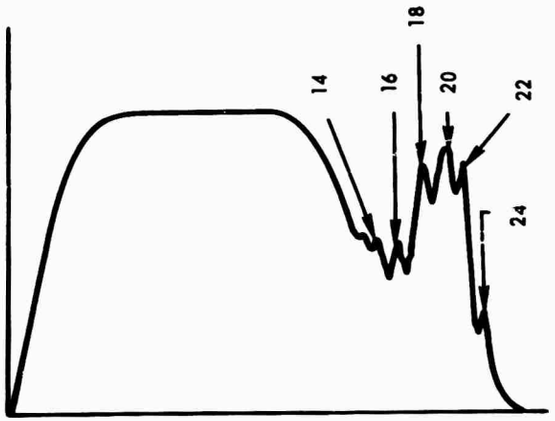

(a) CARBON DIOXIDE

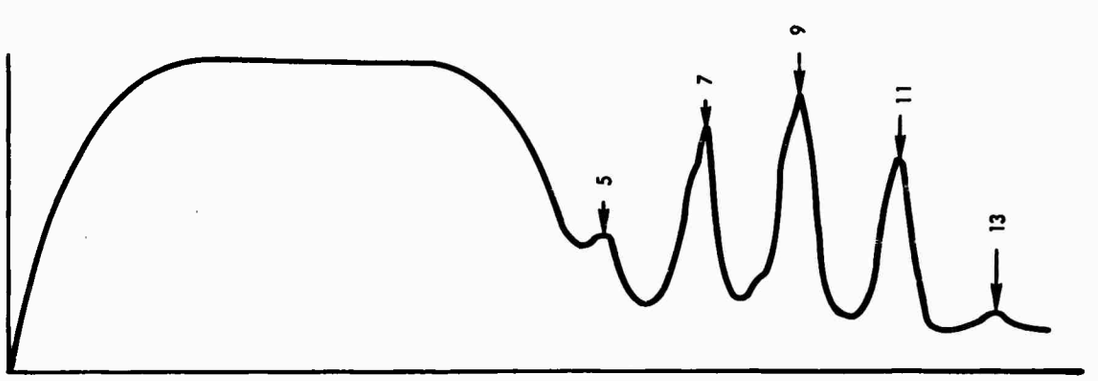

(B) OXYGEN

FIG. 28

SELF-TRAPPING IN N_2O AND CO_2

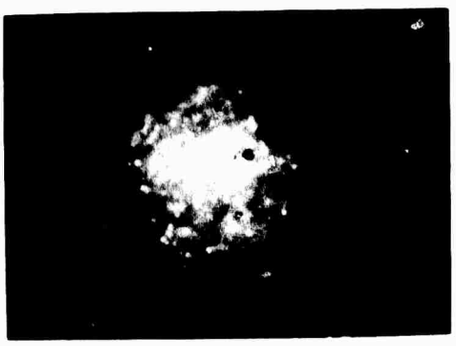

a) N_2O – LASER LIGHT

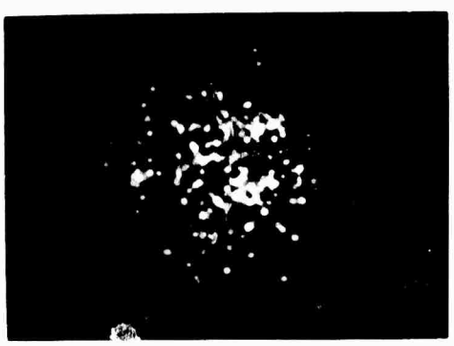

b) N_2O – STOKES LIGHT

c) CO_2 – STOKES LIGHT

FIG. 30

POLARIZATION OF ROTATIONAL SCATTERING IN N_2O

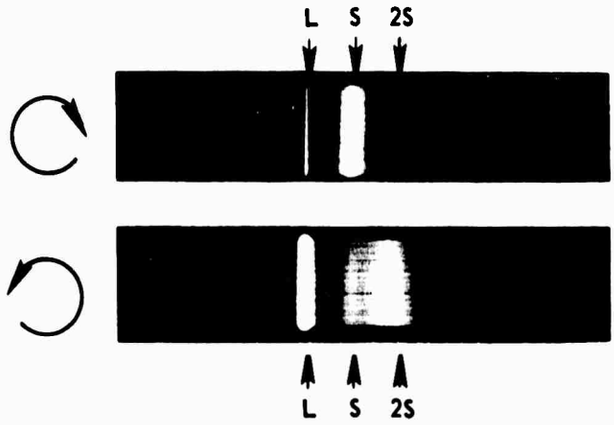

J920479-21

FIG. 31

HF DECAY MEASUREMENT

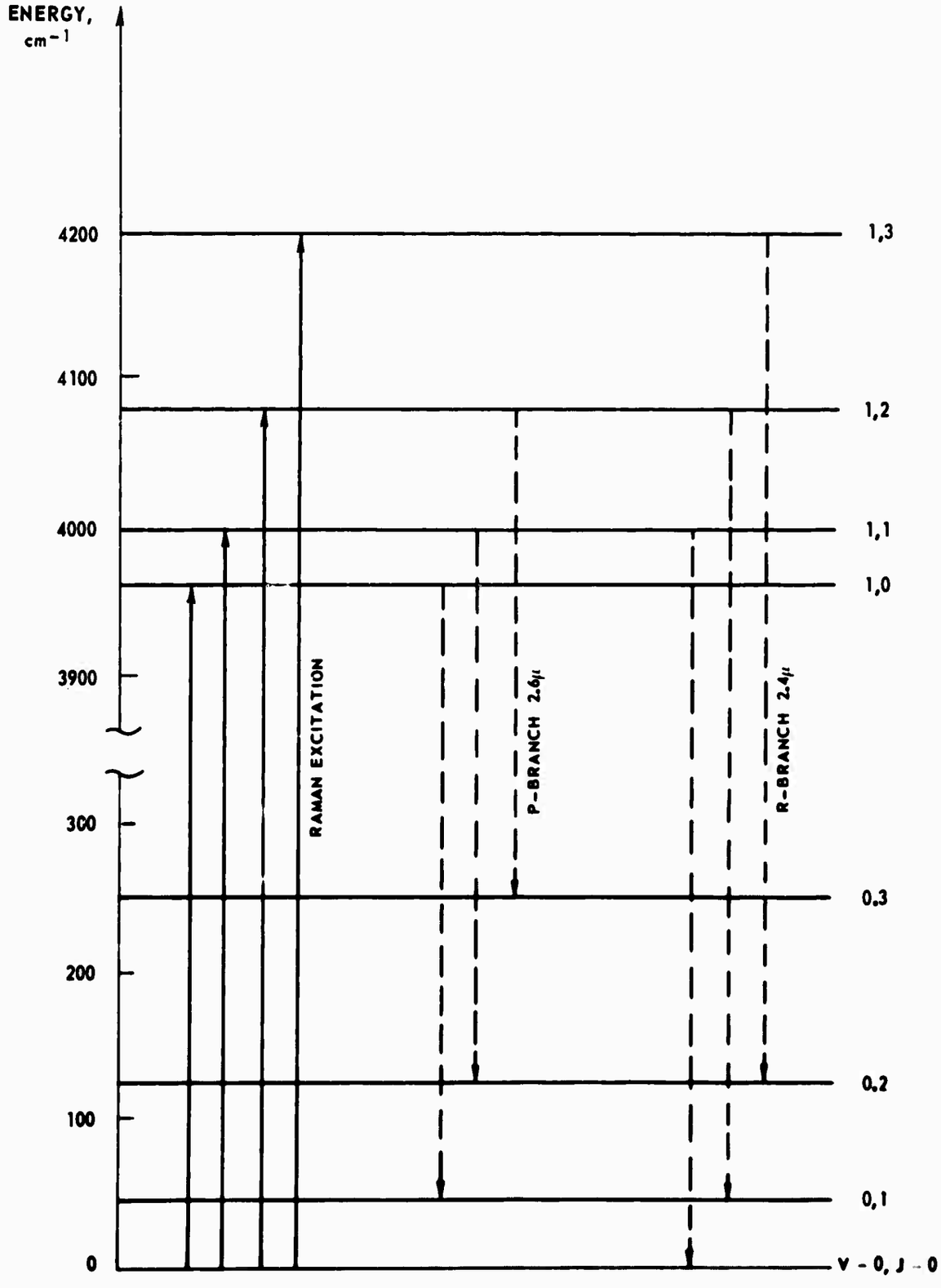

J920479-21

FIG. 32

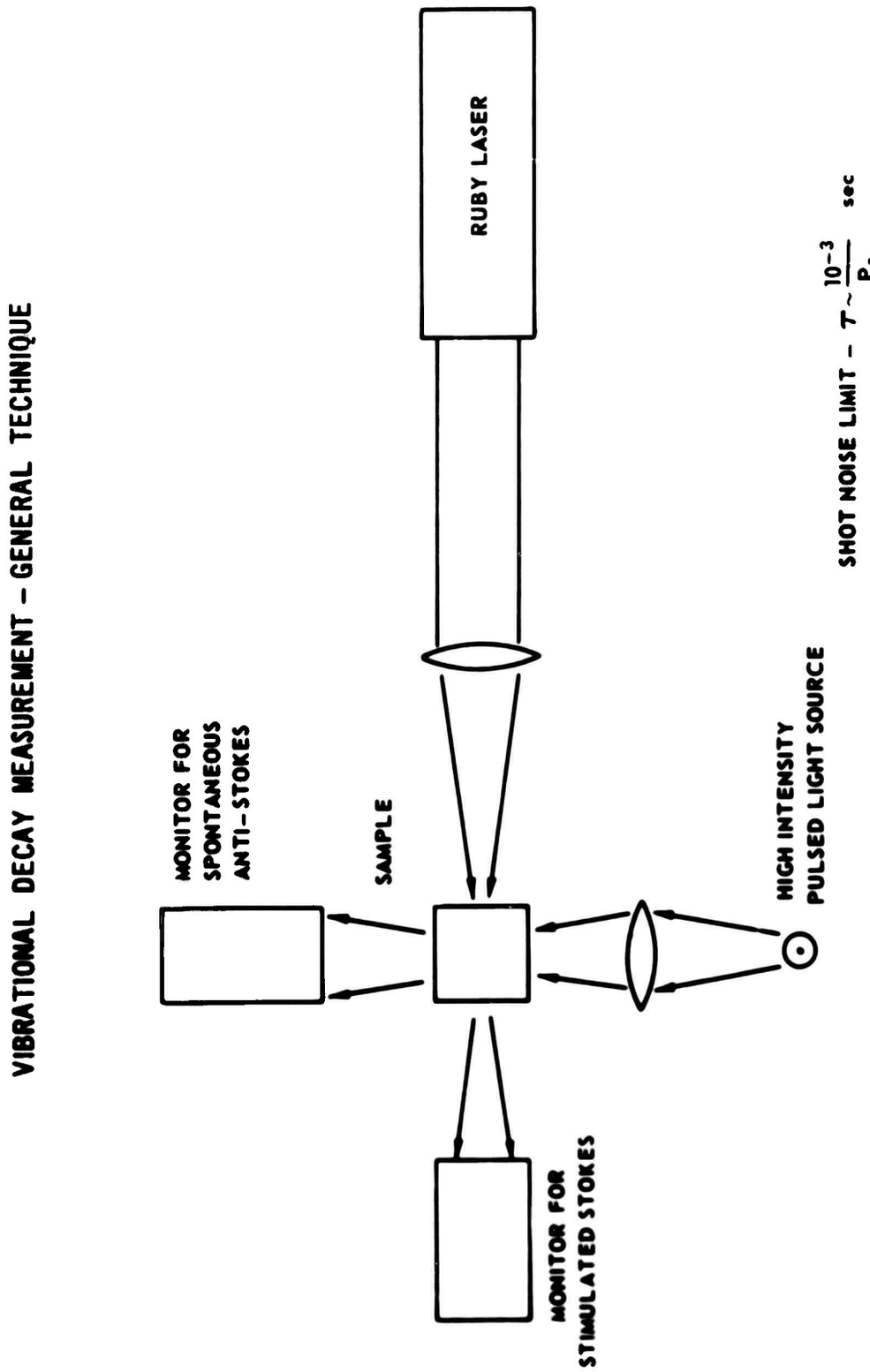

FIG. 33

a) STRAIGHT LAMP

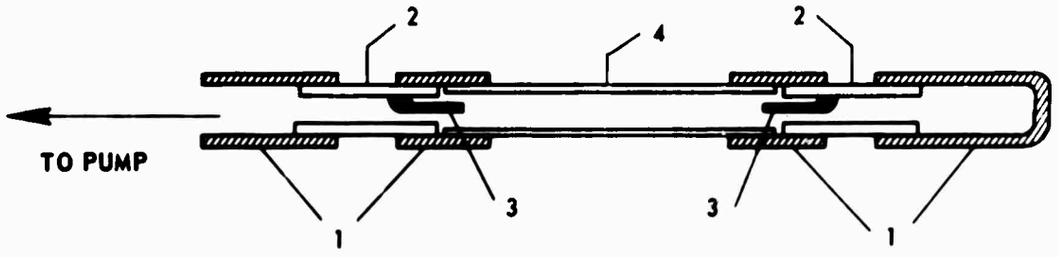

b) LOW INDUCTANCE LAMP

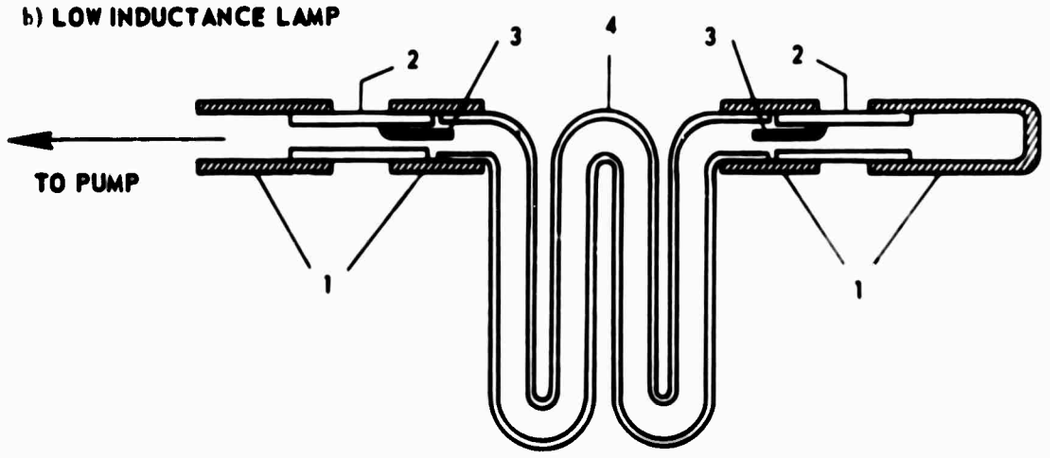

1 SEMI-FLEXIBLE PLASTIC TUBING
2 METAL SLEEVE
3 WIRE ELECTRODE
4 QUARTZ TUBING

FIG. 34

CIRCUIT FOR RELIABLE LAMP TRIGGERING

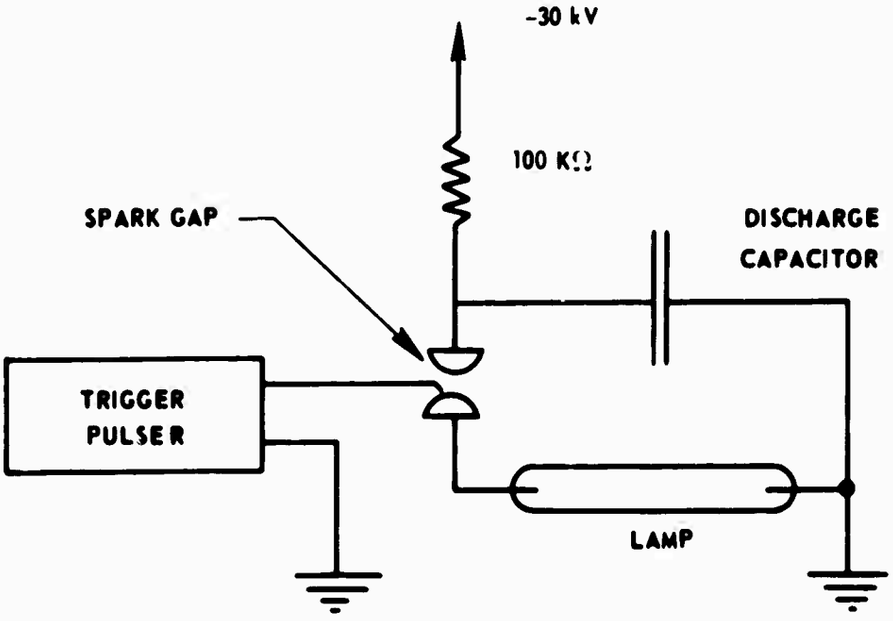

J920479-21

FIG. 35

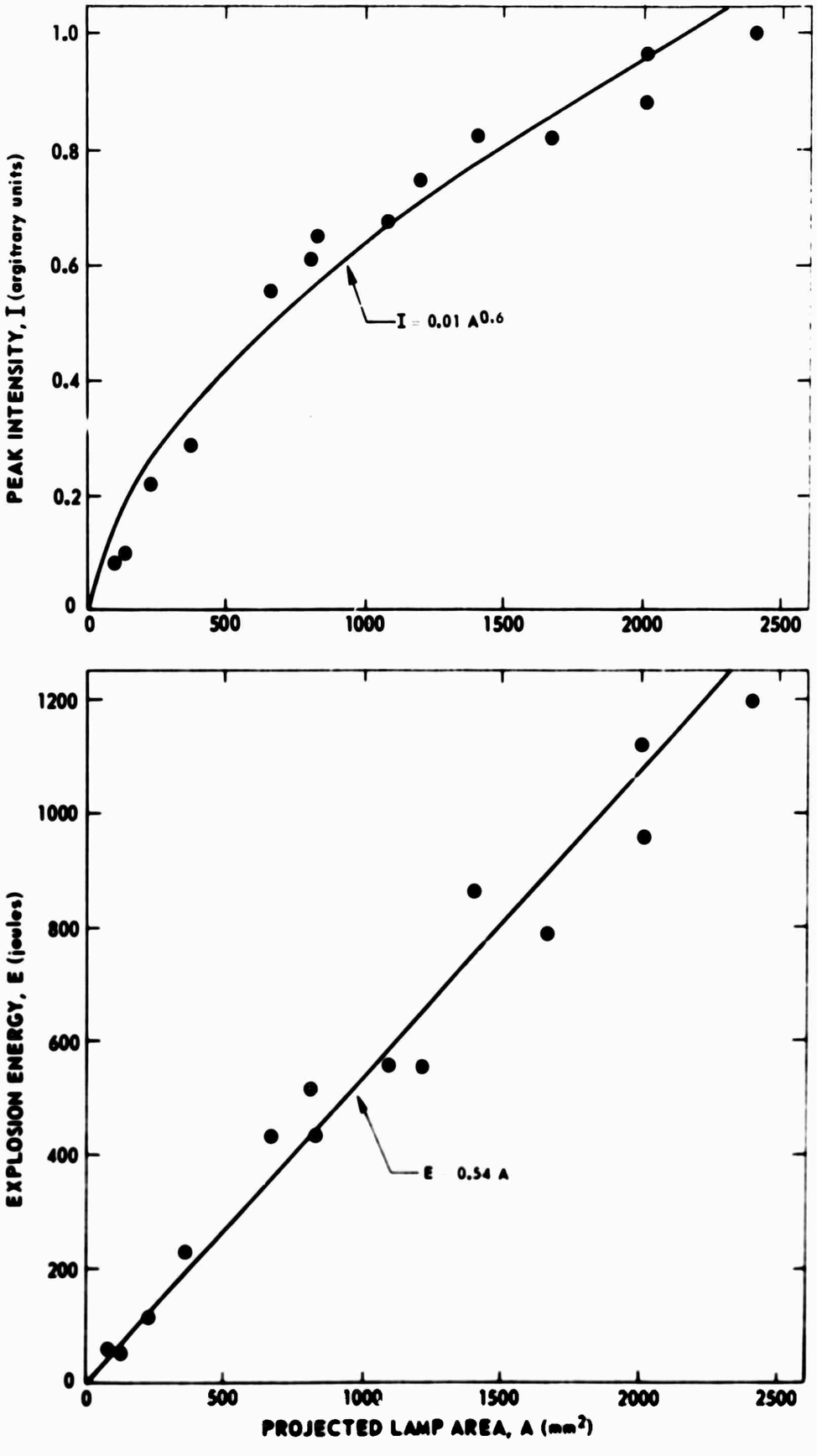

J920479-21

FIG. 36

a) LAMP PULSE

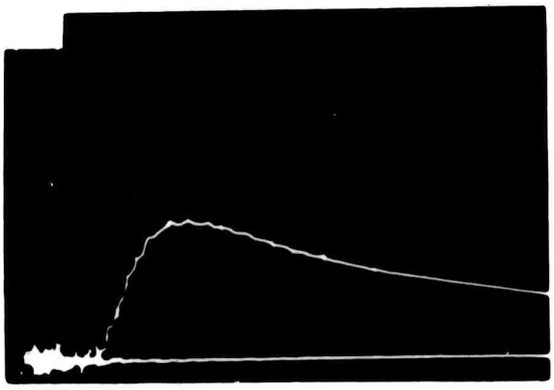

b) OUTPUT OF COUMARIN LASER PUMPED BY LAMP

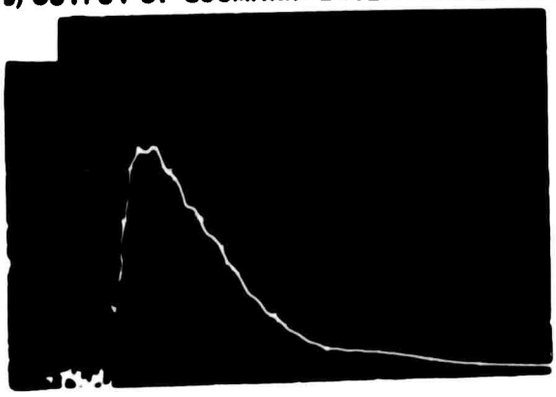

0.5 μsec/div

J920479-21

FIG. 37

FAST-RISE DYE LASER FLASHLAMP

20 nsec/cm

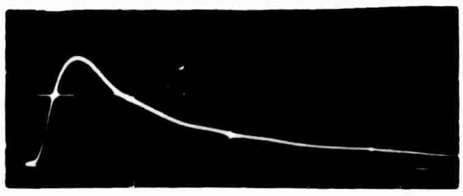

a) OPEN ARC

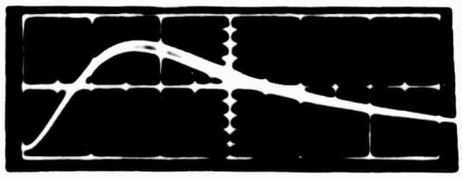

b) CONFINED ARC

J920479-21

FIG. 38

OUTPUT OF MODE-LOCKED COUMARIN DYE LASER

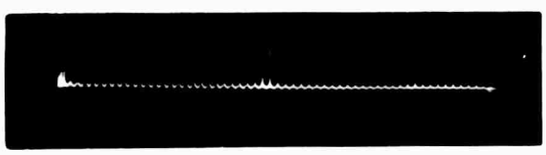

SWEEP SPEED: 100 nsec/div

TRAVELING WAVE DYE LASER

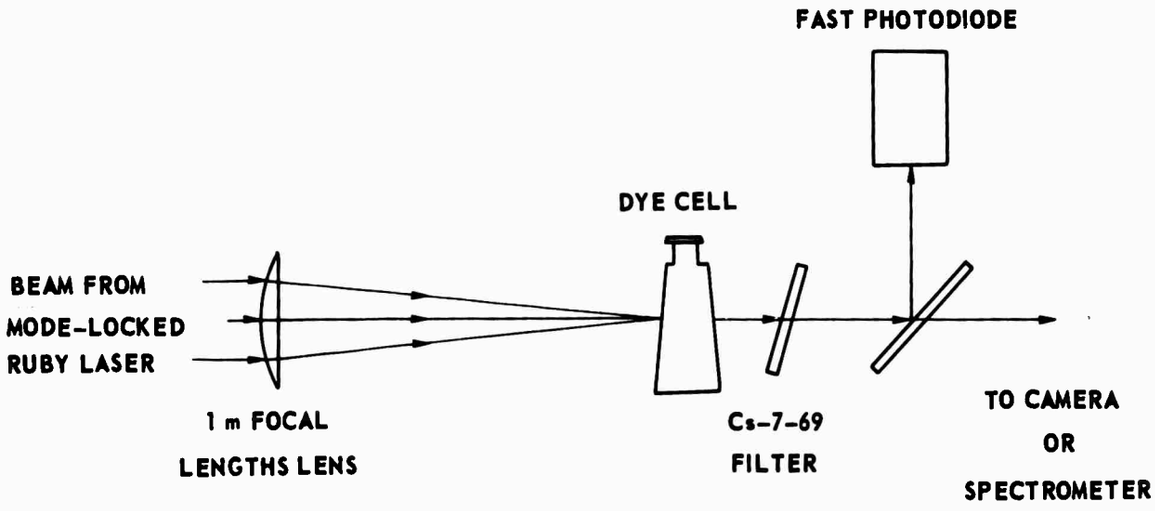

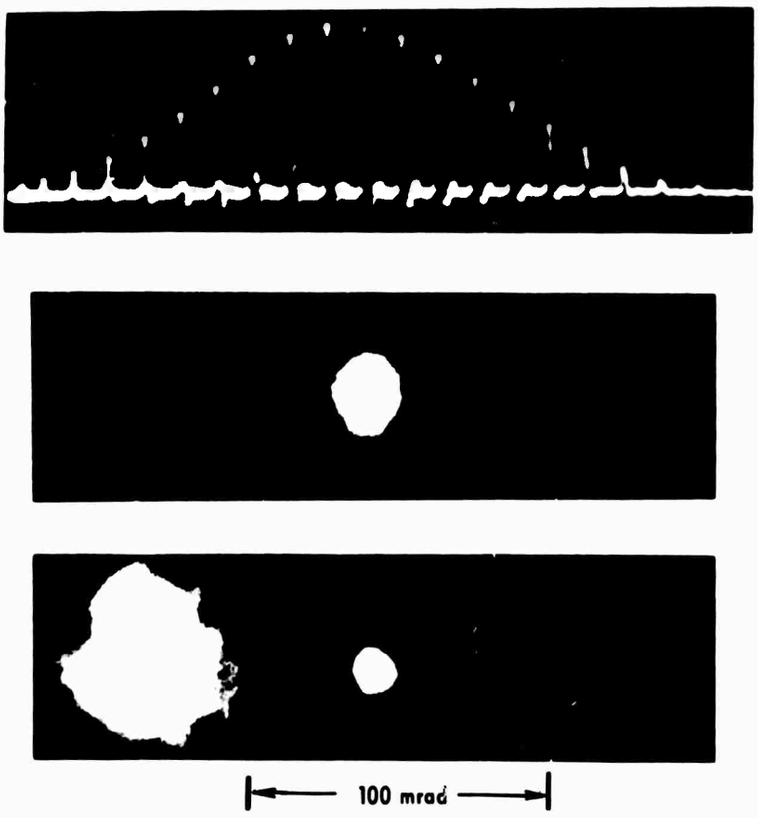

J920479-21

FIG. 40

OUTPUT PULSE DURATION VS PEAK TRAVELI NG WAVE GAINS

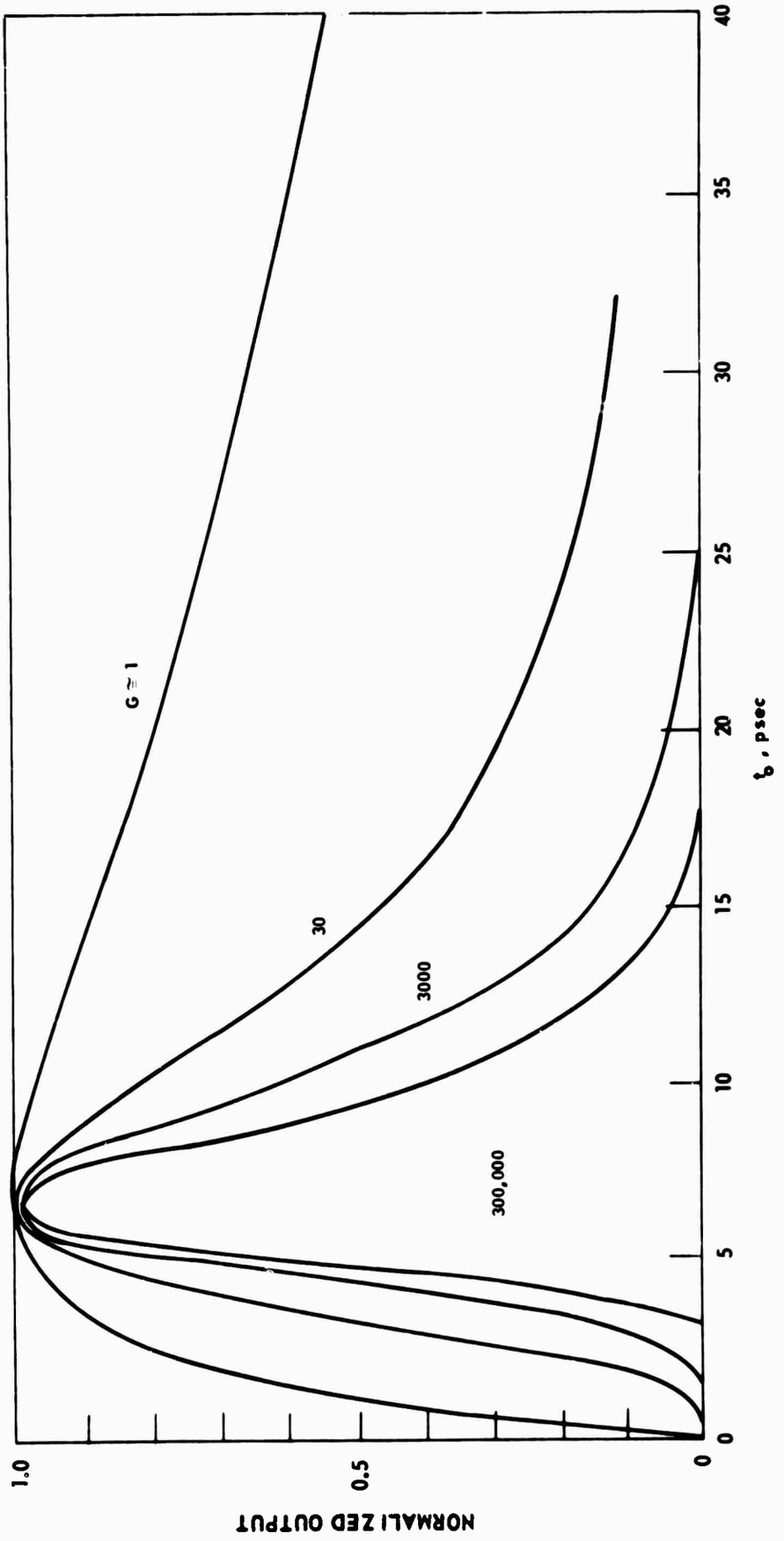

J920479-21

FREE-FREE ABSORPTION VS PRESSURE AND WAVELENGTH

FIG. 41

($T = 5 \times 10^5\,^\circ K$, $Z = 5$)

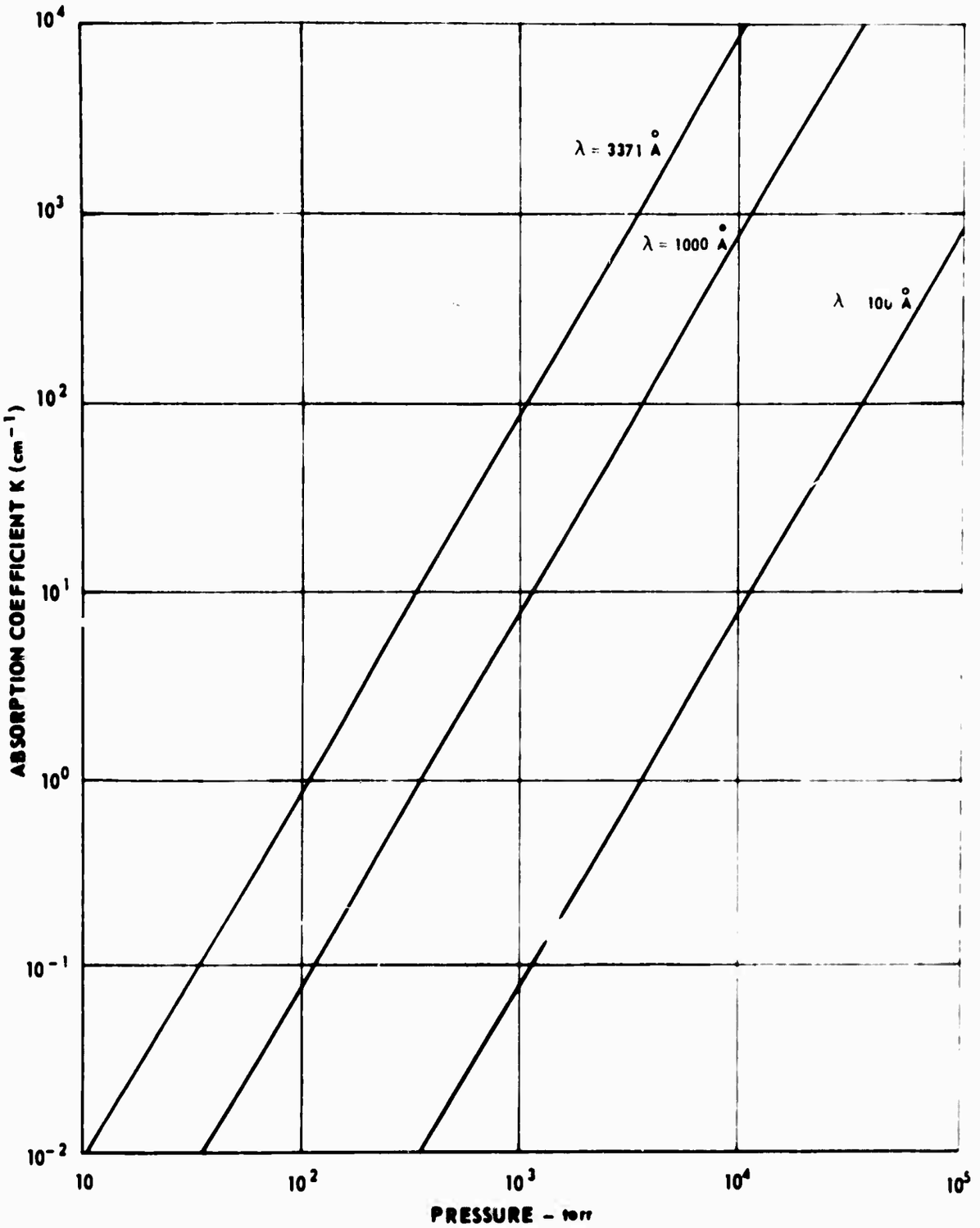

J920479-21

NET GAIN COEFFICIENT FOR 3371 Å EMISSION IN NITROGEN

FIG. 42

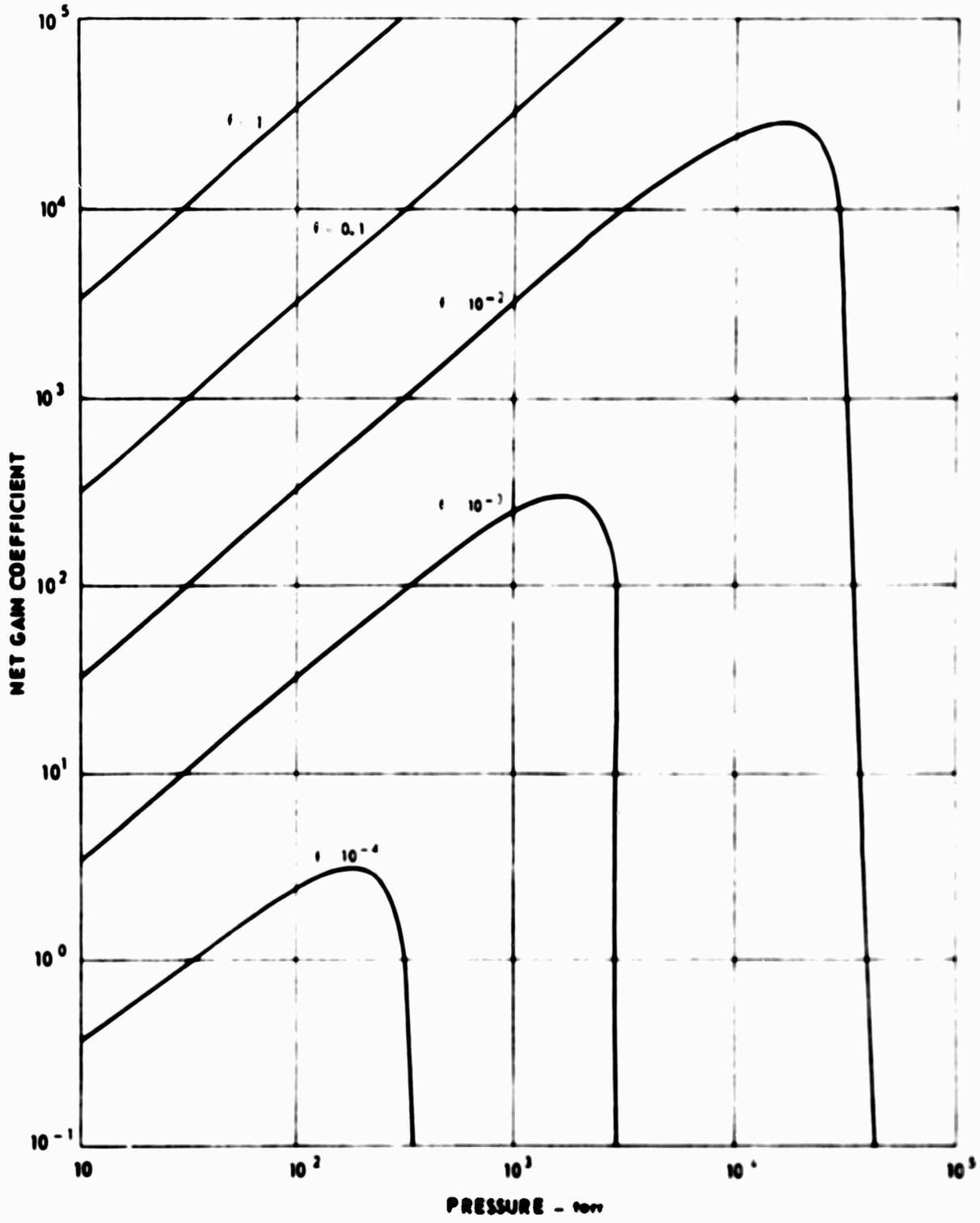

J920479-21

FIG. 43

NET GAIN COEFFICIENT

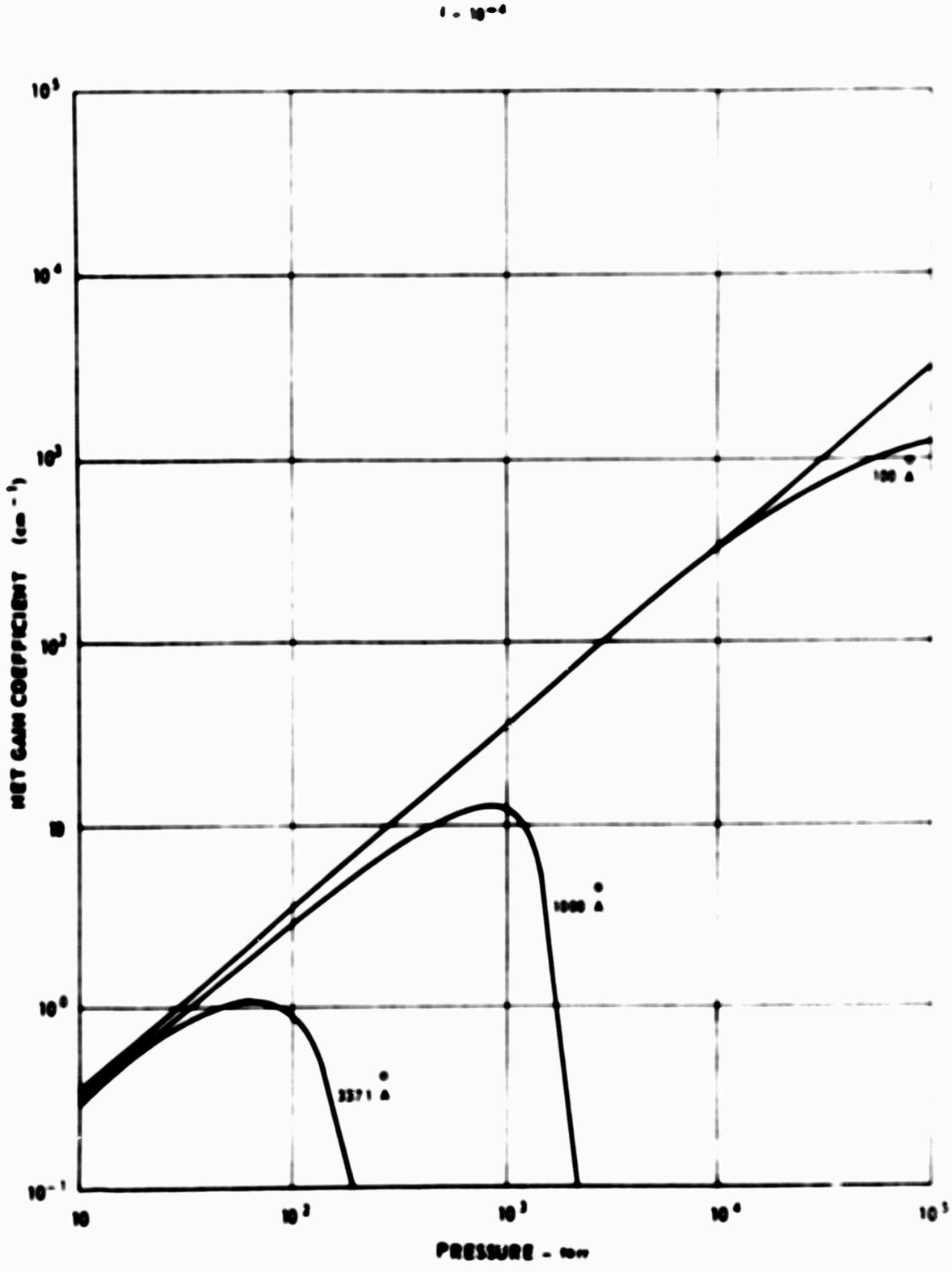

J920479-21

FIG. 44

GAIN IN COPPER VAPOR

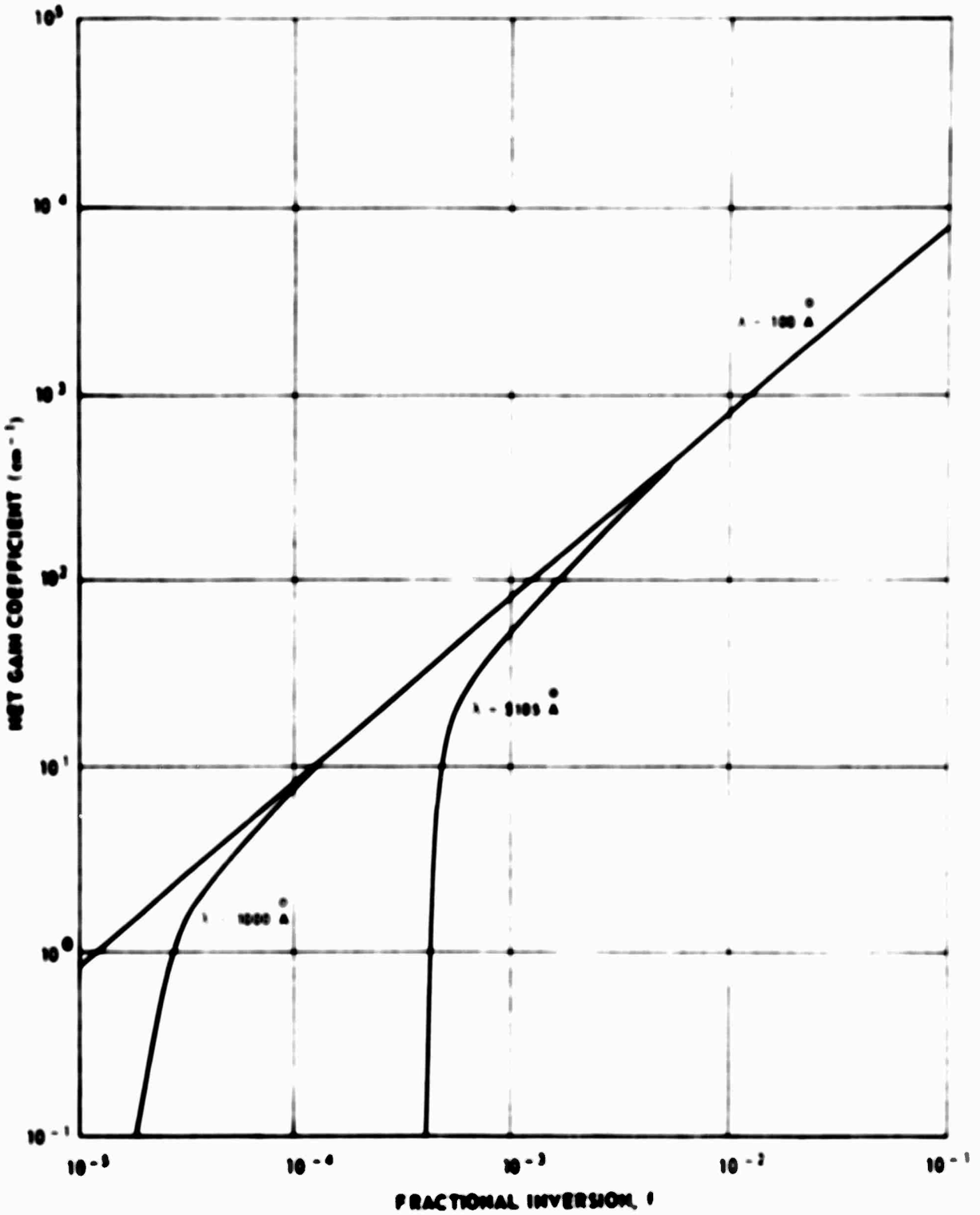

J920479-21

FIG. 45

GAIN IN LEAD VAPOR

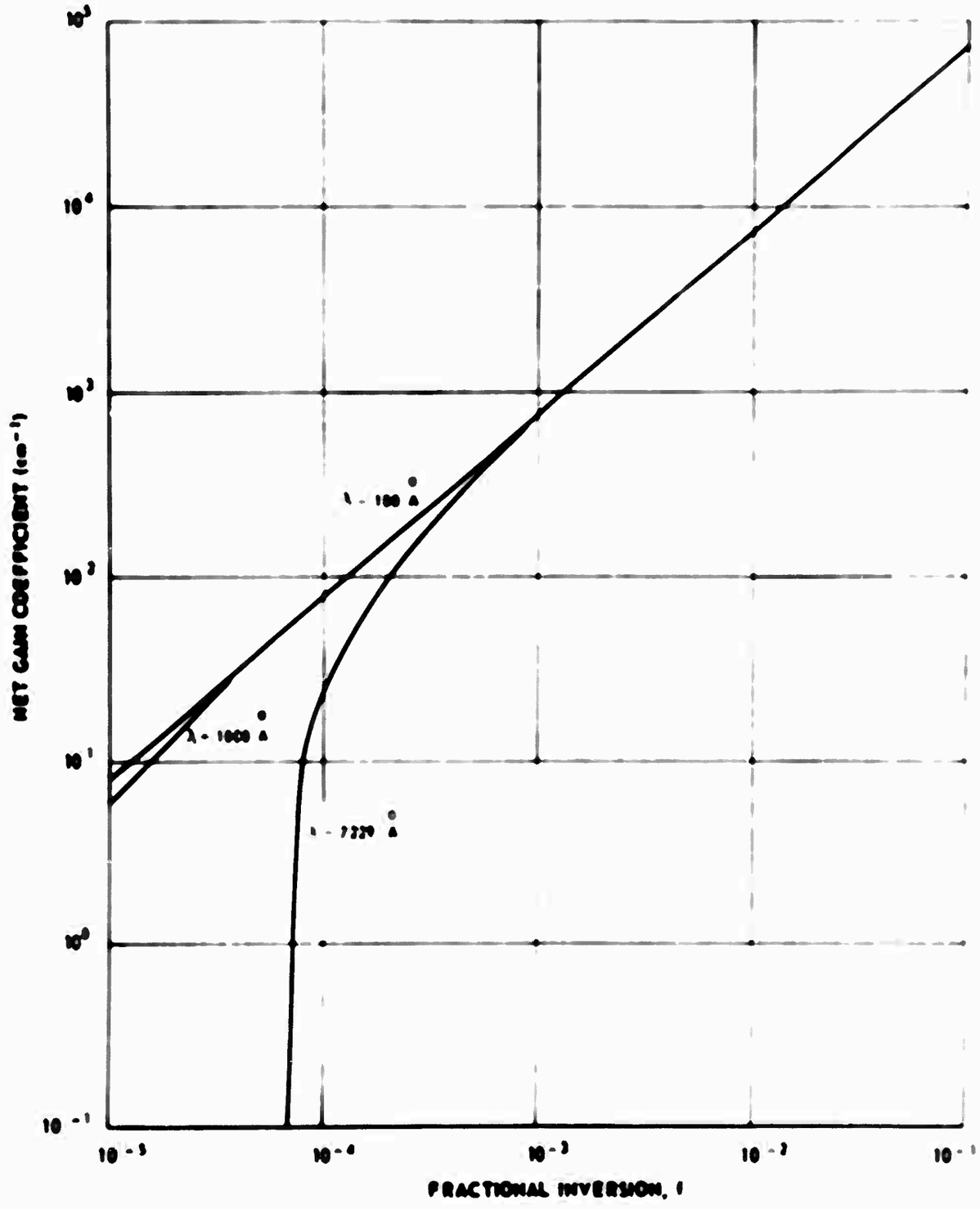

J920479-21

FIG. 46

PLASMA LASER EXPERIMENT

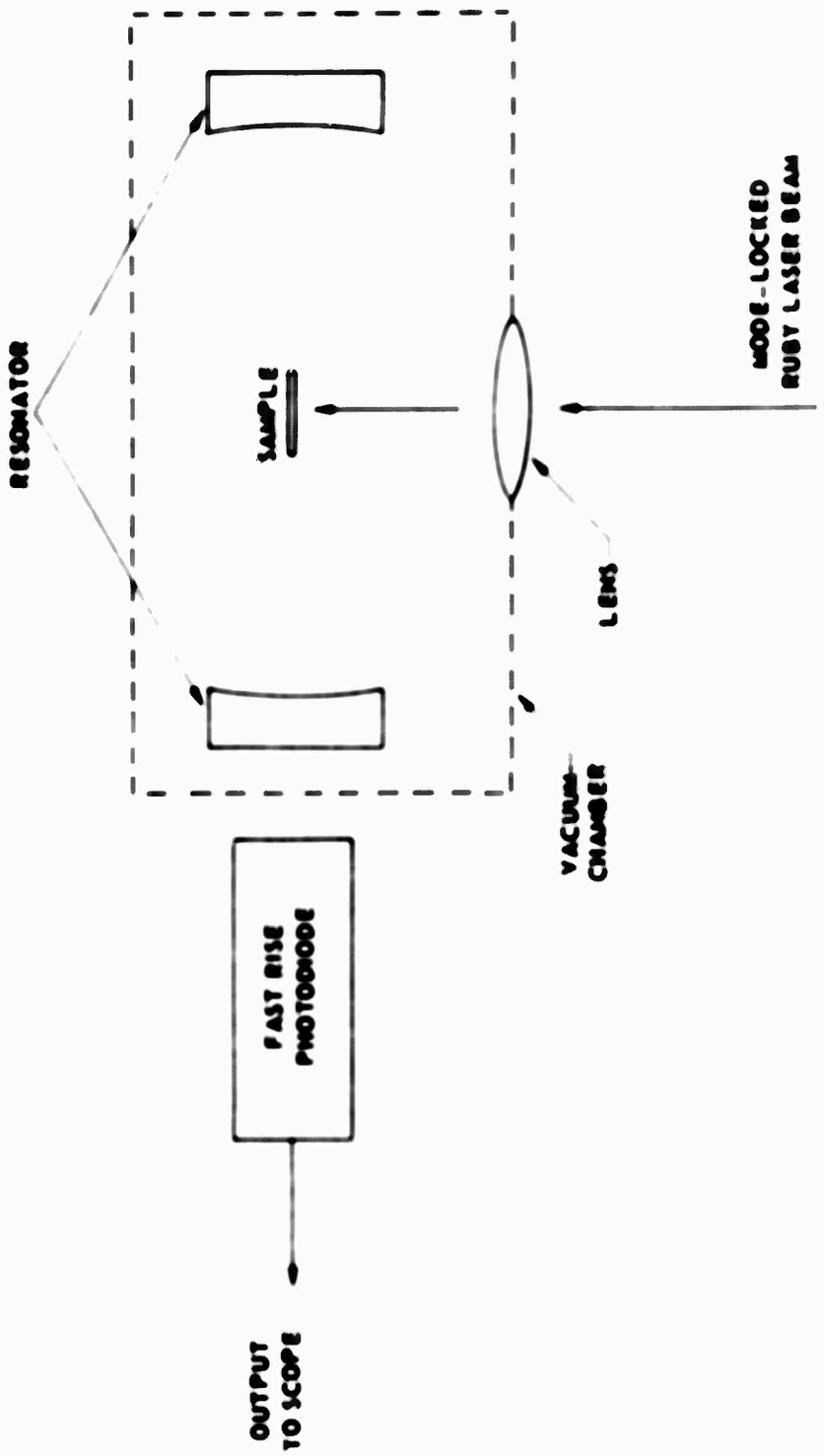

J920479-21

FIG. 47

COPPER VAPOR FLUORESCENCE

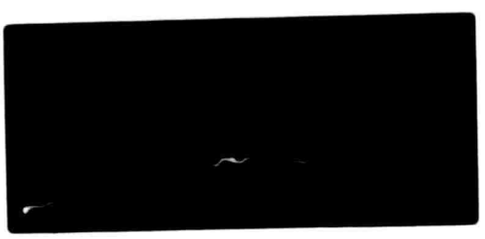

a) 20 nsec cm

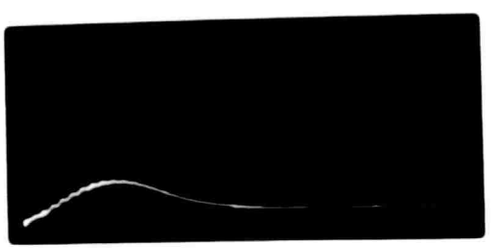

b) 50 nsec cm

BEHAVIOR OF POLARIZATION

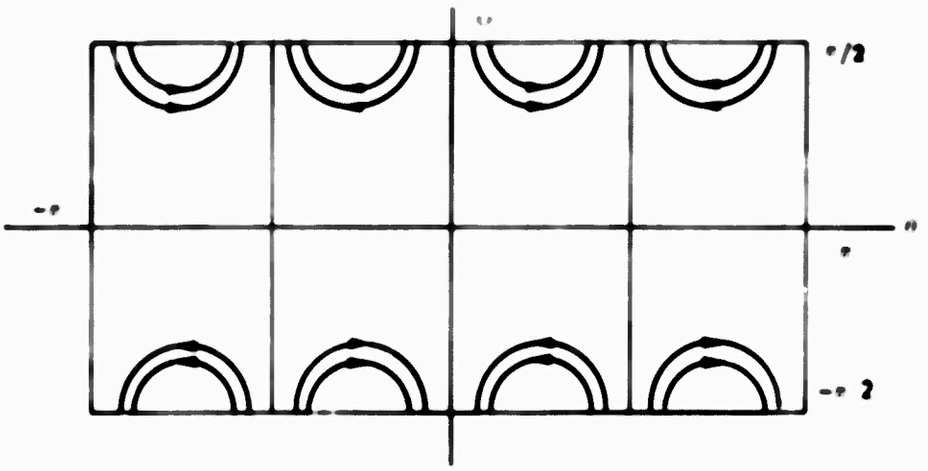

KERR ACTIVE LIQUID

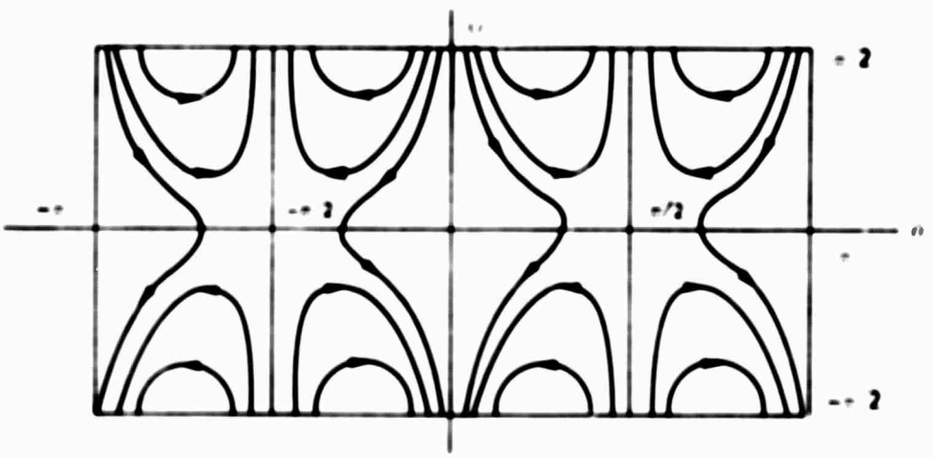

KERR ACTIVE LIQUID WITH INDUCED BIREFRINGENCE

UNCLASSIFIED

Security Classification

DOCUMENT CONTROL DATA - R & D

(Security classification of title, body of abstract and indexing annotation must be entered when the overall report is classified)

United Aircraft Corporation Research Laboratories East Hartford, Connecticut	Unclassified

REPORT TITLE

RESEARCH INVESTIGATION OF PICOSECOND LASER PULSES

Scientific Annual Report for the Period 1 March 1969 to 28 February 1970

AUTHOR(S) (First name, middle initial, last name)

Anthony J. DeMaria, William H. Glenn, Carl M. Ferrar, George L. Lamb, Jr., Michael E. Mack and E. Brian Treacy

REPORT DATE	TOTAL NO OF PAGES	NO OF REFS
March 26, 1970	163	139

CONTRACT OR GRANT NO	ORIGINATOR'S REPORT NUMBER(S)
N00014-66-C-0344	
PROJECT NO ARPA Order No. 306 A # 15 Project Cost Code No. 9E30K21	OTHER REPORT NO(S) (Any other numbers that may be assigned this report) J970479-21

DISTRIBUTION STATEMENT

Reproduction in whole or in part is permitted for any purpose of the United States Government.

SUPPLEMENTARY NOTES	SPONSORING MILITARY ACTIVITY
	Department of the Navy Office of Naval Research

ABSTRACT

This report covers work under contract N00014-66-C-0344 for the period 1 March 1969 to 28 February 1970. Topics discussed include theoretical and experimental work made on the propagation of ultrashort light pulses, stimulated scattering effects, nonlinear propagation, Cerenkov radiation, organic dye lasers, and stimulated emission from laser produced plasmas.

DD FORM 1473

UNCLASSIFIED

Security Classification

14 KEY WORDS	LINK A		LINK B		LINK C	
	ROLE	WT	ROLE	WT	ROLE	WT
Laser Line Profiles						
Picosecond Laser Pulses						
Ultrashort Pulse Propagation						
Stimulated Scattering						
Cerenkov Radiation						
Laser Produced Plasmas						
Organic Dye Lasers						
Mode-Locked Lasers						
Nonlinear Optics						